POOL BOILING FROM ENHANCED STRUCTURES UNDER CONFINEMENT

A Dissertation
Presented to
The Academic Faculty

by

Camil-Daniel Ghiu

In Partial Fulfillment
Of the Requirements for the Degree of
Doctor of Philosophy in Mechanical Engineering

Georgia Institute of Technology
August 2007

POOL BOILING FROM ENHANCED STRUCTURES UNDER CONFINEMENT

Approved by:

Dr.Yogendra K.Joshi, Chair/Advisor
School of Mechanical Engineering

Dr.Said Abdel-Khalik
School of Mechanical Engineering

Dr.Mostafa Ghiaasiaan
School of Mechanical Engineering

Dr.Sushil Bhavnani
Auburn University

Dr.Madhavan Swaminathan
School of Electrical and Computer Engineering

Date Approved: April 10, 2007

ACKNOWLEDGEMENTS

I would like to thank Professor Yogendra Joshi, my advisor and mentor. His guidance, support and patience during my years of graduate studies at the University of Maryland College Park and Georgia Institute of Technology made this possible.

I am also grateful to my dissertation committee members (Professor Said Abdel-Khalik, Professor Mostafa Ghiaasiaan, Professor Madhavan Swaminathan and Professor Sushil Bhavnani) for their constructive comments during the proposal and final dissertation.

Thanks are extended to the members of the Microelectronics and Emerging Technologies Thermal Laboratory for maintaining a pleasant work environment and helping me in many ways.

Special thanks go to my wife Ioana for her continuous support and encouragement throughout my years in Graduate School.

I would like to thank my mother and sister for their incessant belief in me.

TABLE OF CONTENTS

LIST OF TABLES

LIST OF FIGURES

NOMENCLATURE

A	area of the structure (projected) (m^2)
A_b	area available for boiling (m^2)
A_c	area available for conduction (m^2)
A_h	area of the copper rod cross section (m^2)
A_w	structure wetted area (m^2)
c_p	specific heat (J/kg·K)
C	coefficient in equation (3.1)
C_1	empirical constant in equation (6.1)($W/cm^2 \cdot K$)
C_2	empirical constant in equation (6.3) (s/m)
C_3	coefficient in equation (6.6) (m^{-1})
d_p	pore diameter (m)
D_d	bubble departure diameter (m)
f	frequency (Hz)
g	acceleration due to gravity (m/s^2)
h_{fg}	latent heat of vaporization (kJ/kg)
H_t	channel depth (m)
k	thermal conductivity (W/m·K)
L	overall length of the structure (m)
M	factor defined in equation (6.7) ($m^{0.5}$)
n	exponent of ΔT_{wall} in equation (3.1)

n_s nucleation site density (m^{-2})

N number of channels

P_p pore pitch (m)

P_t channel pitch (m)

R thermal resistance ($^oC/W$)

q'' heat flux based on projected surface area (W/m^2)

q_t'' heat flux based on total surface area (W/m^2)

q heat rate (W)

r radius of the flattened bubble (m)

S top gap distance (m)

t time (s)

T temperature (^oC)

v_s velocity of the bubble boundary (m/s)

w_i uncertainty of variable i

W_t channel width (m)

x horizontal direction

y horizontal direction

Subscripts

cond conduction

eff effective

ex external

l liquid

lat	latent
0	initial
sat	saturation
slope	slope
sup	superheat
t	tunnel
v	vapor
w	at the top of the enhanced structure
wall	at the base of the enhanced structure

Greek symbols

δ	thickness of liquid film (m)
Δ	difference in two quantities
μ	dynamic viscosity (kg/m·s)
ρ	density (kg/m^3)
σ	surface tension (N/m)

CHAPTER 1: INTRODUCTION

Modern life is becoming increasingly dependent on sophisticated electronic devices. Advanced features, faster communication and increased portability will be the hallmarks of future electronics. The trend towards miniaturization and increased functionality poses numerous challenges to developing compliant and reliable electronic products.

Thermal characterization of electronic devices is important for several reasons. First, there is a direct link between the reliability of an electronic component and its operating temperature. Since most failure mechanisms commonly encountered in electronic components depend exponentially on the operating temperature, the failure rate increases with increase in device temperature. Additionally, most electronic packages are made up of multiple materials with different coefficients of thermal expansion. Under the thermal loading from the environment or self heating during operation, stresses and strains generate within the package, leading to thermomechanical failures. Second, the electrical performance of an electronic device degrades with the increase in the operating temperature. Therefore, to ensure functionality within the design specifications, it is necessary to maintain the device temperature below the maximum allowable limit. This is the primary objective of thermal management of electronics.

As the heat fluxes dissipated by the new generation of electronic chips continue to increase, the need for new cooling techniques has become more stringent. Existing air cooling hardware has become too large to meet the overall electronic system size requirements of newly developed electronic systems. For these applications the primary

heat sources (chips) are located in a densely packed zone, requiring the removal of heat from tight spaces.

While air-cooling remains the main way of cooling electronics, it is clear that for a number of applications other cooling methods have to be employed. The nearly inevitable adoption of liquid cooling in commercial electronic products will demand affordable thermal management hardware. The simplest method of liquid cooling is through a single phase forced convection scheme. A single phase cooling loop consists generally of a pump, a heat exchanger (attached to the heat source) and a heat sink. Despite the high cooling potential of single-phase liquid convection, such a solution is limited by the need of pumping power and complex plumbing. The use of liquid-vapor phase change to transfer the heat from the source to the ultimate heat sink is an alternative solution attracting the interest of thermal community. Two-phase liquid cooling has the advantage of reaching very high heat transfer coefficients.

Two-phase liquid cooling schemes are typically implemented using heat pipes and thermosyphons. A heat pipe is a thermal transport device utilizing phase change processes to transfer heat with no moving parts and at a nearly constant temperature. It is composed of three sections: the evaporation section at one end, a condenser section at the other end and an adiabatic section. Although a very efficient cooling device, the heat pipe has limitations, nevertheless. These limitations (boiling limit, for instance) spurred the interest for the use of alternative devices utilizing the advantages of two phase cooling.

Such a candidate device is the thermosyphon. Based on geometry, thermosyphons can be classified as single-chamber (closed) or two-chamber (Figure 1.1). A single chamber thermosyphon has the evaporator, the adiabatic mixing section and the

condenser as part of a single tube In a two-chamber thermosyphon, the evaporator and condenser are separated through two tubes, one designed for vapor rise and the other for condensate return. This configuration provides flexibility and assures vapor and condensate separation.

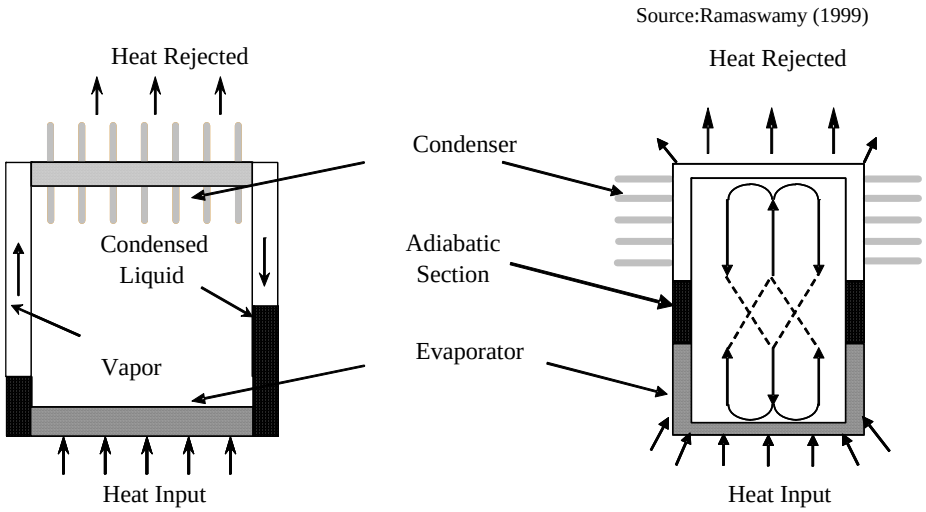

Figure 1.1 Thermosyphon types (a) two-chamber, (b) single-chamber

The overall thermal performance of a two-chamber thermosyphon depends on the evaporator performance. This can be improved by employing the highly efficient nucleate pool boiling regime.

There are two fundamental issues associated with pool boiling heat transfer: incipience overshoot and critical heat flux. Before the initiation of boiling, the heat is transferred from the surface to the surrounding liquid pool through natural convection. There is an excess temperature (incipience overshoot) required for boiling to start. On the other hand, the critical heat flux is the upper limit of the highly thermally efficient nucleate boiling regime. It dictates the maximum limit of heat dissipation attainable.

Electronics cooling applications place specific requirements on using boiling as a heat transfer mode. First of all, the temperature of the electronic component to be cooled must be held below a certain value (typically 85^{o}C for conventional silicon electronics), based on performance and reliability considerations. Secondly, only certain fluids are suitable for direct contact with electronics. The candidate fluids should have low boiling points, be chemically stable, inert, and with high dielectric strength. While distilled water may be used in a limited number of situations, the requirement of compatibility of coolants with electronic packaging materials narrows the choice of candidate liquids. Other liquids, like the chlorofluorocarbons, have been considered suitable for use in electronic systems, but their use has been phased out due to environmental concerns. The perfluorinated liquids from 3M (Fluorinert class) appear to be the best suitable candidates for direct liquid cooling applications. Unfortunately, these dielectric liquids have poor thermal transport properties. Moreover, the incipience overshoot issue is exacerbated for low surface tension fluids (fluorocarbons, for instance). In addition, the heat source surface area is small, which leads to high heat fluxes to be dissipated. The critical heat flux was found to be only 17 W/cm^2 for boiling FC 72 from plain surfaces under atmospheric pressure (Nakayama et al. (1984)). This is well below heat fluxes of interest in electronics cooling, typically 40 W/cm^2 or higher.

To reduce the incipience overshoot and increase the critical heat flux, special surfaces have been developed (Figure 1.2). They feature sub-surface tunnels communicating with the liquid pool through small opening called pores. The efficient performance of enhance structures in pool boiling makes them suitable candidates for incorporation into the evaporator section of a thermosyphon.

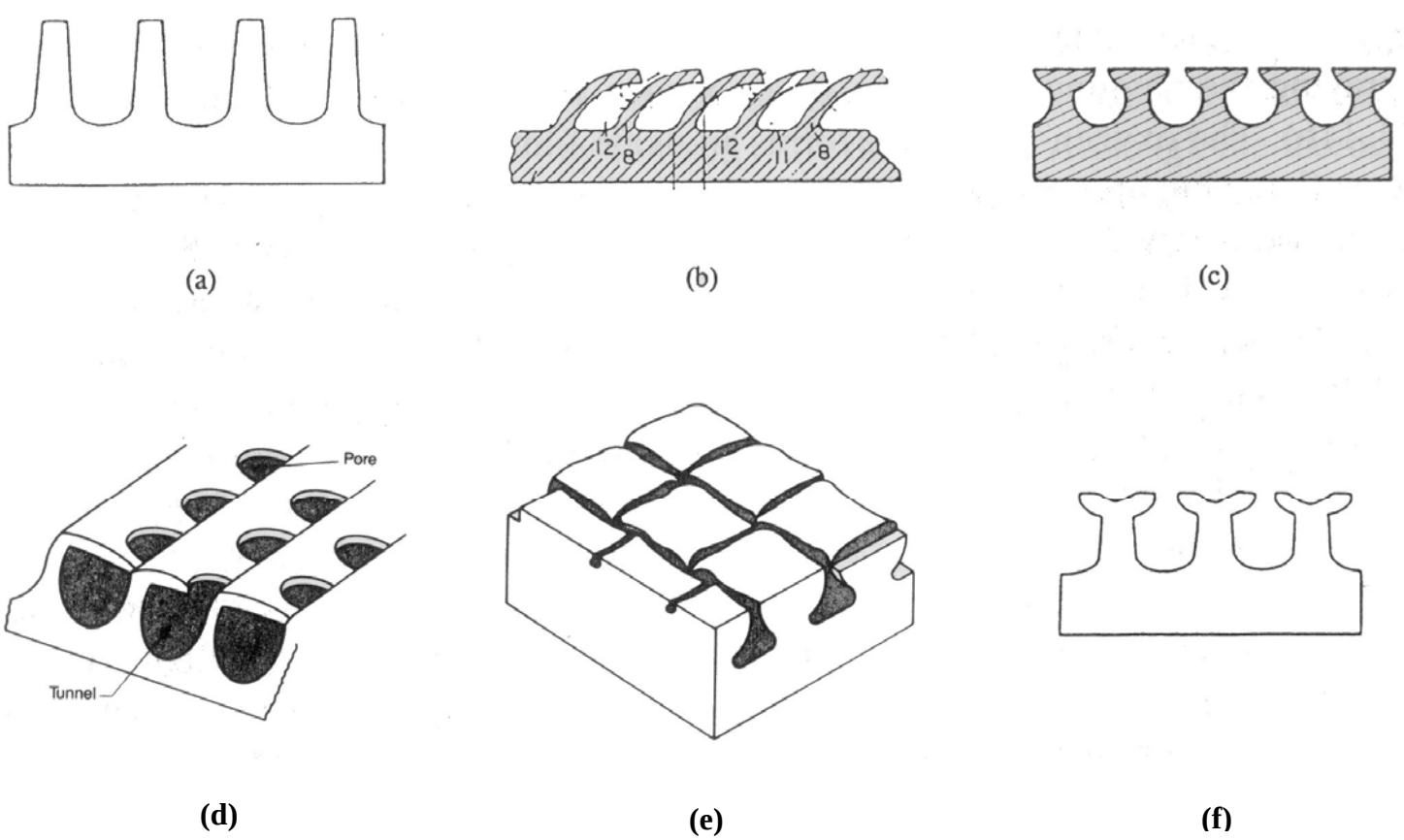

Figure 1.2 Representative enhanced boiling structures (a) Integral-fin tube (b) Trane bent fin (c) Weiland GEWA-TW (d) Hitachi Thermoexcel-E (e) Wolverine Turbo-B and (f) Weiland GEWA-SE

1.1 Motivation for the current study

The electronics miniaturization process poses new challenges for the thermal engineer. Reduction in electronic chip sizes (going down to a few square millimeters for certain applications) places a space constraint on the micro-geometric features to be provided on the cooling device. While boiling from enhanced structures has been studied extensively, there is virtually no information for enhanced structures featuring small channel width (65-105μm) and channel pitch (0.2-0.7 mm). While the small channel width and pitch allow an increase in pore density, it is unclear whether such an increase results in a commensurate increase in the overall heat removal capability of the structure.

The trend to move away from two-dimensional chip architectures to three-dimensional electronics presents new issues to the thermal community. 3D packages containing stacked die are common today in portable devices like mobile phones and digital cameras. The presence of a high-power component, such as a processor, into a stack of memory or other chips exacerbates the thermal issue. The lack of an adequate cooling scheme limits 3D stacking to only low power electronics such as memory circuits. For such cooling applications, the common approach of a metallic spreader is no longer valid. It is therefore necessary to assess the viability of new cooling schemes. Figure 1.3 presents such a possible future application, a thermosyphon implemented in a PC.

The vast majority of boiling studies dealing with enhanced structures was performed in an unconfined space. However, several future applications (for instance, in next generation of three-dimensionally stacked layers of powered electronic chips (Banerjee et al. (2001)), require complete confinement in the vertical direction.

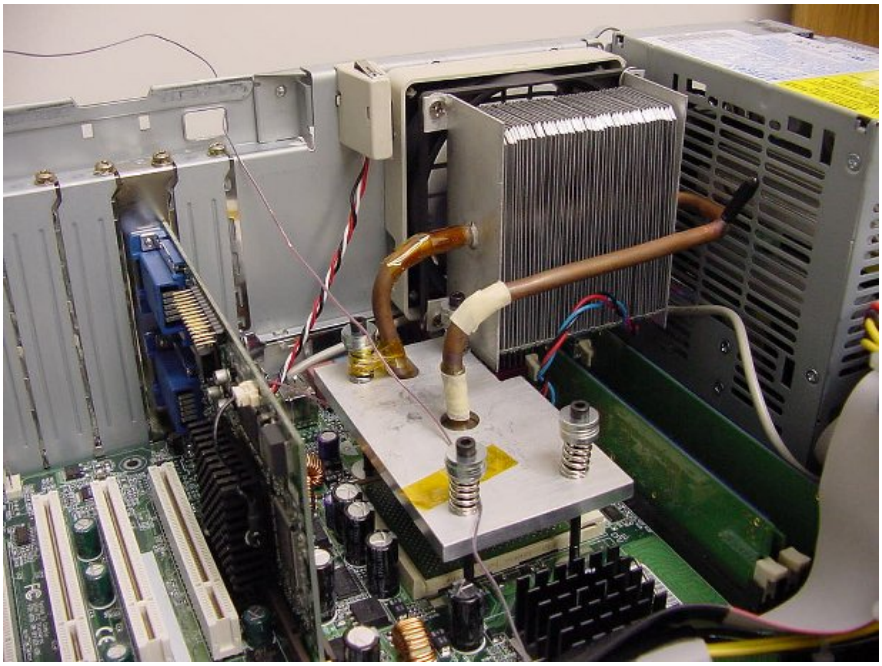

Figure 1.3 Thermosyphon implemented in a PC (Pal et al. (2002))

Moreover, the single-layered structures studied here are often used in a stacked configuration to enhance the overall thermal performance. In this case, the bonding between individual layers may require the presence of a thin metallic foil (for instance, gold; see Ramaswamy (1999)). Hence the completely covered top situation may be encountered in many practical implementations. There is virtually no data on the boiling performance of the single-layered enhanced structures in such closed-top configuration.

A less severe constraint occurs when there is limited space above the enhanced structure. A cooling scheme utilizing little space on vertical direction would be extremely useful in electronics cooling, where the available space is at a premium. However, the confinement alters the conventional boiling in a manner that needs to be understood.

Figure 1.4 depicts a thin two-phase heat spreader designed for space constrained cooling applications.

The previous studies employing enhanced structures under constraint did not include flow visualizations as an aide in illuminating the boiling phenomena. Therefore, the specific heat transfer mechanisms were hypothesized based on the limited information offered by the boiling curves. The present study aims at a deeper understanding of the physics underlying the boiling under top confinement using enhanced structures.

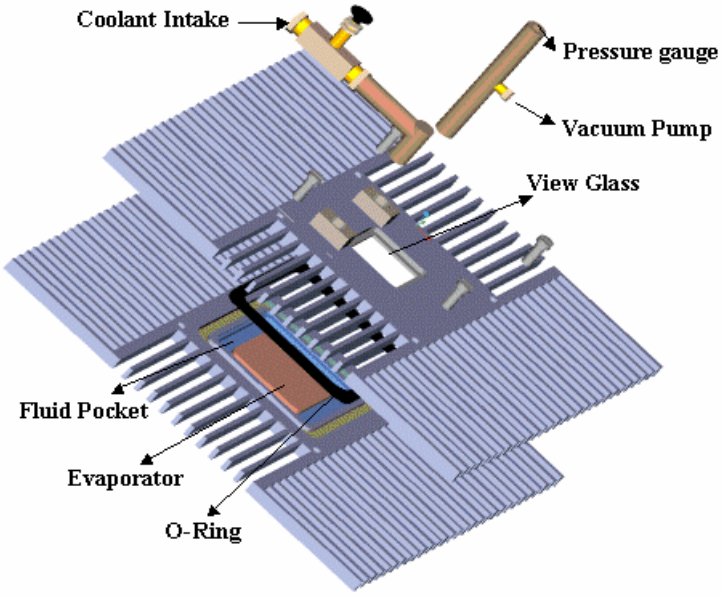

Figure 1.4 Exploded view of a two-phase spreader (Murthy (2004))

The few models existent in literature cover only the unconfined pool boiling case. Pool boiling in confined spaces can occur in many practical heat transfer devices. It is necessary to extend the range of models to the confined case.

1.2 Objectives of the current study

Boiling from enhanced structures has been the topic of many studies in recent years. Despite this effort, there areas still areas requiring further investigation. The objectives of this study are:

1) Investigate the effect of reduction in geometrical dimensions on the boiling heat transfer performance of enhanced structures under open top conditions.

There is virtually no information for enhanced structures featuring small channel width (65-105μm) and channel pitch (0.2-0.7 mm). While the small channel width and pitch allow an increase in pore density, it is unclear whether such an increase results in a commensurate increase in the overall heat removal capability of the structure.

2) Investigate the boiling thermal performance of the enhanced structures in the limiting case of insulated top confinement.

For the applications with the vertical dimension at a premium, the placement of a thin thermal management layer sandwiched between active layers is a possible cooling solution. It is useful to understand the boiling phenomena, as well as identify the boiling regimes, that might establish from the enhanced structures with insulated top, through high speed visualizations.

3) Investigate the boiling thermal performance of the enhanced structures with limited top space.

A less severe constraint occurs when there is limited space above the enhanced structure. This study aims at characterizing the boiling phenomena through identification of the regimes (modes) established for different top gaps and heat flux levels.

4) Develop a semi-analytical model applicable to pool boiling from enhanced structures under confinement.

The process of boiling under confinement from an enhanced structure can be simulated using a semi-analytical model. Such models are very useful in practical applications, serving as prediction and sizing tools in the design stage of a product development.

1.3 Literature review

Over the years, pool boiling from enhanced structures has been the topic of numerous studies. The investigations most relevant to the present work are reviewed in the sections below. First (section 1.3.1) the studies of conventional (unconfined) pool boiling from enhanced structures are presented. The flow visualization investigations are included in section 1.3.2. Section 1.3.3 reviews studies dealing with boiling under total confinement, while section 1.3.4 presents the relevant investigations of pool boiling under partial confinement. The modeling work is presented in sections 1.3.5 (for unconfined pool boiling from enhanced structures) and 1.3.6 (for the case of confined pool boiling from plain surfaces).

1.3.1 Unconfined pool boiling from enhanced structures

Despite the high heat transfer coefficients associated with nucleate boiling, attempts have been made to enhance the heat transfer process (increase the heat transfer coefficient). This has been driven by applications requiring removal of high heat rates at low superheats.

An established way of improving the heat transfer in nucleate boiling is by employing enhanced structures. Two types of such structures exist: porous coatings and re-entrant grooves. A number of investigations on porous coatings have been carried out (Thome (1990), Webb (1994), O'Connor and You (1995)). The latter category of structures, the focus of the present paper, has special surface microgeometry (small features), which promotes high performance nucleate boiling. The heat transfer coefficients achieved with these structures are much greater than those obtained with smooth surfaces. (Thome (1990), Webb (1994)).

Several researchers have investigated the boiling phenomena pertaining to re-entrant grooved enhanced structures. Nakayama et al. (1980a) developed flat boiling enhancement structures simulating the Hitachi Thermoexcel-E commercial surface (Fujie et al. (1977)). These structures consisted of interconnected internal cavities (tunnels) communicating with the external liquid pool through small openings (pores). Water, R-11 and liquid nitrogen constituted the working fluids. This type of enhanced structure proved to be highly efficient in transferring heat especially for small wall superheats (in the range 0.5-5 K). The surface structure having a pore diameter of around 0.1 mm achieved the best heat transfer performance for all fluids.

Arshad and Thome (1983) studied surfaces similar to ones of Nakayama et al. (1980a). Their structures had rectangular, triangular and circular cross-section subsurface channels connected with the liquid pool through pores of diameters 0.18 and 0.25 mm. The working fluid was water and the range of investigated heat fluxes 1- 20 W/cm^2. The structure having pores of 0.25 mm diameter showed as much as seven times improvement in performance over the smooth surface of Nakayama et al. (1980a).

Chien and Webb (1998a) employed refrigerants R-11 and R-123 for heat fluxes in the range 0.1-8 W/cm^2. By soldering a thin copper foil (50 μm) around a 19.1 mm diameter horizontal integral-fin tube they obtained a surface similar to Nakayama et al. (1980a). Round pores of 0.12 mm, 0.18 mm, 0.23 mm and 0.28 mm diameter were provided on the cover foil by piercing. The heat transfer coefficient was found to strongly depend on pore size at a given heat flux. For heat fluxes less than 3.5 W/cm^2 the optimum pore diameter was 0.23 mm. For higher heat fluxes the surface with the largest diameter pores (0.28 mm) showed the best performance.

The enhanced surfaces employed in the studies described above had discrete pores through which the structure communicates with the liquid pool. This particular configuration could not assure the high heat flux dissipation needed in electronics cooling. The critical heat flux was found to be 17 W/cm^2 in boiling FC 72 under atmospheric pressure (Nakayama et al. (1984)). This is well below heat fluxes of interest in electronics cooling, typically 40 W/cm^2 or higher. To address these issues, Nakayama et al. (1984) developed enhanced multi-layer structures especially for use in electronics cooling. By placing a five-layer stack on top of a 5 mm long cylindrical stud, a heat flux of 110 W/cm^2 (calculated using the projected surface area) was dissipated at a surface superheat of 35 K in pool boiling with FC-72 as the working fluid.

Anderson and Mudawar (1989) tested three categories of surfaces (smooth, drilled and low-profile structures) placed vertically in a stagnant pool of FC-72 maintained at atmospheric pressure. It was found that low-profile surface geometries resulted in significant enhancement of nucleate boiling. The CHF was 34.6 W/cm^2 for microfin structures and 51.1 W/cm^2 for microstud surfaces.

Mudawar and Anderson (1993) subsequently constructed and evaluated a surface with multiple levels of enhancement. Low profile microstructures were machined on the lateral surface of a single extended cylindrical stud. Additionally, microscopic surface characteristics were obtained by blasting the surface with air/water/silica slurry prior to testing. A CHF value of 105.4 W/cm^2 at a wall superheat of 90 K was obtained with saturated FC-72.

Ramaswamy et al. (2003a) employed the type of enhanced structures proposed by Nakayama et al. (1984) in a compact (50 mm x 50 mm x 40 mm) evaporator chamber of a thermosyphon loop. They investigated 0.5 mm thick silicon structures having channel widths in the range 0.090 mm-0.320 mm and channel pitches between 0.5 mm and 2.1 mm. For a constant channel pitch, the heat dissipation increased with increase in the pore size, particularly at low to intermediate wall superheats (4-12 K). The single-layered silicon structures performed similarly for a wall superheat beyond 30 K. This effect was explained in light of the "dried-up" mode of boiling in a tunnel proposed by Nakayama et al. (1982). The effect of channel pitch on heat transfer performance was found to be more significant. The heat dissipation increased significantly through reduction in pitch at all superheats.

1.3.2 Visualizations of boiling from enhanced surfaces

A few investigators performed visualizations of boiling from enhanced structures. Nakayama et al. (1980a) were the first to perform a visualization study on a porous structure. Figure 1.5 shows a representative optical micrograph from their study. Their single-tunnel, horizontally orientated apparatus permitted side observation of the internal

evaporation. Tunnel heights were varied between 0.5 and 1.0 mm, with the width held fixed at 1.0 mm. The visualization study suggested that vaporization inside the tunnel played an important role in enhancing heat transfer. The results from the study formed the basis of the semi-analytical model developed by the authors.

In continuation of Nakayama et al. (1980a) work, Arshad and Thome (1983) devised a visualization experiment aiming at explaining the enhancement mechanism established in enhanced structures. They employed a brass block having triangular, rectangular and circular cross-section grooves on its top surface. A thin copper sheet having discrete pores covered the grooves. The observation was along the axis of the groove so that the ends of tunnels were observed.

The main conclusion of their study was that the evaporation of the thin liquid film is the principal boiling mechanism for the structured surfaces. Figure 1.6 sketches the thin film formation for three groove geometries.

Chien and Webb (1998b) conducted visualizations of boiling taking place on an enhanced tubular surface having rectangular cross-section sub-surface tunnels and surface pores. The experiments were conducted in horizontal and vertical orientations using saturated and subcooled methanol at atmospheric pressure. For the vertical tube, they found that all the tunnels were vapor filled except for liquid menisci in the corners.

This also held true for the horizontal tube at high heat flux. The authors also concluded that the principal boiling mechanism for the structured surfaces is evaporation of liquid menisci in the tunnel corners.

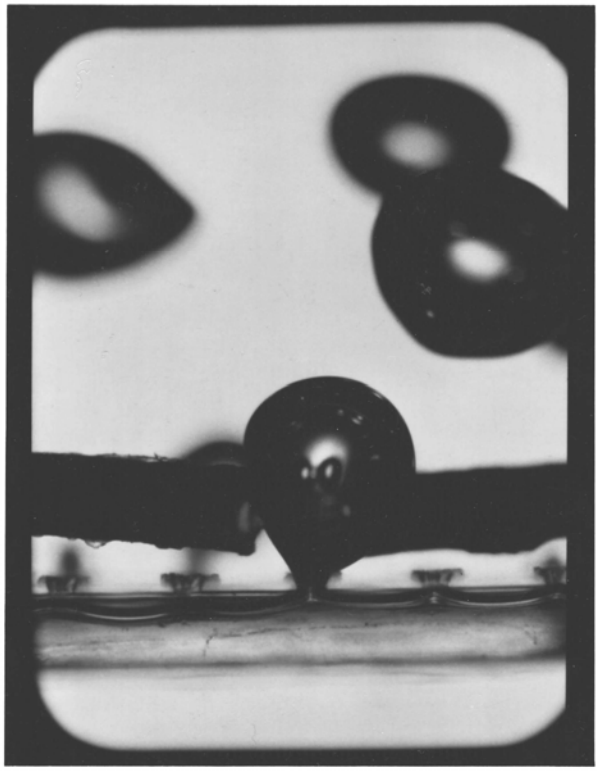

Figure 1.5 Bubble ejection in Nakayama (1980a) visualization study

Bhavnani et al. (2001) employed high-speed photography to record parameters (such as bubble size, bubble departure frequency, bubble interactions and active site density) during pool boiling of FC-72 from an enhanced surface. The surface consisted of an array of discrete re-entrant cavities etched into a silicon wafer. The cavities, having a characteristic dimension of approximately 40 μm, were arranged in a square cluster 12.7 mm on each side. It was concluded that the contribution of latent heat as a heat dissipation mechanism is only minor (less than 16 %).

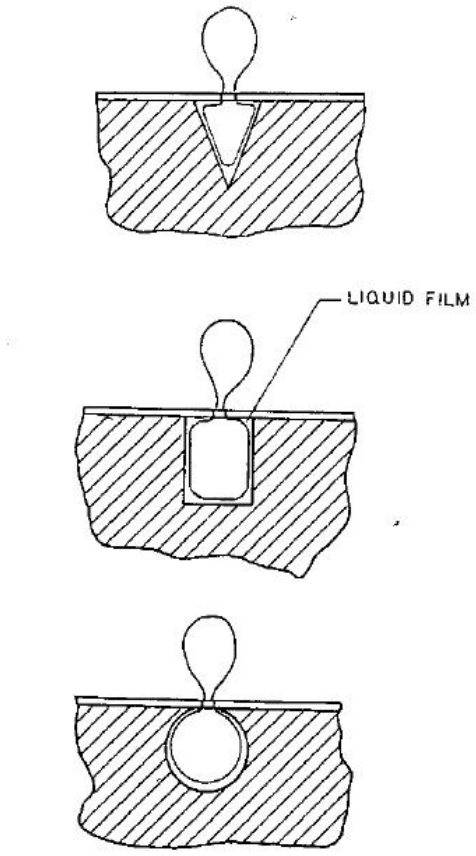

Figure 1.6 Shape of liquid film for three geometries (Arshad and Thome (1983))

Ramaswamy et al. (2002) performed a visualization study of boiling from enhanced structures similar to the ones used in this study in the wall superheat range 4-30 ^{o}C. The enhanced structures, manufactured of silicon, were 0.5 mm thick. It was found that the boiling regimes established for the enhanced structures are similar to that for plain surfaces. For 4-12 ^{o}C superheat, the boiling was in the isolated bubble regime. As the wall superheat increases, coalescence occurs, resulting in formation of vapor mushrooms above the boiling surface.

1.3.3 Pool boiling from enhanced structures under total top confinement

The experimental studies mentioned in Section 1.3.1 treated pool boiling under unconfined conditions. However, for future applications, the space available for thermal management hardware is limited. It is therefore desirable to asses the thermal performance of the enhanced structure under confinement. Nakayama et al. (1989) were the first to study boiling from enhanced structures in a fully confined configuration. They sandwiched an enhanced structure between two chip heaters in vertical position. The single layer enhanced structure served to model one subsurface layer of a stacked porous stud. The boiling curve obtained with the structure produced the heat transfer coefficient applied to the open surface of the stud. The mechanism of boiling from fully confined enhanced structures was not revealed since no visualizations were performed. Ghiu et al. (2001) performed a visualization study of pool boiling from transparent quartz structures of the present form. The channel widths studied were 0.090 mm and 0.285 mm. The top of the structures was covered with a quartz plate having the same overall dimensions (10 mm × 10 mm × 1 mm). Three boiling regimes were identified: *slug formation* (in either top or bottom channels), *slug migration* between the top and bottom channels and *slug predominance* (most of channels vapor filled). Their study did not contain data for structures made of higher thermal conductivity materials (copper, silicon).

1.3.4 Pool boiling under partial top confinement

Nucleate pool boiling from plain surfaces in narrow spaces constituted the subject of several experimental investigations, starting with the pioneering work of Katto and Yokoya (1966) and Katto et al. (1977). They investigated the pool boiling of water in the

narrow space created between two parallel, horizontal discs of 10 mm in diameter brought in close proximity. For low to intermediate heat fluxes, the top confinement has a surprisingly beneficial effect, enhancing the heat transfer. The reason for the enhancement is believed to be the formation and subsequent evaporation of a thin liquid film beneath the squeezed bubbles. On the other hand, the performance decreases in the high heat flux regime. The magnitude of the critical heat flux is also diminished with increased confinement. Ishibashi and Nishikawa (1969) studied the boiling in an annular vertical narrow space between two concentric cylinders, one heated and one not. Two flow regimes (isolated bubbles and coalesced bubbles) were identified. A correlating expression was also proposed. Yao and Chang (1983) developed a boiling map having the Bond number and a specially defined boiling number as coordinates. Several boiling regimes (termed isolated deformed bubbles, slightly deformed bubbles and coalesced deformed bubbles) were identified based on visual observations. Fujita et al. (1988) performed systematic experiments on heat transfer characteristics of pool boiling in a confined space formed between a rectangular heating surface and an opposed unheated plate. The heat transfer coefficients were found to increase with decrease of gap size at moderate heat fluxes. Bonjour and Lallemand (1998) identified three regimes (nucleate boiling with isolated deformed bubbles, nucleate boiling with coalesced bubbles and

The vast majority of studies dealing with boiling from enhanced surfaces were performed in an unconfined space. Very few authors investigated boiling from enhanced surfaces under spatial constraints. Nowell et al. (1995) studied the influence of a confining plate on boiling FC-72 from a microconfigured heat sink. The heat sink was manufactured by etching discrete re-entrant cavities in a silicon wafer. Five different gap

sizes were tested (unconfined, S = 1 mm, S = 2 mm, S = 4 mm, S = 6 mm). The thermal performance decreased significantly for S = 1 mm, whereas all the other gap sizes tested yielded approximately the same results as the unconfined case, within experimental uncertainty. Ramaswamy et al. (1999) found that the top and side spacing have only a marginal effect on the boiling performance of a stack of 6 layers of structures of present form (Figure 2.1). A possible explanation for no marked difference between the various gap sizes is the three-dimensional morphology of the structure under consideration. Each layer contributes to the total heat flux so that constricting the top alone does not affect the thermal performance in a significant way. Chien and Chen (2001) were apparently the only authors to study the effect of confinement from a single layered enhanced structure. They tested a structure having cross-grooves in a special dielectric liquid (HFC 4310) at 75.5 ^{o}C. The effective surface opening diameter and the total opening area were the most influential parameters for the boiling performance. A slight enhancement of heat transfer for confined case versus the unconfined case was noticed at low heat fluxes. In summary, no significant heat transfer enhancement resulting from top confinement could be recorded, for the range of heat fluxes tested.

The previously mentioned studies employing enhanced structures under constraint did not include visualizations of the boiling phenomena. Therefore, the specific heat transfer mechanisms were hypothesized based on the limited information offered by the boiling curves.

1.3.5 Mathematical models for pool boiling from enhanced structures

A multitude of models have been proposed for nucleate pool boiling from plain surfaces. Despite the widespread use of enhanced structures and their proved efficiency, the understanding of their functioning mechanisms lacks. Only a few modeling attempts targeted the enhanced structures.

1.3.5.1 Nakayama's dynamic model

The first dynamic model developed for a structured surface was proposed by Nakayama et al. (1980b). Their model is applicable to a specific type of structure attempting to model the Hitachi Thermoexcel surface. The model was developed for tube application; therefore there is no communication between the tunnels and the liquid pool other then the pores. The authors recognized the cyclic nature of the boiling process and divided the bubble process into three phases. Figure 1.7 presents the envisioned boiling mechanism. The authors divided the events into three phases:

a) Phase I (pressure build-up): During this stage the pressure inside the tunnel increases due to internal evaporation. The end of this phase is reached when the menisci at the pores become hemispherical.

b) Phase II (pressure reduction): The vapor will flow into bubbles at some pores. As a result, the tunnel internal pressure will decrease, preventing the growth of menisci at inactive pores.

c) Phase III (liquid intake): For a short interval, the pressure in the tunnel decreases below the pool pressure; it is then when the liquid enters the tunnel through the

inactive pores. This phase ends with the bubble departure and closing of the pores by the menisci.

Based on the envisioned physical mechanism, mathematical expressions were developed for each phase. A prediction procedure, which requires use of eight empirical constants, is also proposed. In a subsequent paper, Nakayama et al. (1982) identified three possible boiling modes (regimes) that might exist in a subsurface tunnel. Figure 1.8 illustrates the proposed boiling regimes. The investigators recommended that any attempt of modeling boiling phenomena from an enhanced structure should begin with the identification of the boiling regime taking place in the subsurface channels. In retrospective, their initial model was tailored for the suction - evaporation mode of heat transfer.

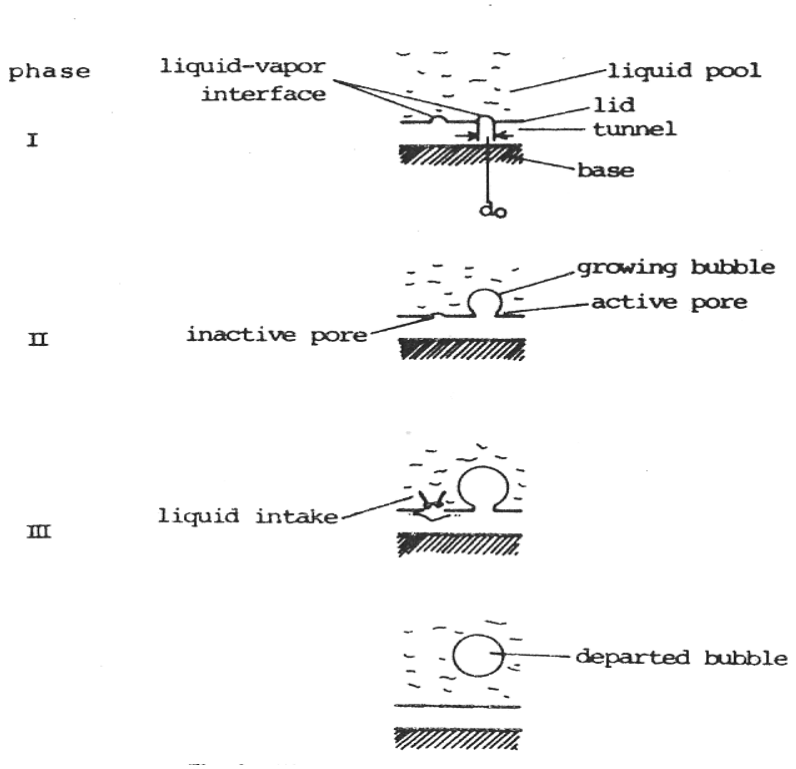

Figure 1.7 Physical model for the dynamic model (Nakayama et al. (1980b))

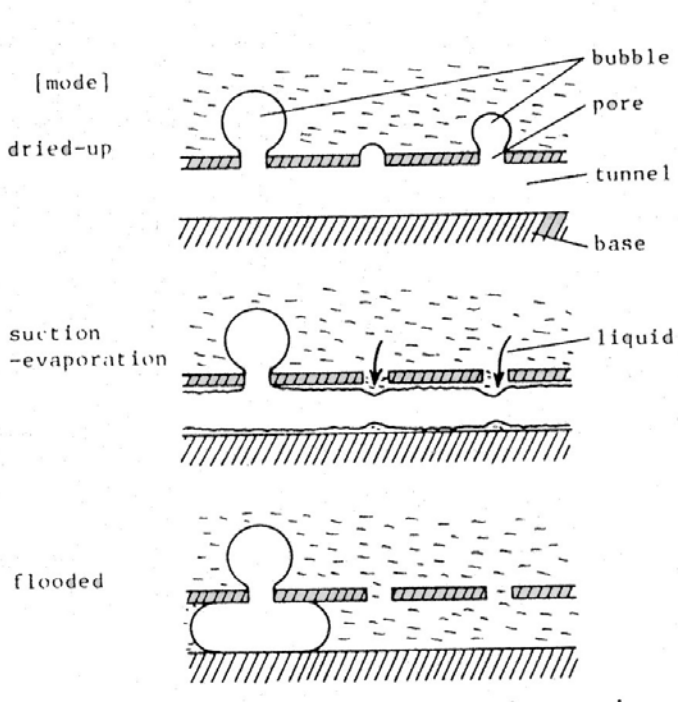

Figure 1.8 Possible modes of boiling in a subsurface tunnel (Nakayama et al. (1982))

1.3.5.2 Webb and Haider model

Webb and Haider (1992) proposed a model for the flooded mode of boiling. The basic assumption in their model was that portions of liquid and vapor existed in the subsurface channels. Figure 1.9 summarizes the envisioned boiling cycle.

The model was developed for a geometry consisting in subsurface channels with a circular cross-section having a continuous opening at the top. The evaporation was assumed to take place from menisci formed at the liquid –vapor interface. For the external convection component of the heat flux the authors used a new model taking into consideration the micro-convection.

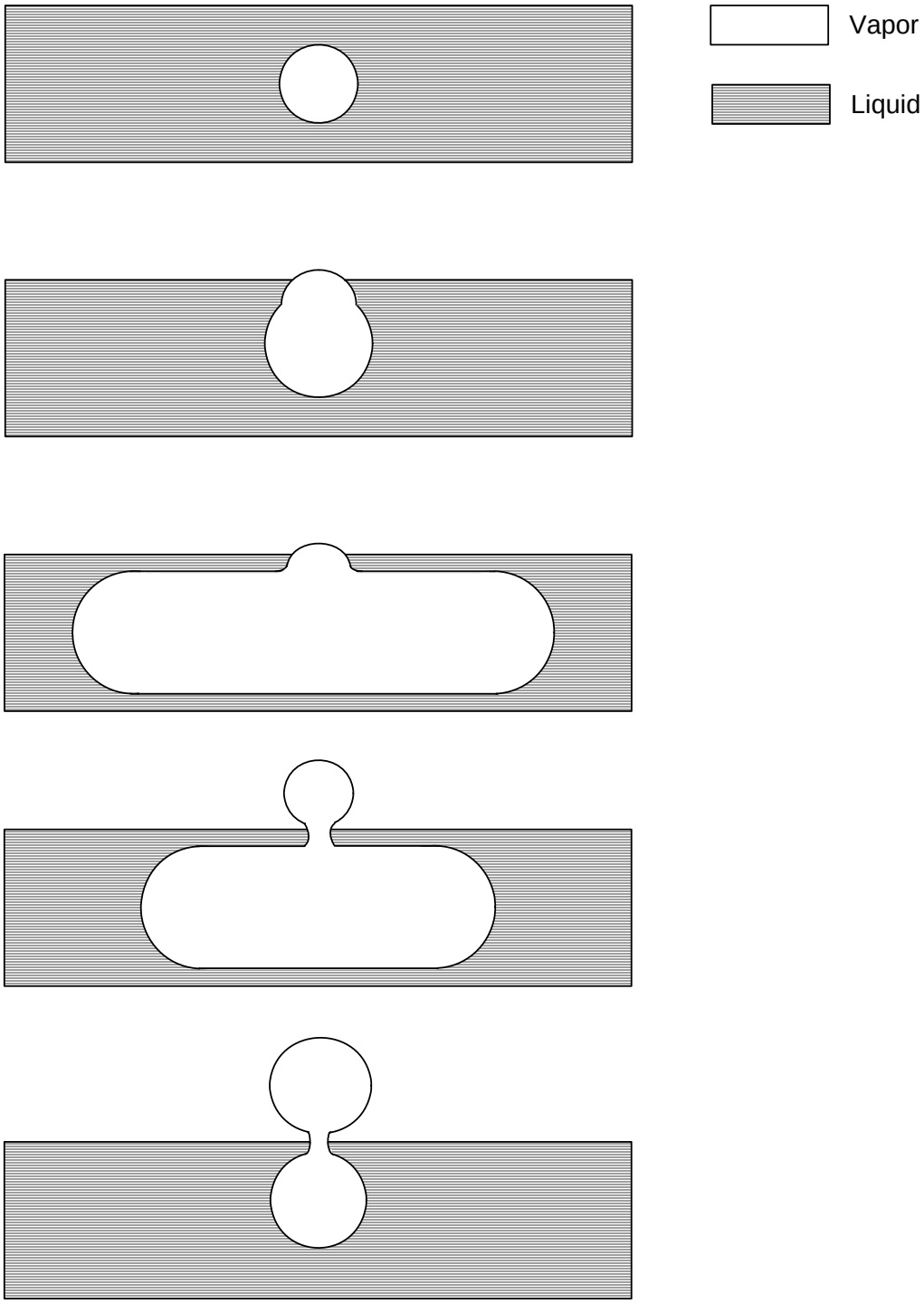

Figure 1.9 Webb and Haider (1992) bubble cycle for the flooded mode

1.3.5.3 Chien and Webb model

Chien and Webb (1998c) improved upon Nakayama et al. (1980b) dynamic model. As a novel feature, the temporal variation of the evaporation process of the liquid inside the channels was taken into account. The liquid evaporation and bubble growth cycle is depicted in Figure 1.10. The initial meniscus radius was assumed uniform along the length of the tunnel. To compute the external heat flux, the Haider and Webb (1997) formulation was utilized.

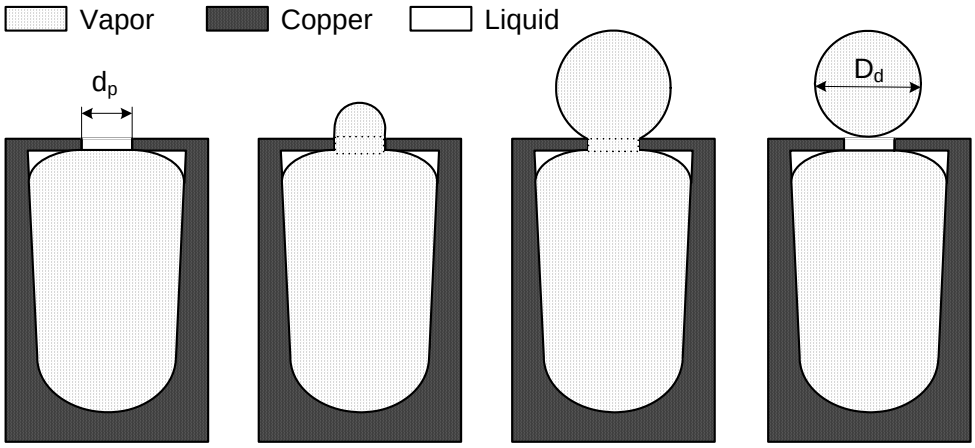

Figure 1.10 Evaporation and bubble growth process in a subsurface tunnel (Chien and Webb (1998c))

1.3.5.4 Xin and Chao model

Xin and Chao (1987) used a different approach in their modeling effort. It was hypothesized that, under developed nucleate boiling conditions, the cycle of the vapor-liquid flow is so short that it may be approximated as a countercurrent two phase flow (vapor flows continuously out of the channel and liquid continuously enters the channel).

The authors developed their model for a planar Gewa-T surface (see Figure 1.11) and extended it to Thermoexcel-E surfaces.

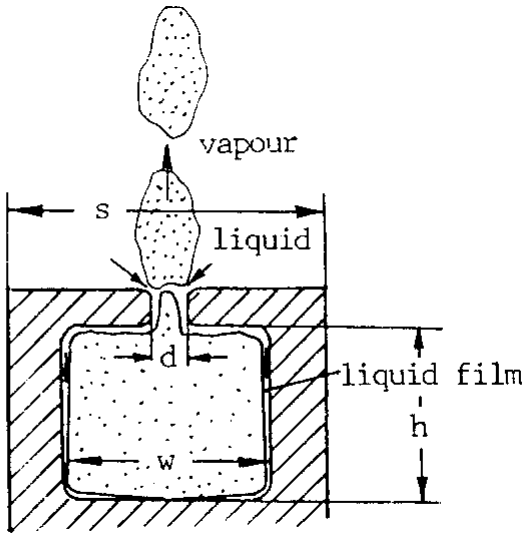

Figure 1.11 Geometry used in Xin and Chao (1987) model

Ayub and Bergles (1987) adapted Nakayama et al. (1980b) model for the GEWA-T surface. Their model is simpler in formulation and relies completely on a heat balance. The event of a bubble formation is presented in Figure 1.12. The model does not have predictive capabilities since the empirical constants used need to be obtained from experiments.

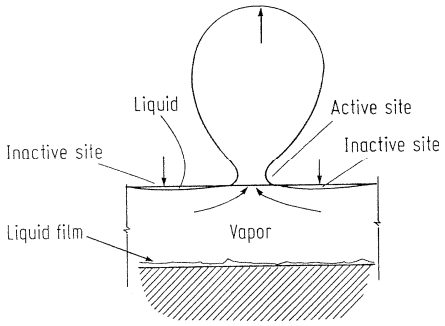

Figure 1.12 Bubble formation in Ayub and Bergles (1987) model

1.3.5.5 Ramaswamy et al. model

Ramaswamy et al. (2003b) developed a semi-empirical model for the suction-evaporation mode of boiling proposed by Nakayama et al. (1982). The type of structure employed was similar to the one used in the present study. The authors adapted Chien and Webb's model to the new, more complex, geometry. The novelty of this model consisted in the improvements on sub-models for bubble departure diameter, internal evaporation and convective heat transfer from the envelope surfaces of the enhanced structure.

The model was used to predict the total heat flux dissipated from the enhanced structure. The bubble departure diameter is predicted within ± 10%, frequency within ± 30% for the vast majority of data points, nucleation site density within ± 40% and the heat flux within ± 50%. The model proves useful in optimization of geometrical parameters for maximizing heat transfer. The heat transfer can be maximized using a structure with numerous pores having small pore diameter. However, this will result in a structurally weak structure. It was concluded that the process of designing an optimum structure must include factors other than heat transfer.

1.3.6 Mathematical models for confined pool boiling from plain surfaces

Despite the recognized practical importance of confined boiling from enhanced structures and their proved efficiency, the understanding of the effect of a confined space on heat transfer is limited. Very few investigators attempted modeling confined pool boiling from plain surfaces. To date, there is no model for confined boiling from enhanced structures.

1.3.6.1 Katto and Yokoya model

Katto and Yokoya (1966) developed a model for boiling from horizontally oriented plain surfaces under top confinement. Their boiling surface was a disk of 10 mm in diameter facing upward. A horizontal disc of the same diameter held above the boiling surface at various top gaps constituted the confining factor. The model assumes that the main heat transfer mechanism is vaporization of a thin liquid film formed on the heating surface by a laterally spreading vapor bubble. Assuming an initial distribution of the liquid film thickness, the mass of liquid vaporized in a certain time interval is calculated. The mean heat flux is then obtained dividing the latent heat by the surface area and time interval. The predicted heat flux is 57 % higher than the measured one for a value of heat flux $q'' = 18.6\ W/cm^2$. The authors concluded that thin film evaporation contributes about 67 % to the total heat transfer, the remaining 33 % being performed through other mechanisms.

1.3.6.2 Fujita et al. model

Fujita et al. (1988) proposed a method for predicting the heat flux in confined boiling heat transfer. The authors conducted experiments with boiling water in a confined space from a plain rectangular surface oriented vertically. Their model accounted for both sensible and latent heat transport and included the top gap as a parameter. It is assumed that the heating surface is alternately in contact with the liquid slug (for a time interval Δt_l) and a vapor bubble (for a time interval Δt_v). Periods Δt_l and Δt_v were measured 0.5 mm above the heating surface at three vertical locations. For a top gap S = 2 mm, the agreement between prediction and experiment was good. The prediction was higher than

the measurement for S =0.6 mm indicating the drying of the heating surface at some locations.

1.4 Outline of thesis

The tendency to move away from two-dimensional chip architectures to three-dimensional configurations presents new issues to the thermal community. A cooling scheme utilizing little space on vertical direction would be extremely useful for future electronic products, where the available space is at a premium. However, the confinement alters the conventional boiling in a manner that needs to be understood. This study aims at addressing some of the issues associated with enhanced boiling heat transfer under confinement.

Chapter 2 describes details of the enhanced structures fabrication, experimental set-up, experimental procedures as well as uncertainty estimates for the measurements performed.

Chapter 3 investigates the effect of reduction in the geometrical dimensions on the boiling heat transfer performance. Predictive correlations for the nucleate boiling regime are proposed for the proper design and employment of the enhanced structures.

Chapter 4 examines the thermal performance of the enhanced structures in the limiting case of insulated top confinement. Also, the effect of channel width W_t on the thermal performance is clarified.

Chapter 5 presents the influence of partial top confinement on boiling heat transfer from enhanced structures. The boiling is characterized by identifying the regimes (modes) established for different top gaps and heat flux levels. The gap between the

enhanced structure and the confinement plate constitutes the main geometrical parameter varied in several steps.

Chapter 6 describes a semi-analytical model intended to simulate the boiling under confinement. It also includes comparisons between predictions of the model and experimental results.

Chapter 7 summarizes the entire study, presents a few possible applications of confined boiling from enhanced structures and provides recommendations for future work.

1.5 Summary

This chapter introduces the topic addressed in this study. It presents the motivation for performing this investigation and lists the objectives to be reached at the completion of the study. A detailed literature review section is also included in this chapter. Finally, the order and brief content of the subsequent chapters is presented.

CHAPTER 2: EXPERIMENTAL SETUP AND PROCEDURES

The experiments conducted in this study consisted of temperature and voltage measurements as well as flow visualizations to elucidate the influence of confinement and geometric parameters on the boiling from enhanced structures. The single-layered structures were included in a thermosyphon loop to simulate the employment of the structures in a real electronics cooling environment. The experiments were divided into two main categories: unconfined pool boiling and pool boiling under confinement. Details of the enhanced structures fabrication, experimental set-up, data acquisition procedures as well as uncertainty estimates for the measurements performed are presented in the following sections.

2.1 Enhanced structures

The Hitachi Thermoexcel surface (Fujie et al. (1977)) has been developed and proved successful in enhancing nucleate boiling heat transfer at low heat fluxes. In order to ensure a similar good performance at the high heat fluxes encountered in electronic applications, the original Hitachi design was modified by providing rectangular fins on the top external surface by Nakayama et al. (1984). The present study utilizes the same structure geometry, but with significantly smaller feature sizes than previously studied.

A schematic diagram and optical micrographs of representative enhanced structures are presented in Figure 2.1. The single layer structures were fabricated in copper and quartz. Their geometrical parameters are summarized in Tables 2.1 and 2.2. The structure identification code employed indicates the constitutive material (copper or

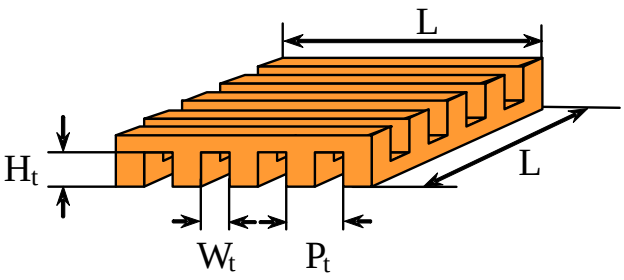

(a)

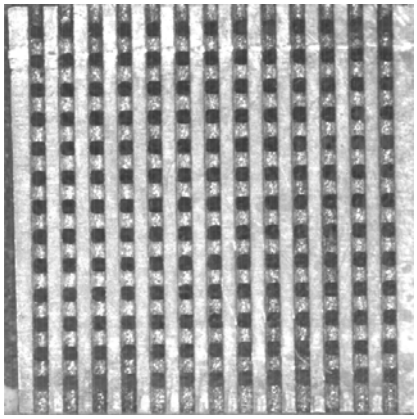

(b)

(c)

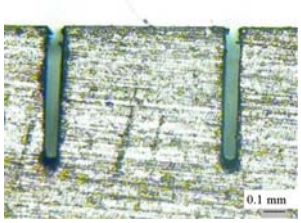

(d)

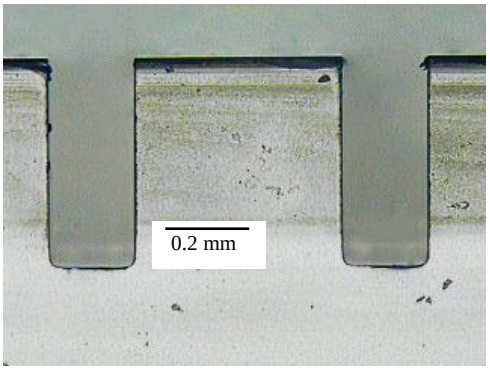

(e)

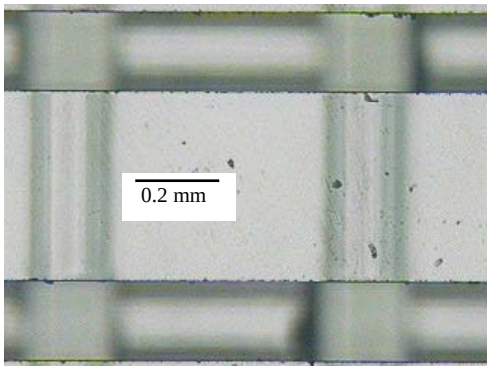

(f)

Figure 2.1 Enhanced structures used in the present study (a) sketch of the enhanced structure (b) pore formation at the intersection of microchannels. Top view of structure C-0.360-0.7 is shown (c) top view of structure C-0.105-0.7 (d) magnified (50 X) picture of the structure C-0.065-0.7, lateral view (e) magnified (50 X) picture of the structure Q-0.200-0.7, lateral view (f) magnified (50 X) picture of the structure Q-0.200-0.7, top view

Table 2.1 Copper structures employed in the present study

Structure identification	Structure length L (mm)	Channel width W_t (mm)	Channel pitch P_t (mm)	Channel depth H_t (mm)	Increase in wetted area (A_w/A)
C-0.065-0.20	10	0.065	0.20	0.6	8.05
C-0.065-0.35	10	0.065	0.35	0.6	5.21
C-0.065-0.50	10	0.065	0.50	0.6	4.08
C-0.065-0.70	10	0.065	0.70	0.6	3.26
C-0.085-0.70	10	0.085	0.70	0.6	3.26
C-0.105-0.35	10	0.105	0.35	0.6	5.12
C-0.105-0.50	10	0.105	0.50	0.6	4.06
C-0.105-0.70	10	0.105	0.70	0.6	3.26
C-0.360-0.70	10	0.360	0.70	0.6	3.12
C-0.470-0.70	10	0.470	0.70	0.6	2.97
C-5-0.105-0.70	5	0.105	0.70	0.6	2.97
C-5-0.365-0.70	5	0.365	0.70	0.6	2.97
C-15-0.365-0.70	15	0.365	0.70	0.6	2.97

C-copper

Table 2.2 Quartz structures employed in the present study

Structure identification	Structure thickness (mm)	Structure length L (mm)	Channel width W_t (mm)	Channel pitch P_t (mm)	Channel depth H_t (mm)
Q-0.065-0.70	1	10	0.065	0.70	0.6
Q-0.085-0.70	1	10	0.085	0.70	0.6
Q-0.105-0.70	1	10	0.105	0.70	0.6
Q-0.105-0.35	1	10	0.105	0.35	0.6
Q-0.200-0.70	1	10	0.200	0.70	0.6
Q-0.200-0.70	0.5	10	0.200	0.70	0.3
Q-0.250-0.70	1	10	0.250	0.70	0.6

Q-quartz

quartz) followed by the channel width and channel pitch. When utilized, the additional number indicates the overall structure width. Two manufacturing procedures were employed for making the enhanced structures: wafer dicing and wire-EDM. An automated dicing saw was at the center of the manufacturing process. While the quartz structures were easy to manufacture, the fabrication of copper ones posed some challenges. The structures with small channel widths (C-0.065-0.7, C-0.085-0.7 and C-

0.105-0.7) were produced by employing an automated wafer dicing saw. The cutting element consisted of nickel blades (having diamond particles embedded at the periphery) rotating at 30,000 rpm. A row of parallel microchannels was cut on the bottom surface. The top surface also had parallel microchannels aligned 90^o to those on the bottom surface (Figure 2.1(a)). Since the depth of the microchannels (0.6 mm) was more than half the thickness of the structure, an array of pores resulted at the intersections. (Figure 2.1(b)). Wire electro-discharge machining was used to fabricate the structures with large channel width (C-0.360-0.7 and C-0.470-0.7).

The external surfaces of the structure were mirror-polished with fine sand paper. The roughness of the top surface was 0.15μm (root-mean square (rms)) as measured with a profilometer. The roughness of the internal surfaces (produced by the blades in the cutting process) could not be determined exactly. Visual observation indicates that these surfaces are fairly smooth.

2.2 Experimental set-up

The single-layered structures were included in a thermosyphon loop consisting of a boiling chamber, connecting tubes and a condenser (Figure 2.2). The condenser is placed at a higher elevation than the boiling chamber to allow liquid return by gravity. The boiling chamber was made of 12.54 mm thick Plexiglas and had inner dimensions of 40 mm × 40 mm × 30 mm. Four auxiliary foil heaters were placed on the lateral walls inside of the chamber to maintain the liquid pool at saturation temperature. A dielectric, inert liquid (PF 5060) was used as the working fluid. Its thermophysical properties closely match FC 72 and are included in Appendix C.

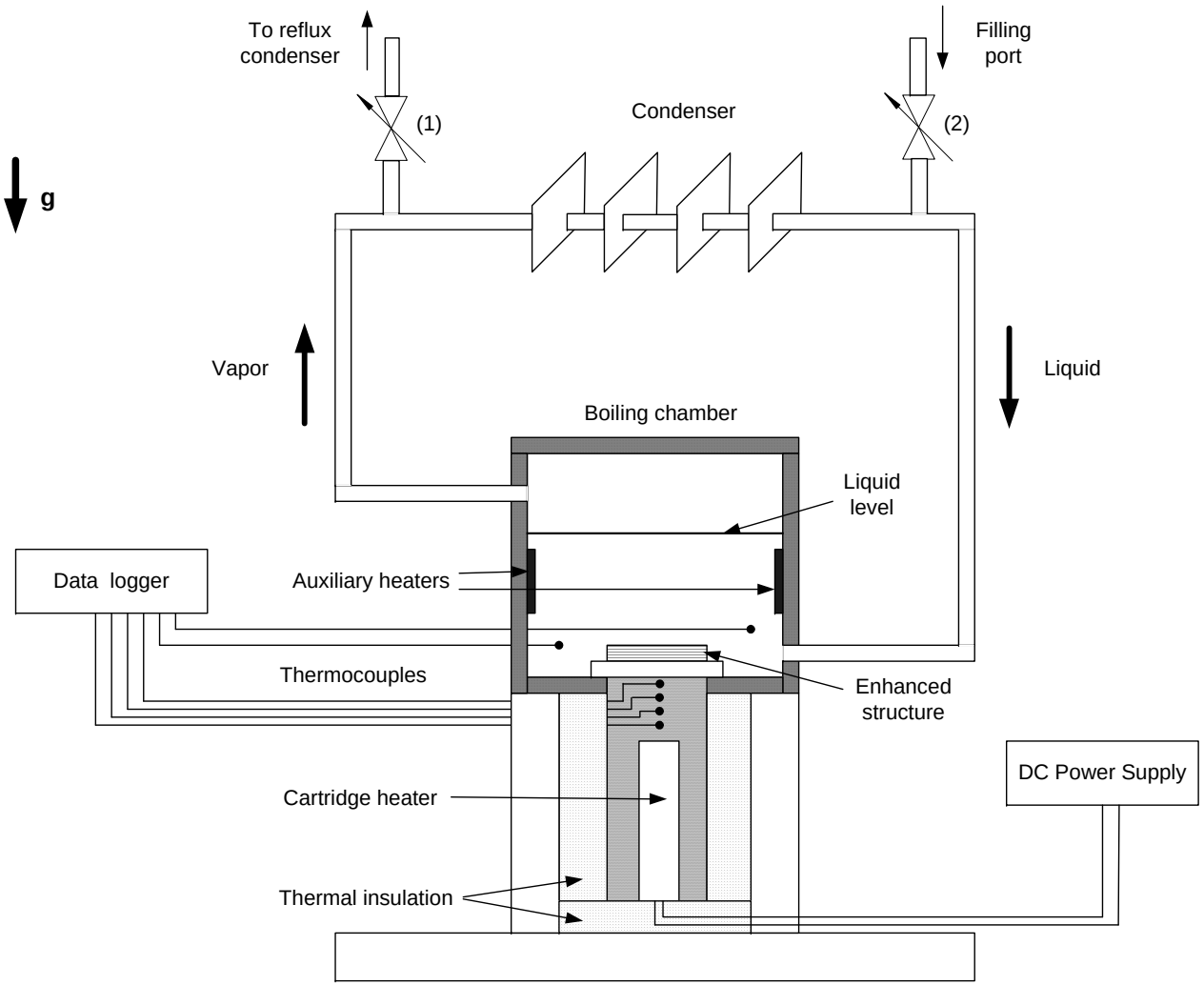

Figure 2.2 Thermosyphon loop

In an actual implementation, a thermosyphon loop will be hermetically sealed with the system operating pressure set by the level of heat input (for constant cooling conditions at the condenser). Ramaswamy et al. (1998) found that the performance of a thermosyphon similar to the one employed in the present study does not depend on the internal pressure that once the saturated boiling regime is reached ($q'' > 9$ W/cm^2). Therefore, by maintaining the system open to atmosphere a close simulation of the real case was reached, along with experimental convenience.

A plate fin condenser (11 fins) was utilized to close the loop. A reflux condenser was placed at a higher elevation in order to trap any escaping vapor. The structures were attached to the heating surface using 63Sn 37Pb solder alloy. The thickness of the solder layer was ~50μm. The thin solder layer provided a strong mechanical bond with a low thermal contact resistance. An Omega cartridge heater embedded in a copper rod with square cross section (9 mm x 9 mm) was used to provide heat to the structure. For the structure size effect study, two additional heater assemblies were used: one with the cross section 4.5 mm × 4.5 mm (for structure width L = 5 mm) and the other with the cross section 14 mm × 14 mm (for structure width L = 15 mm). Figure 2.3 (a) illustrates an enhanced structure with a confining plate; the top surface of the copper heater is shown in Figure 2.3 (b). The black rectangles represent the portions of the heater top surface in contact with the fluid, while the white regions represent the portions covered by the structure.

To firmly fit the heater into the rod, a high temperature, high thermal conductivity paste (Omegatherm® '201', k_{eff} = 2.31 W/m K) was employed. In order to minimize the heat losses, the copper rod was peripherally surrounded with a glass sheath. Thermal

insulation and plexiglass provided additional insulation. At the end of the rod four copper-constantan sheathed thermocouples (0.128 mm wire diameter) were embedded, starting from 4 mm below the enhanced structure.

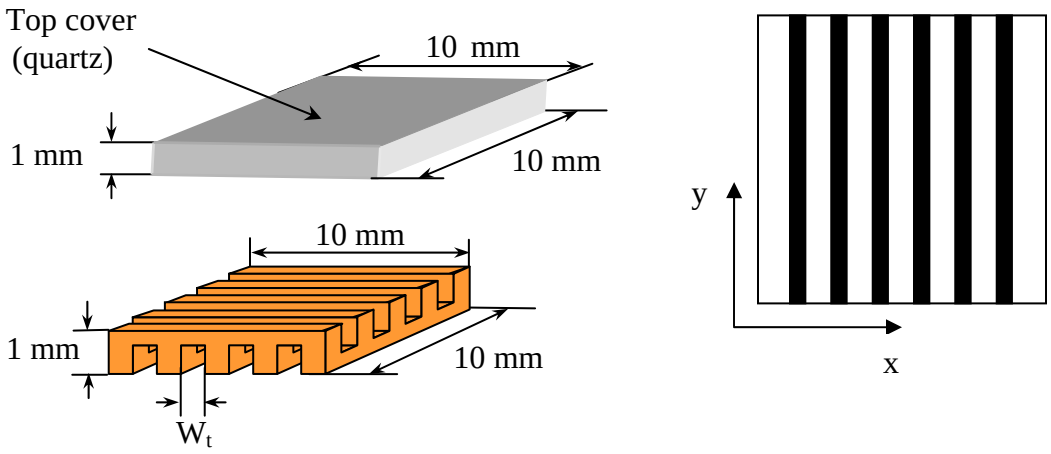

Figure 2.3 Enhanced structure shown with the confining plate
(a) sketch illustrating microchannels on the top and bottom faces
(b) sketch of the top surface of the heater

Figure 2.4 shows details of the cartridge heater assembly, which was utilized for heating and surface temperature measurement. The thermocouples were used to calculate the surface temperature (by extrapolation) and the heat flux at the base of the enhanced structure, assuming one-dimensional heat conduction. The temperature of the liquid pool was monitored using two copper-constantan thermocouples (0.128 mm wire diameter). All temperatures were measured using an automated data acquisition system.

A regulated direct current power supply (0-100 V, 0-0.5 A) was used to provide power to the cartridge heater. The auxiliary heaters were supplied with power from a

separated power supply. A precision resistor (1 Ω ± 0.01 Ω) connected in series with the power supply served to measure the current. The voltage drops across the heater and the precision resistor were also measured.

This base test vehicle was changed to perform boiling under confinement experiments. For the variable space top, a quartz tube mounted vertically on top of the structure permitted the variation of the top spacing S (Figure 2.5). The tube had a square cross-section. A square quartz plate with the same dimensions as the enhanced structure (10 mm × 10 mm × 1 mm) was attached at one end of the tube and served as the confining surface/visualization port.

A Phantom high-speed CCD camera was used to perform the flow visualizations. For stability and alignment purposes, a tripod equipped with a multi-axis bubble level supported the camera. The camera can capture a maximum of 1,000 frames per second at full resolution (512 × 512 pixels). With a reduction in the field of view, higher frame rates can be achieved. A range of frame rates (minimum 100 fr/s, maximum 2100 fr/s) was employed. A zoom lens (Navitar 12 X Zoom) attached to the camera through an adapter (Navitar 0.67 X) was used to magnify the area of interest and work at close distances to the enhanced structure. The lens is capable of a variable magnification of 1 – 12 times the original size of the object. A 150 W Moritex fiber optic light source was used for providing light to the structure. Movies and still pictures were acquired from the top and sides of the structures. After capture, the movies were played back at slower speed. From the movies selected frames (single pictures) were extracted.

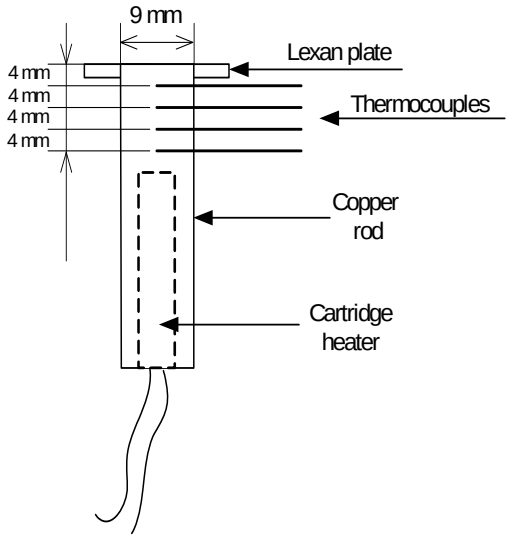

Figure 2.4 Heater assembly

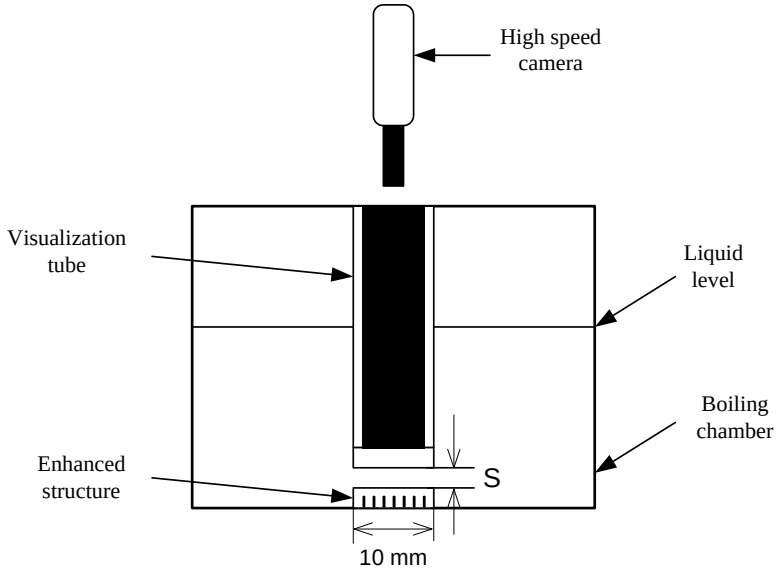

Figure 2.5 Boiling chamber equipped with the visualization tube

2.3 Experimental Procedure

The working fluid was maintained at saturation (~ 56^{o}C at 1 atm) throughout the experiments. For heat inputs q > 5 W through the copper rod saturated conditions existed. For lower heat inputs the auxiliary heaters were employed in conjunction with the main heater to maintain saturation conditions during the experimental run. The liquid level in the boiling chamber was maintained at 20 mm above the top surface of the structure under un-powered conditions. The system pressure was set at 1 atm in all the experiments by keeping the valve (1) open and valve (2) closed (see Figure 2.2). One of the characteristics of PF 5060 is its high affinity for common atmospheric gases. Therefore, a degassing operation preceded every experimental run. For degassing, the system was kept at atmospheric pressure, while an electrical power input of ~11 W was applied via the cartridge heater. The dissolved gas content (by volume) was measured with a Seaton-Wilson AD-4000 Aire-ometer (Figure 2.6). The Aire-Ometer operates based on Henry's Law which states that the amount of gas dissolved in a fluid id directly proportional to the absolute pressure on the fluid. The air content before charging the system (from the bottle) was 50 %, decreasing to 40 % after one hour of vigorous boiling and going up to 46 % after cooling down (at the beginning of the run).The liquid was boiled vigorously for about one hour, and then allowed to cool down until it reached room temperature. This procedure ensured that the dissolved gas concentration was around 46 % (by volume) at the beginning of every run. Bhavnani et al. (2001) found that the dissolved gas content did not decrease below a certain level (39 % in their case) even after several days of degassing.

The electrical power to the cartridge heater was provided in incremented or decremented steps. The power steps were 0.5 W until 2 W, 2 W until 10 W and 5 W until the highest heat flux tested. The experiments were performed for power inputs resulting in a maximum temperature at the base of the enhanced structure of 85^{o}C.

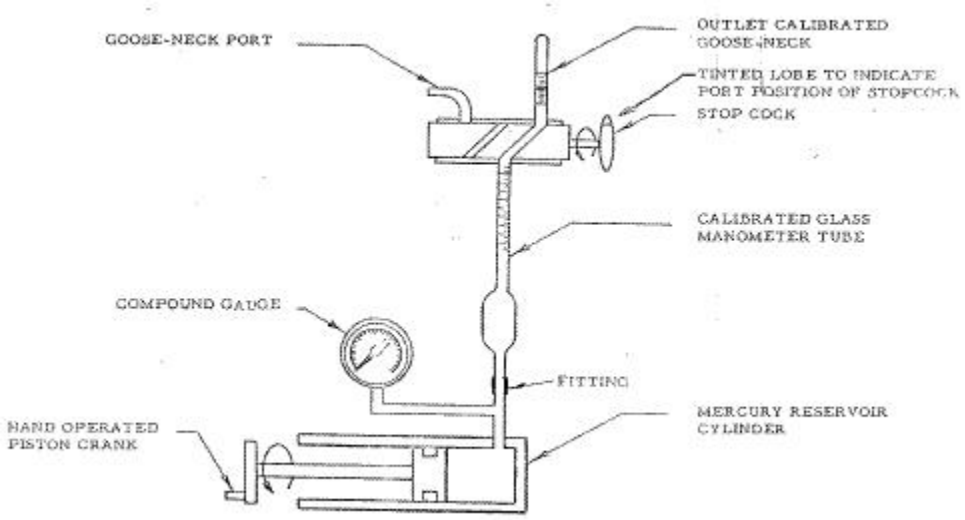

Figure 2.6 Aire-meter used for air concentration measurements

It should be noted that the highest heat fluxes reported in the present study do not represent critical heat flux values, but maximum values for which the wall temperature stays below 85^{o}C. This has been done in light of the possible application of this study to electronics cooling. For these applications the maximum junction temperature is typically limited to 85^{o}C. In experiments performed with decreasing heat flux, the first heat flux level was established by trial and error. Initially, the highest power input that resulted in a steady wall temperature was imposed. The surface temperature was above 85^{o}C at this condition. The corresponding heat fluxes were 5-10% higher than the highest values

presented in this study. It is believed that the critical heat flux will be reached in this region, as also reported by Anderson and Mudawar (1989) and Mudawar and Anderson (1993).

The six temperatures were monitored continuously, with readings taken after steady state was reached. After reaching steady state, temperatures were recorded for 35 minutes and mean values were calculated. These values were subsequently used to calculate the surface temperature and the heat input. The electrical power input was calculated by multiplying the voltage drop across the heater with the line current. The heat loss (defined as the difference between the electrical power input and the heat input) was always within 10 %. The heat flux was calculated based on the surface projected area (10 mm × 10 mm). The experiments were performed for power inputs resulting in a maximum temperature at the base of the enhanced structure of 85^{o}C.

Usually, after an experimental run, the structure was kept immersed under a non-boiling condition overnight. Under these conditions, the performance degraded in time due, perhaps, to variation in surface finish. The decrease in the performance was more pronounced at low heat fluxes.

2.4. Uncertainty Estimates

The thermocouples and the data acquisition system were calibrated against a precision mercury thermometer at ice point to an uncertainty of 0.1 K. The precision resistor employed for current measurement was accurate to 1 %. The voltage measurement uncertainty was specified by the instrument manufacturer as being 0.045 % of the reading. The uncertainty in the channel width (5 μm) was due to the uneven width

across the depth of the channel. The uncertainty in the top spacing measurement S was estimated at 25 μm. The Kline and McClintock (1953) technique was used to estimate the uncertainty for the derived quantities.

The resulting maximum uncertainty in the heat flux was ± 15 % (with over 90 % of the data within ±10 %). The maximum uncertainty in the wall superheat values was ± 0.25 K. Details of the uncertainty estimates are included in Appendix A.

Repeatability runs have been conducted on different days to verify the reliability of the experimental data. Measurements were taken with increasing and decreasing heat flux. At the same (imposed) heat flux the day-to-day variations of the temperature measured below the surface (T_1) were within + 1^oC.

2.5 Summary

This chapter presents the experimental set-up and procedures used for the current study. The components of the basic set-up (for unconfined boiling) are described and the alterations introduced for the purpose of studying confined boiling shown. The chapter contains a section about the tools employed for flow visualizations. Also, the procedure employed for carrying out heat transfer and flow visualization experiments is detailed. The uncertainty associated with measured and derived quantities has been evaluated and included in this chapter.

CHAPTER 3: BOILING PERFORMACE OF SINGLE-LAYERED ENHANCED STRUCTURES

The reduction in electronic chip sizes (going down to a few square millimeters in certain applications) places a space constraint on the micro-geometric enhancement features to be provided on the cooling device. There is virtually no information on the effectiveness of enhanced structures in the range of small channel width (65-105 μm) and channel pitch (0.2-0.7 mm). While the small channel width and pitch allow an increase in pore density, it is unclear whether such an increase results in a commensurate increase in the overall heat removal capability of the structure. This study investigates the effect of reduction in the geometrical dimensions on the heat transfer performance. The enhanced structure employed is similar to one proposed by Nakayama et al. (1984). Geometrical details of the structure have been included in Chapter 2. Predictive correlations for the nucleate boiling regime are explored for the proper design and employment of the enhanced structures.

3.1 Influence of channel width on thermal performance

For this set of experiments the channel pitch was maintained constant at 0.7 mm. The enhancement of boiling due to the structured surfaces is obvious from the boiling curves shown in Figure 3.1. The curves were obtained with decreasing heat flux (to avoid hysteresis effects), the fluid being at saturation point throughout the run. It is evident that the enhanced structures are highly efficient in promoting boiling heat transfer, especially in the low heat fluxes range ($q^{"} < 8$ W/cm^2). The superheat required to transfer a certain

heat flux is reduced to nearly one fifth, at best (structure C-0.105-0.7, $q^{"}$ = 2 W/cm^2). Since the wetted area is increased by only a factor of 3.26 (at most), this enhancement cannot be attributed to the increase in wetted surface area alone. The maximum attainable heat flux was 34.8 W/cm^2 for structure C-0.105-0.7, as opposed to 15.4 W/cm^2 for the C-plain structure.

In general, the performance improves with increase in channel width. This effect diminishes for heat fluxes exceeding 15 W/cm^2. Table 3.1 summarizes this enhancement.

Table 3.1 Relative enhancement (percentage) in heat dissipation compared to a plain surface for the enhanced structures with P_t = 0.7 mm.

$q^{"}$ (W/cm^2)	Relative enhancement in heat dissipation (%)				
	C-0.065-0.7	C-0.085-0.7	C-0.105-0.7	C-0.360-0.7	C-0.470-0.7
2	96	206	513	188	151
4	80	143	343	188	153
6	71	115	311	194	157
8	62	91	224	195	161
10	69	81	180	200	184
15	93	85	141	214	218
20			25	38	43
25			33	33	34
29			49	38	42

The improvement is presented relative to the plain structure for heat fluxes less than 15 W/cm^2. For 15 W/cm^2 < $q^{"}$ < 29 W/cm^2 the reference is structure C-0.065-0.7. Since the maximum heat flux attainable with structure C-0.065-0.7 is $q^{"}$ = 29 W/cm^2, data for $q^{"}$ > 29 W/cm^2 were not included in Table 3.1. It is noted that structures C-0.065-0.7 and C-0.085-0.7 perform similarly within the heat flux range 20-29 W/cm^2, within

experimental uncertainty. The same observation can be made about structures C-0.360-0.7 and C-0.470-0.7 for heat fluxes 12 W/cm^2 < q'' < 35 W/cm^2.

Three distinct regions can be delineated from Figure 3.1. For low heat fluxes q'' = 1-10 W/cm^2 the structure C-0.105-0.7 displays the best performance. For intermediate heat fluxes q'' = 10-25 W/cm^2 the structures C-0.360-0.7 and C-0.470-0.7 show better heat transfer characteristics. For high heat fluxes q'' = 25-35 W/cm^2 the structures perform similarly. Two observations can be made from the data shown in Figure 3.1. First, no decrease in performance was present in the high heat flux region. For their porous structures, Nakayama et al. (1982) noted a decrease in performance for heat fluxes larger than 15 W/cm^2, and the boiling curves of the porous structures converged towards the boiling curve of the plain surface. This decrease in performance was attributed to the "dried-up" mode of boiling. It was hypothesized that the structure will revert towards the plain surface behavior once the tunnel space is filled with vapor. For the present surfaces no such trend was noticed. It must be noted that the construction of the present structures lets the top finned face open to the liquid pool (see Figure 2.1a). This feature is believed to be the reason for the superior heat transfer performance over the entire range of heat fluxes. Second, the performance of the enhanced structures does not deteriorate even for the largest channel tested (0.47 mm), over the entire range of heat fluxes tested. In the low heat flux region (q'' < 10 W/cm^2) the flooded mode may take place for larger channel widths, decreasing the heat transfer coefficient. A change in slope occurs at around 10 W/cm^2 indicating a change in the boiling mode. The superior performance in the intermediate and high heat flux regions it is believed to be due again to the presence of fins on the external surface.

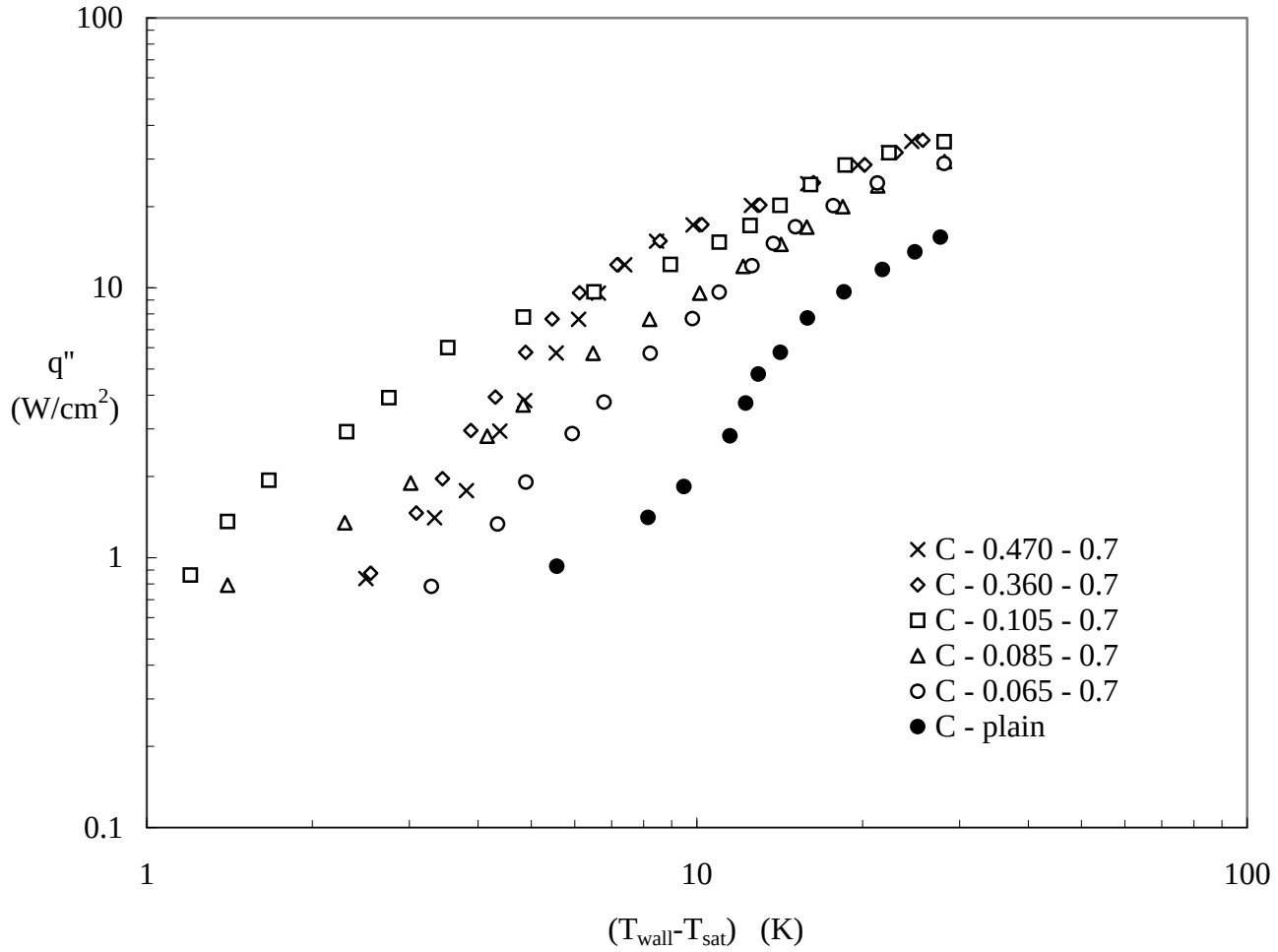

Figure 3.1 Boiling curves at saturation for various channel widths. The maximum uncertainty is ± 0.2 K for (T_{wall}-T_{sat}) and ± 13 % for q"

Figure 3.2 compares the performance of enhanced structures with that of plain structure when the heat flux is computed based on the total wetted area. It is clear from this figure that, for wall superheats less than 14 K, the enhancement is not a sole result of the increased surface area. However, in the high superheat region (14 K < ΔT_{wall} < 28 K), the increase in the wetted surface area does not translate into a corresponding increase in performance.

Very few data are available for the structured surface-coolant combination employed in this study. Ramaswamy et al. (2003a) studied the same type of enhanced structure with the same working fluid. However, the majority of their data were taken with structures made of silicon and having a 0.5 mm overall thickness. Their copper structures had larger channel widths (see Table 3.2) due to limitations of their fabrication methods. The data of Nakayama et al. (1984) are for a similar but larger channel widths structure and a different coolant (R-11), whereas the data of Nakayama et al. (1980a) and Chien and Webb (1998a) refer to structures similar to the Hitachi Thermoexcel-E. The geometrical parameters of the structures used in prior related studies are summarized in Table 3.2.

Table 3.2 Geometrical parameters of the structures presented in Figure 3.3.

Authors	Nakayama et al.		Chien and Webb (1998a)	Ramaswamy et al. (2003a)
	(1980)	(1984)		
Fluid	R-11	R-11	R-11	FC-72
W_t	0.25	0.25	0.40	0.2, 0.27
P_t (mm)	0.55	0.55	0.73	0.5, 0.63
H_t	0.4	0.55	0.5	0.55
d_p	0.1	0.25	0.12	0.2,0.27
P_p	0.7	0.55	0.75	0.5, 0.63

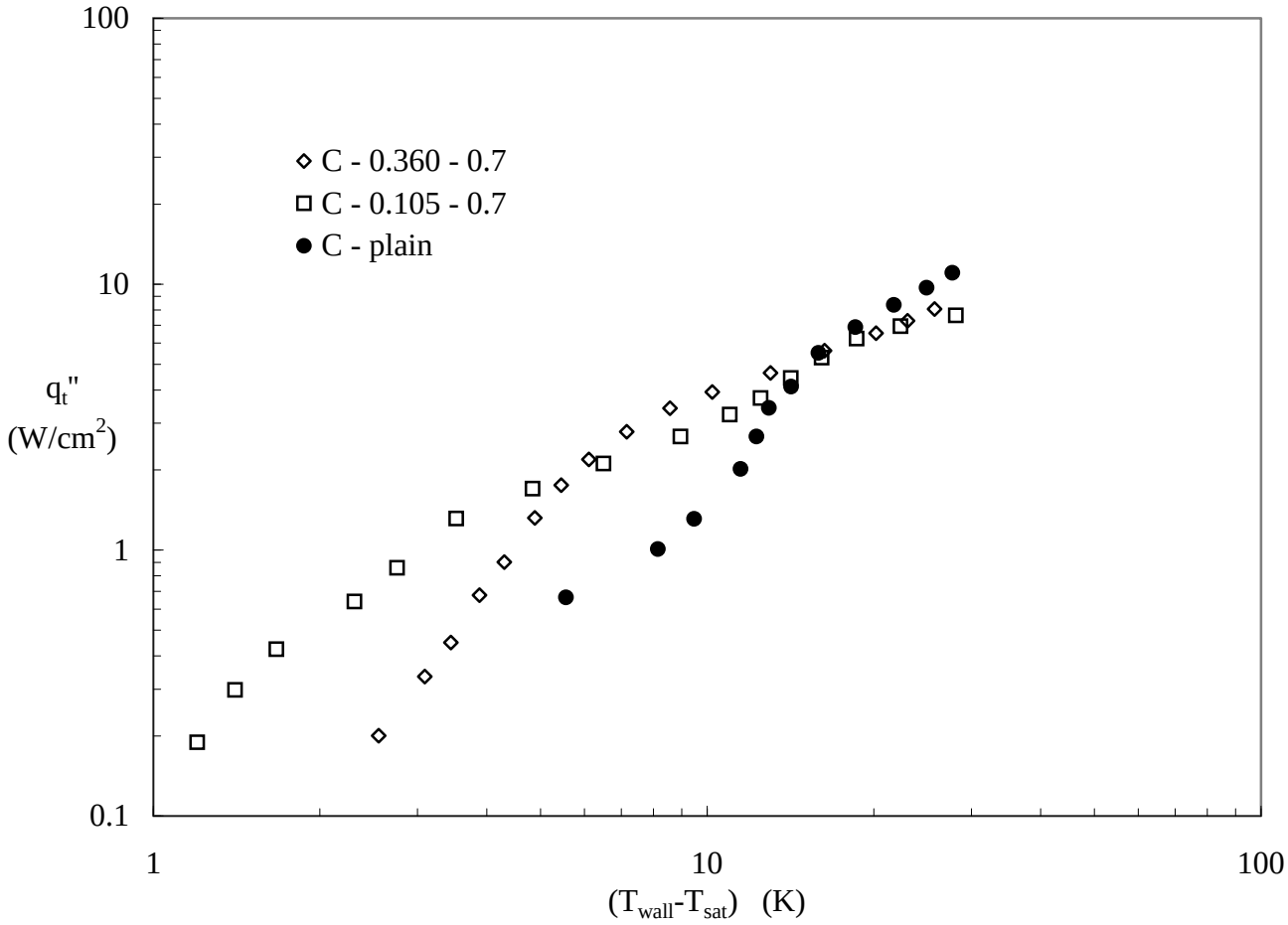

Figure 3.2 Boiling curves based on total surface area.
The maximum uncertainty is ± 0.2 K for (T_{wall}-T_{sat}) and ± 13 % for q"

From Figure 3.3 it can be seen that the structure C-0.105-0.5 exhibits good performance over a wide range of heat fluxes. As pointed out by Nakayama et al. (1984), the working fluid influences the heat transfer performance of the enhanced structures greatly. In general, the refrigerants (h_{fg} = 147 kJ/kg for R-113) tend to produce better heat transfer performance than the fluorocarbons (h_{fg} = 88 kJ/kg for PF 5060). This can explain the superior performance exhibited by the porous surface (Nakayama et al. (1980a)) in the low heat flux range. Another factor is believed to be the higher channel width (0.2 mm and 0.25 mm). The structure C-0.200-0.5 (Ramaswamy et al. (2003a)) displays the best heat transfer performance in Figure 3.3 for heat fluxes in excess of 11 W/cm^2. The highest attainable heat flux was 61.2 W/cm^2 at a wall superheat of 31 ^{o}C. In addition to the larger channel width, the data reported by Ramaswamy et al. (2003a) were obtained using a slightly different heater assembly (see Ramaswamy (1999)) presumably resulting in higher conductive heat spreading.

3.2 Channel Pitch Effect

The effect of varying the channel pitch was investigated for two channel widths: 65 μm and 105 μm. The ranges investigated were 0.2-0.7 mm for the 65 μm wide channel and 0.35-0.7 mm for the 105 μm wide channel. By reducing the pitch, the area of the structure wetted by the liquid increases up to a maximum of ~8 times of that of the plain surface. Therefore the heat transfer performance is expected to increase over the entire range of heat fluxes. The boiling curves for the channel width of 65 μm are presented in Figure 3.4. The structure C-0.065-0.2 exhibits the best heat transfer performance up to 29 W/cm^2. Beyond that, the slope of the boiling curves changes,

signaling deteriorating performance for all the structures tested. The maximum heat flux of 34 W/cm^2 at a wall superheat of 28.3 K was attained with structure C-0.065-0.35. The improvement showed by the structure C-0.065-0.5 over structure C-0.065-0.7 is only marginal up to a heat flux of ~17 W/cm^2. For q'' > 17 W/cm^2 the improvement is significant. The enhancement over the structure with the largest channel pitch (C-0.065-0.7) is summarized in Table 3.3.

Table 3.3 Heat transfer enhancement (percentage) relative to the structure C–0.065–0.7

q'' (W/cm^2)	Heat transfer enhancement (%) relative to C-0.065-0.7		
	C-0.065-0.2	C-0.065-0.35	C-0.065-0.5
5	166	64	7
10	97	58	9
15	78	25	4.5
20	74	35	19.4
25	77	46	33
29	89	63	42

A deviation from the expected behavior occurs in the case of 0.105 mm channel width, as seen in Figure 3.5. In the low heat flux region (1 < q'' < 12 W/cm^2) the best performance is shown by the structure with the largest channel pitch (C-0.105-0.7). A second region (12 < q'' < 25 W/cm^2) is characterized by a similar performance for the structures C-0.105-0.5 and C-0.105-0.7, with a slightly higher boiling curve for the structure C-0.105-0.35. Finally, the last region (q'' > 25 W/cm^2) exhibits a clear differentiation between the structures, with the expected hierarchy in performance (the smaller the channel pitch, the better the performance).

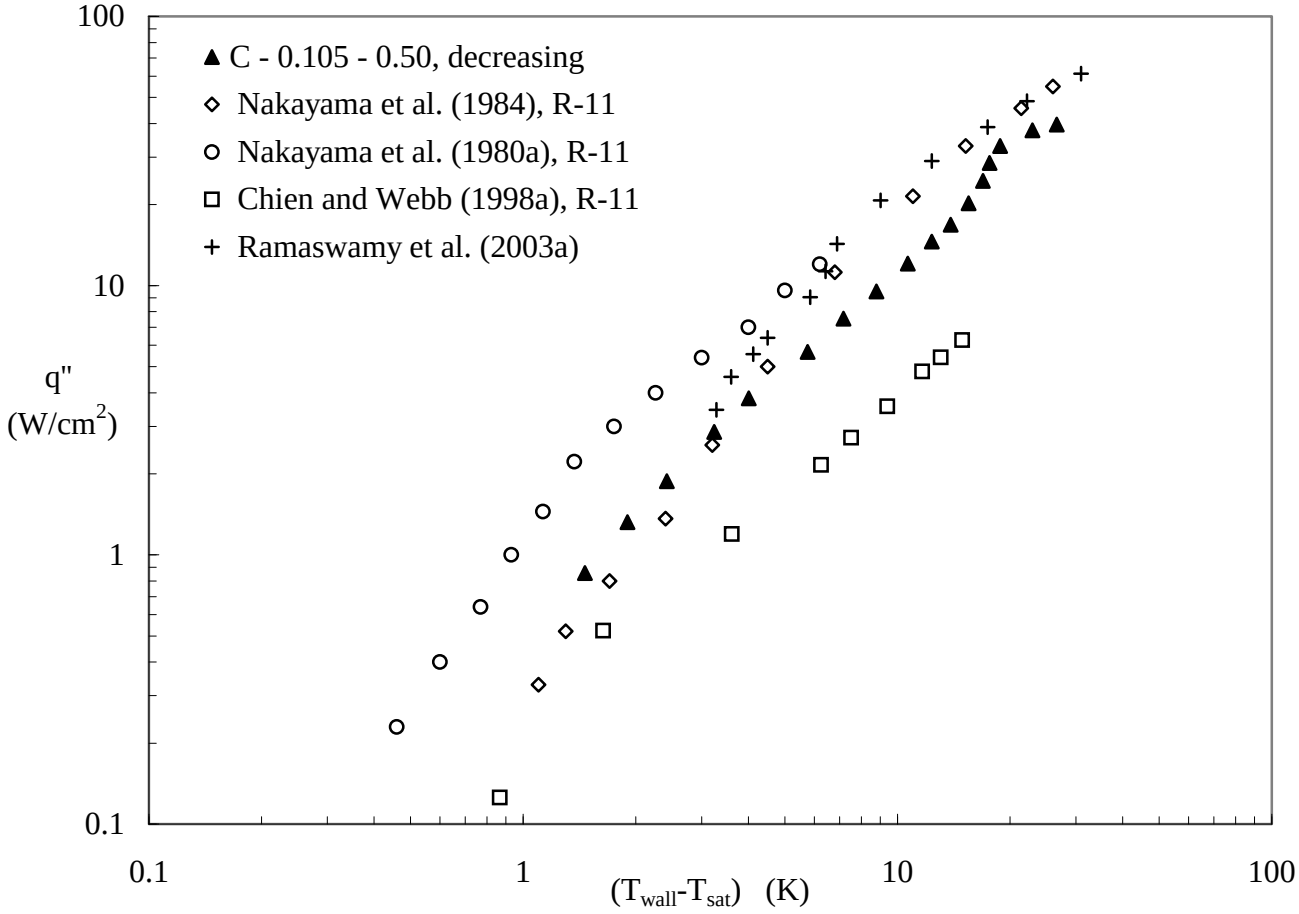

Figure 3.3 Boiling performance of structure C – 0.105 – 0.5 compared with existing data. The maximum uncertainty is ± 0.21 K for (T_{wall}-T_{sat}) and ± 14 % for q"

The boiling curve for structure C-0.105-0.35 presents an almost vertical portion (for $25 < q'' < 35$ W/cm^2). This structure exhibits an excellent performance for high heat fluxes: the maximum heat flux dissipated was 43 W/cm^2 at a wall superheat of 24.4 ^{o}C.

Ramaswamy et al. (2003a) found that, in general, a smaller channel pitch resulted in a better heat transfer performance. The exception was constituted by the structure with a 1.4 mm channel pitch. For a wall superheat of around 15 K this structure dissipated less heat than a structure with a 2.1 mm channel pitch. The authors attributed this phenomenon to a difference in surface areas participating in boiling. For the 2.1 mm channel pitch structure the entire channel network contributed to boiling, whereas for the 1.4 mm channel pitch structure just the pores were active.

3.3 Hysteresis Effect

Nakayama et al. (1984) reported that the hysteresis shown by the porous and microfinned surfaces is more pronounced than for the plain surfaces. The hysteresis effect induced by the enhanced structures employed in this study is presented in Figure 3.6 and Figure 3.7. Similar to the plain structure, the boiling curve for structure C-0.065-0.7 (Figure 3.6) presents insignificant hysteresis. The intermediate channel size structure (C-0.085-0.7) exhibits a more pronounced hysteresis (from the boiling incipience up to ~15 W/cm^2). Structure C-0.105-0.7 shows significant hysteresis at the boiling incipience. After this initial region the two curves almost coincide.

A peculiar phenomenon is observed for structures C-0.105-0.5 and C-0.105-0.35. As illustrated in Figure 3.7 for structure C-0.105-0.35, the boiling curves show the expected hystersis behavior at boiling incipience: the boiling curves taken with increasing

heat flux are to the right of those constructed with decreasing heat flux. However, a "reverse" hysteresis was present in the heat fluxes range 4-20 W/cm^2 (well into the established boiling region of the nucleate boiling curve). This is true for all the structures but is particularly noticeable for C-0.105-0.5 and C-0.105-0.35. For heat fluxes beyond 20 W/cm^2 this effect diminishes. Arshad and Thome (1983) reported a similar behavior of the boiling curves for water. The structures employed in their study had rectangular, triangular and circular cross-section subsurface channels connected with the liquid pool through pores of diameters 0.18 mm and 0.25 mm. Kovalev et al. (1987) reported the same phenomenon for porous coatings. They hypothesized that a vapor layer forms at the base of the porous structure at high heat fluxes that insulates the base and deteriorates the heat transfer. If the heat flux is not raised above this threshold level then there is no hysteresis. It is believed this explanation for porous coatings may apply for the present structures as well.

3.4 Effect of structure width

A few investigators have addressed the effect of the heater dimensions on the heat transfer performance. Park and Bergles (1988) boiled R-113 from small thin foil heaters intended to simulate electronic chips. It was found that for established boiling, the size of the heater has little effect on the measured boiling curve. Rainey and You (2001) studied the effect of heater size on the thermal performance for pool boiling from a microporous coated surface. They tested heaters having 10 mm × 10 mm, 20 mm × 20 mm and 50 mm × 50 mm. The experimental nucleate boiling curves were found insensitive to the heater size due to the nature of the nucleation sites formed on the surface.

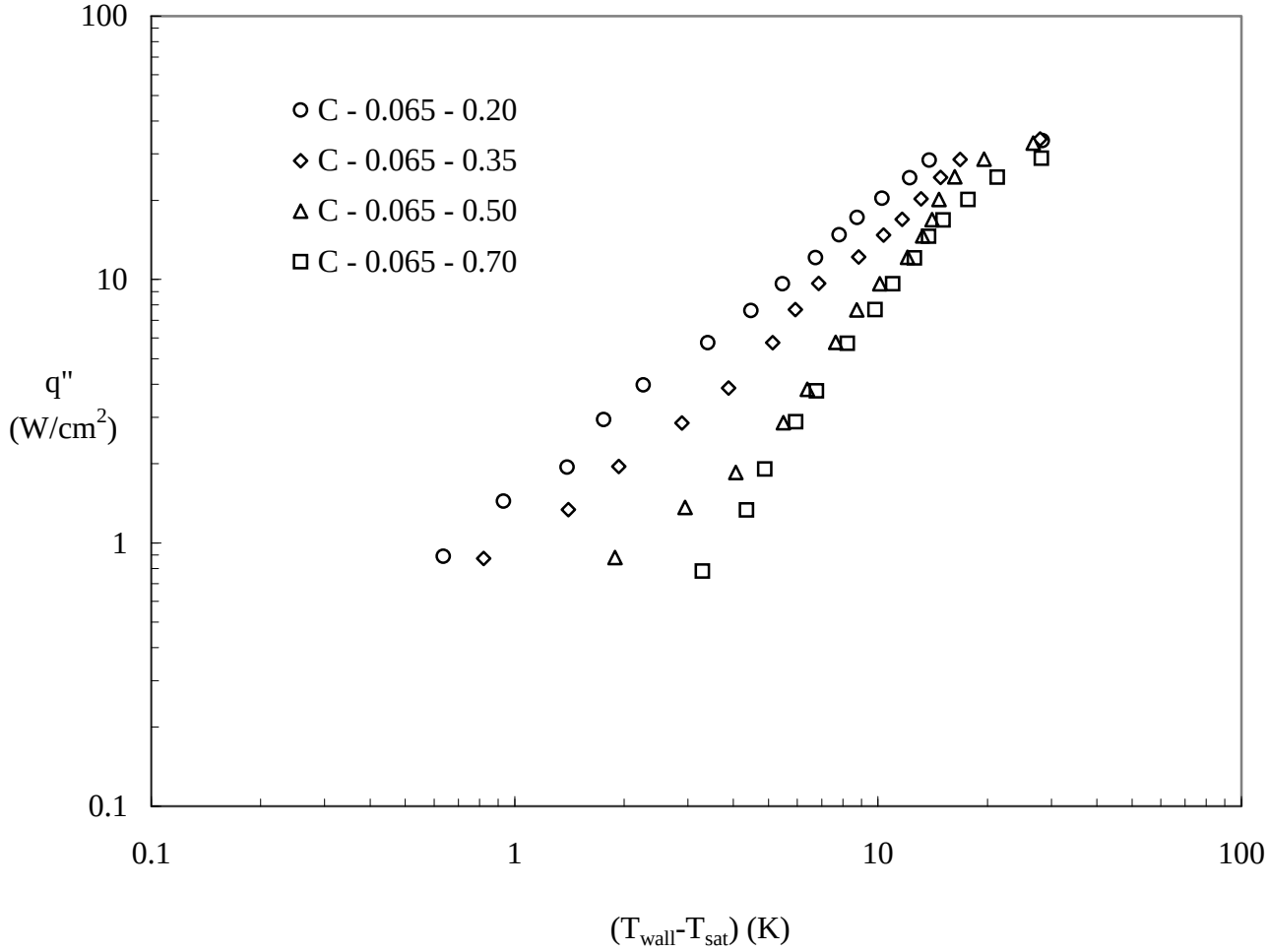

Figure 3.4 Effect of channel pitch on boiling heat transfer (W_t = 65 μm). The maximum uncertainty is ± 0.2 K for (T_{wall}-T_{sat}) and ± 13 % for q"

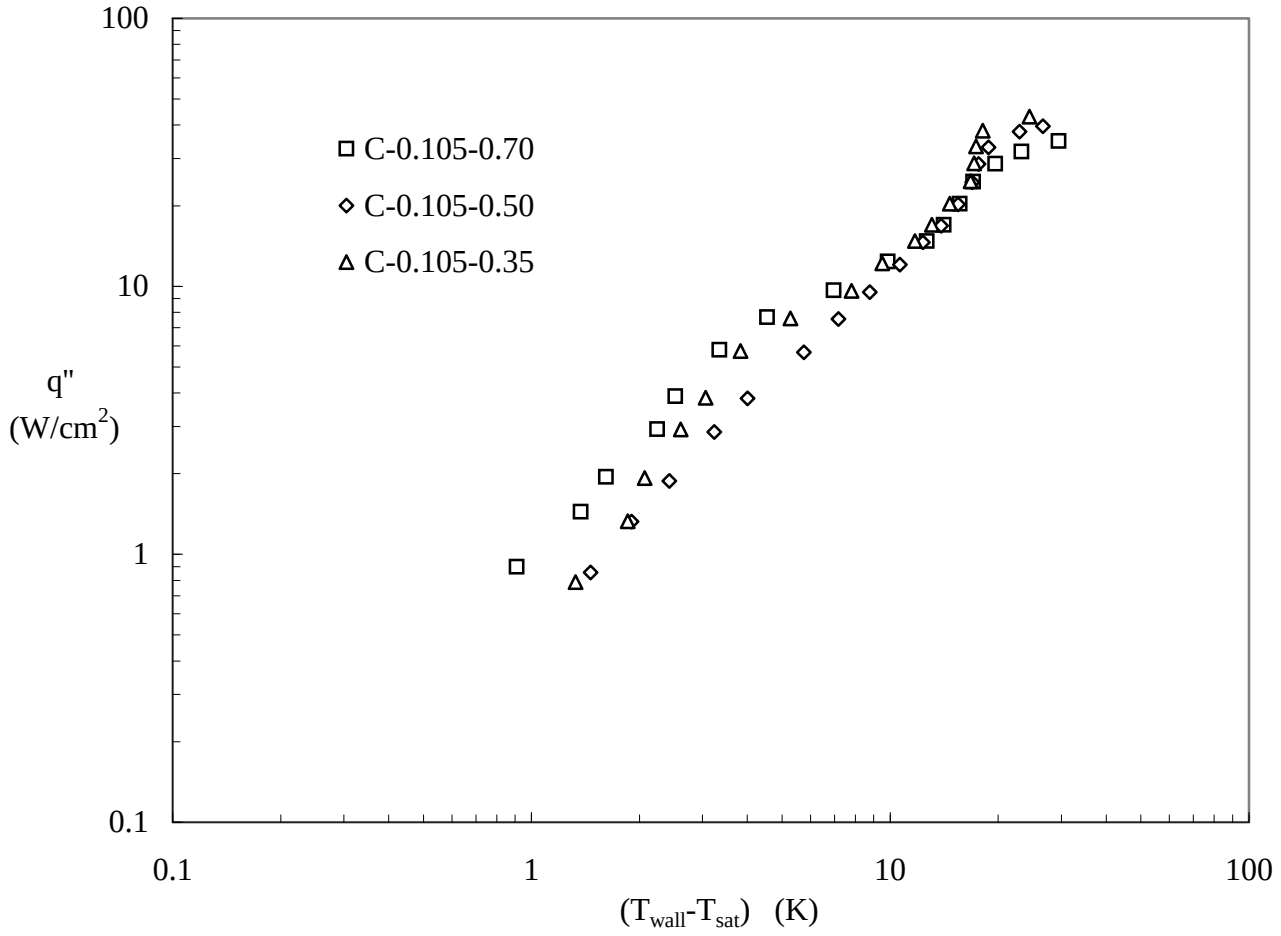

Figure 3.5 Effect of channel pitch on boiling heat transfer (W_t = 105 μm). The maximum uncertainty is ± 0.21 K for (T_{wall}-T_{sat}) and ± 14 % for q"

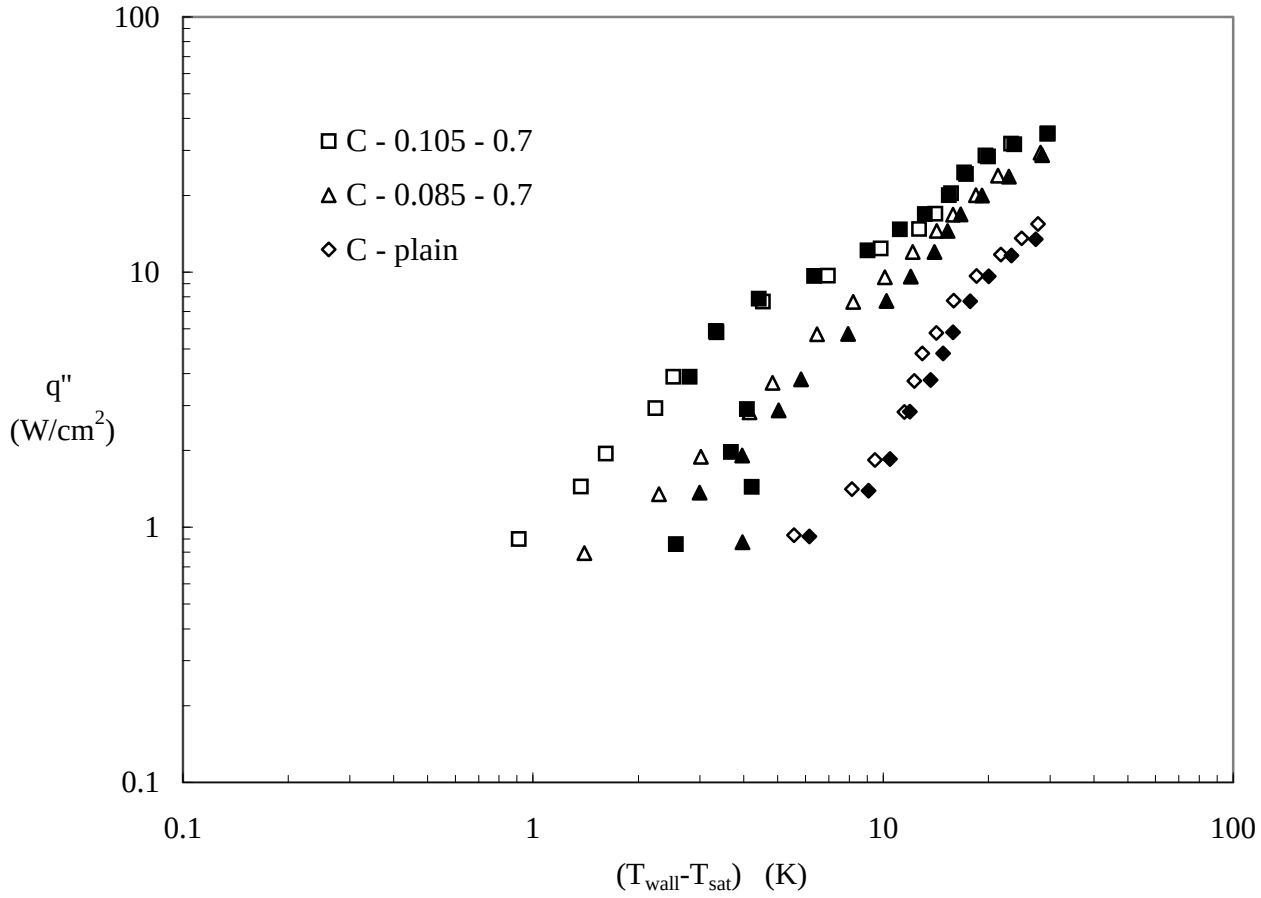

Figure 3.6 Hysteresis of boiling curves for different channel widths. The solid symbols correspond to increasing heat fluxes and open symbols to decreasing heat fluxes. The maximum uncertainty is ± 0.22 K for (T_{wall}-T_{sat}) and ± 13.6 % for $q^{"}$

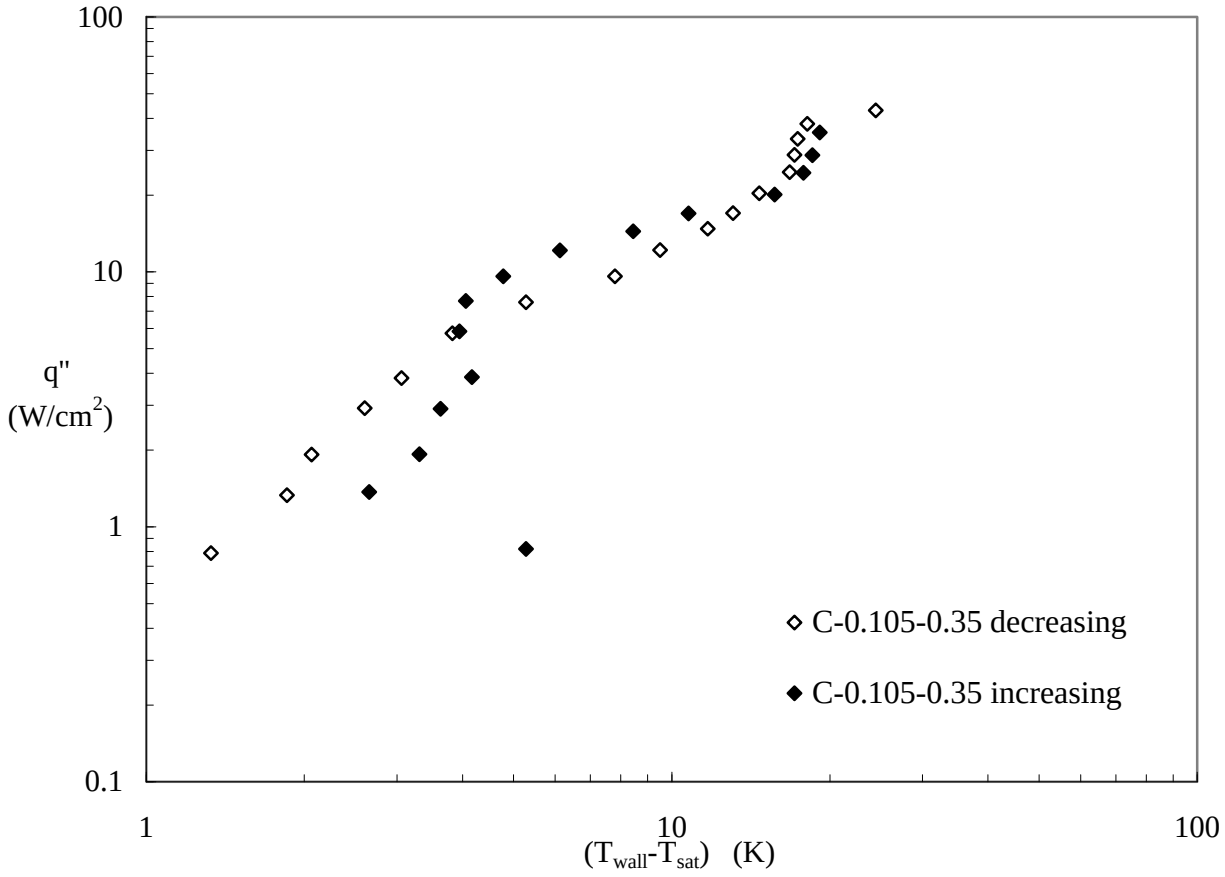

Figure 3.7 Hysteresis effect for structure C-0.105-0.35. The solid symbols correspond to increasing heat fluxes and open symbols to decreasing heat fluxes. The maximum uncertainty is ± 0.23 K for (T_{wall}-T_{sat}) and ± 13.7 % for q"

Figure 3.8 includes data for channel width W_t = 0.105 mm along with the boiling curve obtained with the plain structure. Two overall structure widths were tested: L = 5 mm and L = 10 mm. The channel pitch was maintained constant at 0.7 mm. As can be seen, the boiling curves are nearly identical for heat fluxes beyond q'' = 12 W/cm^2. For the low heat fluxes region the structure C-10-0.105-0.7 displays a slight superior thermal performance. This is believed to be due to the experimental uncertainty, larger for the low heat fluxes. The maximum heat flux attainable with structure C-5-0.105-0.7 was q'' = 35.2 W/cm^2 corresponding to a power input of 10 W.

Figure 3.9 presents heat transfer data for structures with the channel width W_t = 0.360 mm. Three overall structure widths were tested for this case: L = 5 mm, L = 10 mm and L = 15 mm. Again, the channel pitch was maintained constant at 0.7 mm. It should be mentioned that the maximum heat flux tested with structure C-15-0.360-0.7 was q'' = 20 W/cm^2. This heat flux corresponded to an electrical power input of 50 W, maximum attainable with the present setup. A heat load above 50 W would exceed the cooling capability of the condenser. The boiling curves are in close proximity excepting the very low heat flux zone; the scatter of the data is not believed to be the effect of physics but rather experimental uncertainty. The presented study also suggests an insignificant effect of the structure width for the range of dimensions encountered in electronics cooling.

3.5 Correlation of boiling data

As noted by previous researchers, any attempt to establish a physics based predictive correlation of heat transfer data for enhanced structures should begin with the

identification of the heat transfer modes operating inside the structure. While physics based models for specific sub-regimes have been developed (Nakayama et al. (1980), Ramaswamy et al. (2003b)), they do not apply to the large range of superheats encountered in applications.

If a correlation of the usual simplified form:

$$q'' = C \cdot \left(\Delta T_{wall}\right)^{n} \tag{3.1}$$

is sought, the coefficient $C\left(W/cm^2 \cdot K^{-n}\right)$ and the exponent n should depend on the working fluid, structure geometry (channel width and pitch), as well as the level of heat flux (boiling mode from the structure).

In the present study, a multi line power-law curve fit of the data (155 experimental points) is performed to approximate the boiling curves of the enhanced structures. The results are presented in Tables 3.4 and 3.5. Table 3.6 provides more approximate single line fits to the data for each of the structures tested, in addition to the piecewise linear fits in Tables 3.4 and 3.5. The present curve fits are intended to provide empirical relations to represent thermal performance over the entire nucleate boiling regime.

3.5.1 Structures with 65 μm < W_t < 105 μm

The boiling curves can be approximated by linear segments for the tested range of heat fluxes. In general, two segments suffice for the linearization of the boiling curves. Close to the highest heat flux a decrease in the slope of the boiling curves can be detected. This signals the proximity of the critical heat flux. The decrease in channel pitch P_t for the structures with W_t = 65 μm results in increased thermal performance (see

Figure 3.6). This is reflected in the values of C and n (Table 3.6). While the coefficient C increases from 0.1173 to 1.5844, the exponent n follows the opposite trend: it decreases from 1.7787 to 1.0476. The values of the exponent n listed in Table 3.4 are lower than the traditional 2.5-4 value expected for nucleate boiling. This is attributable to the change in the boiling process induced by the use of enhanced structures. Similar results were obtained by other investigators (Rainey and You (2000)).

Table 3.4 Coefficient C and exponent n for the enhanced structures with W_t < 100 μm

Structure identification	C	n	Heat flux range (W/cm^2)
C-plain	0.1098	1.2387	$0.9 < q'' < 2.1$
	5×10^{-5}	4.461	$2.1 < q'' < 4.8$
	0.0126	2.3189	$4.8 < q'' < 8.5$
	0.3285	1.1589	$8.5 < q'' < 15.4$
C-0.065-0.70	0.0716	2.0449	$0.7 < q'' < 14.6$
	1.2685	0.9503	$14.6 < q'' < 28.9$
C-0.065-0.50	0.477	0.9687	$0.9 < q'' < 2$
	0.1144	1.9052	$2 < q'' < 24.6$
	5.0063	0.5769	$24.6 < q'' < 33$
C-0.065-0.35	0.9061	1.1950	$0.9 < q'' < 28.6$
	10.514	0.3544	$28.6 < q'' < 34.2$
C-0.065-0.20	0.4885	1.1162	$0.9 < q'' < 28.4$
	15.064	0.2412	$28.4 < q'' < 33.8$
C-0.085-0.70	0.4823	1.2865	$0.8 < q'' < 23$
	2.4411	0.7453	$23 < q'' < 29.4$

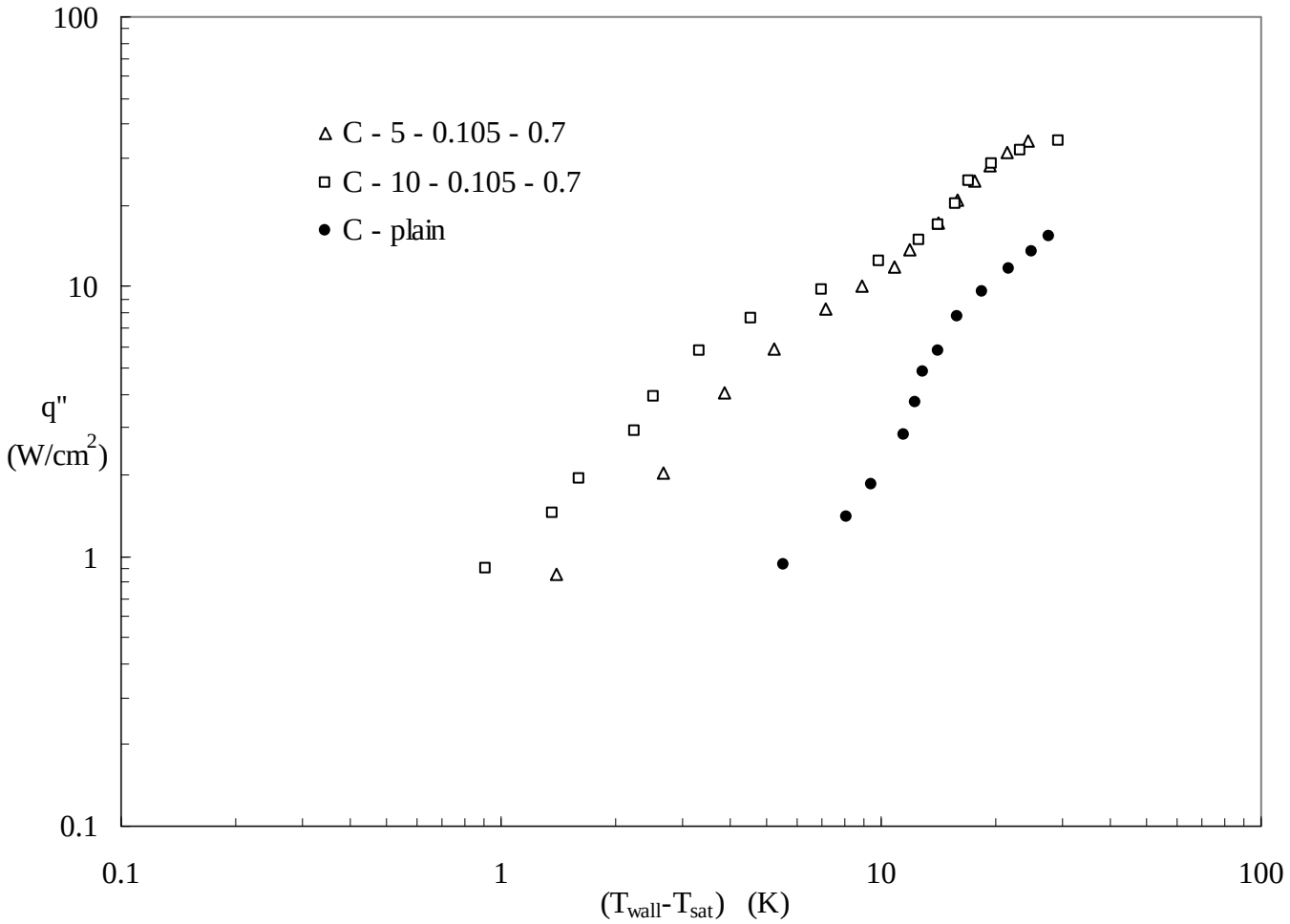

Figure 3.8 Boiling curves for plain structure and enhanced structures with W_t = 0.105 mm. The maximum uncertainty is ± 0.24 K for (T_{wall}-T_{sat}) and ± 14.5 % for q"

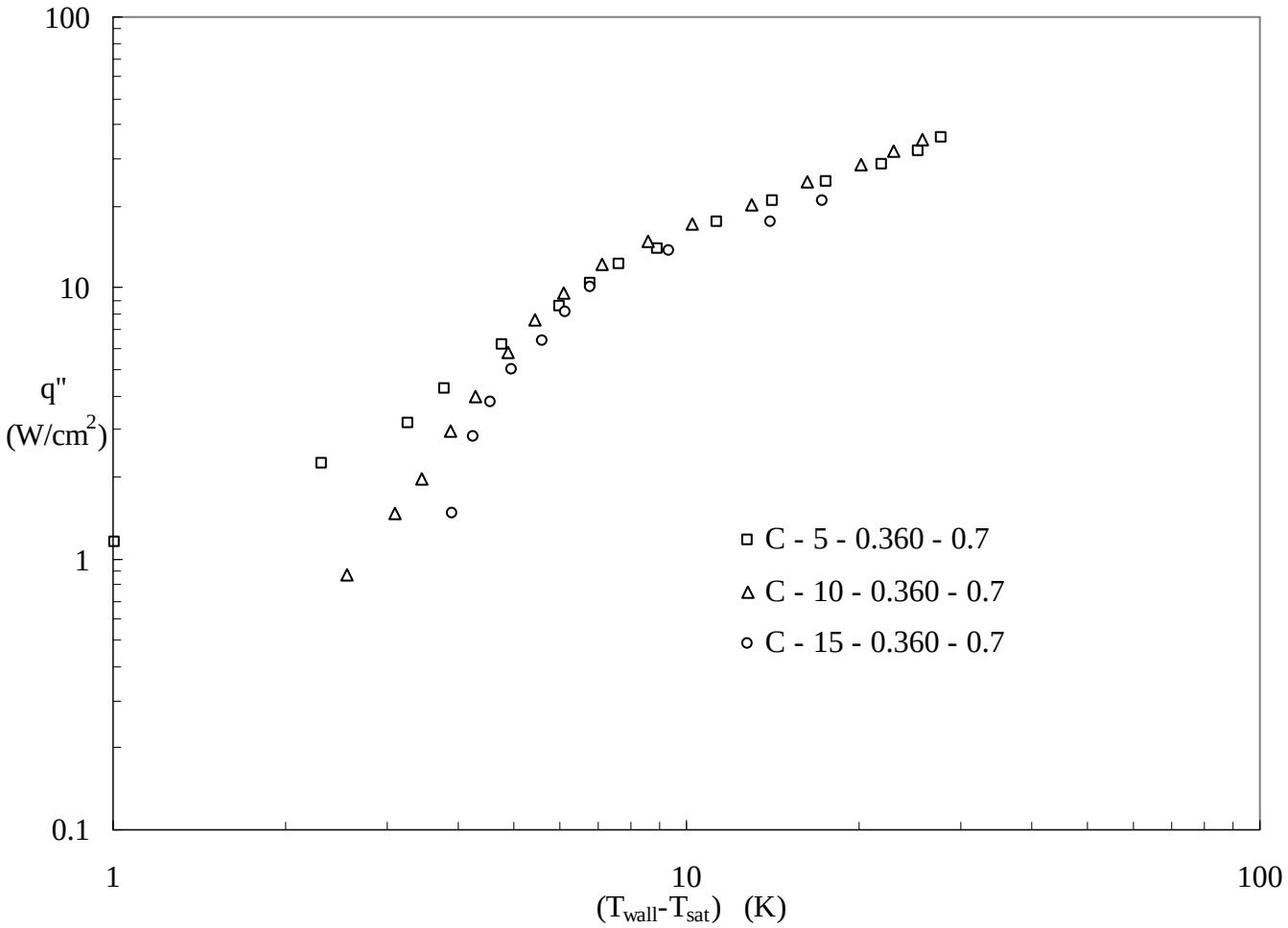

Figure 3.9 Boiling curves for enhanced structures with W_t = 0.360 mm. The maximum uncertainty is ± 0.24 K for (T_{wall}-T_{sat}) and ± 14.8 % for q"

3.5.2 Structures with 105 μm ≤ W_t ≤ 470 μm

The values of C and n for the structures with larger channel widths tested (105 μm, 360 μm and 470 μm) are summarized in Table 3.5. For structures with W_t = 105 μm, multiple linear segments have to be used. Particularly noticeable is the presence of a steep portion before the decline in the heat transfer coefficient. The slope of this curve increases with the increase in the channel pitch, reaching a value of 10.647 for a 0.35 mm pitch.

Table 3.5 Coefficient C and exponent n for the enhanced structures with 105 μm ≤ W_t ≤ 470 μm

Structure identification	C	n	Heat flux range (W/cm^2)
C-0.105-0.70	0.9746	1.4506	$0.9 < q'' < 6$
	2.6231	0.6801	$6 < q'' < 15$
	0.0931	1.9645	$15 < q'' < 25$
	7.0747	0.4736	$25 < q'' < 34.9$
C-0.105-0.50	0.4901	1.5132	$0.8 < q'' < 3$
	0.6765	1.2254	$3 < q'' < 20$
	0.0006	3.7456	$20 < q'' < 33$
	6.9838	0.5324	$33 < q'' < 39.6$
C-0.105-0.35	0.4517	1.4506	$0.8 < q'' < 6$
	2.7993	0.6002	$6 < q'' < 10$
	0.6956	1.2558	$10 < q'' < 25$
	2×10^{-12}	10.647	$25 < q'' < 34$
	11.831	0.4035	$34 < q'' < 43$
C-0.360-0.70	0.0561	2.907	$0.9 < q'' < 10$
	2.6151	0.7995	$10 < q'' < 35.25$
C-0.470-0.70	0.163	1.7854	$0.8 < q'' < 2$
	0.0381	2.9145	$2 < q'' < 14$
	2.8393	0.7786	$14 < q'' < 34.9$

No clear trend can be detected for the values of C and n (see Table 3.6). At the high end of the tested channel widths (W_t = 360 μm and W_t = 470 μm) the boiling curves become linear again, although with a different slope.

Table 3.6 Coefficient C and exponent n for the enhanced structures over the entire nucleate boiling regime

Structure identification	C	n	Heat flux range (W/cm^2)
C-plain	0.0293	1.9366	$0.9 < q'' < 15.4$
C-0.065-0.20	1.5844	1.0476	$0.9 < q'' < 33.8$
C-0.065-0.35	0.9486	1.1566	$0.9 < q'' < 34.2$
C-0.065-0.50	0.2532	1.5593	$0.9 < q'' < 33$
C-0.065-0.70	0.1173	1.7787	$0.7 < q'' < 28.9$
C-0.085-0.70	0.5006	1.2608	$0.8 < q'' < 29.4$
C-0.105-0.35	0.7335	1.2878	$0.8 < q'' < 43$
C-0.105-0.50	0.5583	1.3303	$0.8 < q'' < 39.6$
C-0.105-0.70	1.2493	1.0284	$0.9 < q'' < 34.9$
C-0.360-0.70	0.4168	1.4835	$0.9 < q'' < 35.3$
C-0.470-0.70	0.2969	1.6163	$0.8 < q'' < 34.9$

3.6 Discussion

Nakayama et al. (1982) hypothesized the presence of three modes of boiling from a subsurface channel. The modes were coined “flooded’ (for the large channel sizes at low heat fluxes), “suction-evaporation” and “dried-up” (likely to be present at high heat fluxes on a surface with small pores). The authors assumed that the different boiling modes inside the channels should reflect on the shape of the boiling curves. From their boiling curves, Nakayama et al. (1982) noticed that the exponent n decreases with increase in the diameter of the pores. They also found that, for a constant pore diameter, n

decreases as the population density increases. It was concluded that on a surface having small pores or reduced density of pores, the mechanism of heat transfer approaches the one existent in plain surface boiling. As the dried-up mode prevails, the exponent n approaches that for the plain surface. On the other hand, smaller values of n indicate the predominance of heat transfer inherent to the structured surfaces. Also of interest is the relative invariance of n with the system pressure.

The boiling curves obtained for structures with small channel widths (W_t = 65 μm and W_t = 85 μm) and different channel pitches, do not display a significant variation in shape across the nucleate boiling regime. Therefore the possible modes of boiling are not reflected in the shape of the boiling curves. The "dried-up" boiling mode, expected to occur at high heat fluxes, is not present. As the channel pitch decreases, the exponent n decreases as well, similar to the findings of Nakayama et al. (1982).

On the other hand, the shape of the boiling curves in the case of larger channel widths (W_t = 105 μm, W_t = 360 μm and W_t = 470 μm) indicates the presence of different boiling regimes from the structures. As for the "flooded" mode, the data obtained in the present study do not indicate a sharp decline in heat transfer performance even for the largest channel width tested (W_t = 470 μm) and for $q'' < 2$ W/cm^2.

The above differences between the findings of this study and the hypotheses of Nakayama et al. (1982) can be explained in the light of the differences between the enhanced structures employed in the two studies. The structures employed in this study have an array of microfins on the outside surface, bounding the pores. The morphology of the structures permits the communication with the surrounding liquid pool through continuous channels rather than discrete pores. This is probably the reason why the

"dried-up" mode does not seem to occur. This feature of the present surface is believed to be responsible for the superior performance of the structure in the high heat fluxes region, making it suitable for employing in electronics cooling.

3.7 Summary

The following conclusions can be drawn from the present study:

a) The enhanced structures employed in this study show superior heat transfer performance in comparison with the plain surface. The structures are highly efficient in promoting boiling heat transfer over the entire nucleate boiling curve. The maximum dissipated heat flux was q'' = 43 W/cm^2. In the low heat fluxes range (q'' = 1-8 W/cm^2), the superheat required to transfer a certain heat flux is reduced to nearly one fifth, at best.

b) In general, the performance of the enhanced structure increases with the increase of the channel width. This effect is more pronounced in the low to intermediate heat fluxes range (1-10 W/cm^2). At higher heat flux levels (more than 15 W/cm^2) this effect diminishes, ultimately disappearing.

c) The channel pitch has a large influence on the boiling performance of the enhanced structures. For the 65 μm channel width, the pitch reduction improves the performance at all heat fluxes (except the maximum). For the 105 μm channel width, the improvement is significant only beyond q'' ~ 25 W/cm^2.

d) The best thermal performance is obtained with structure C-0.065-0.2 for q'' < 30 W/cm^2 and with structure C-0.105-0.35 for q'' > 30 W/cm^2.

e) Simple multi-line curve fits are provided as empirical predictive correlations for boiling using enhanced structures. The present curve fits are intended to serve as quick dimensioning tools for the designer of cooling systems and represent the thermal performance of the enhanced structure over the entire nucleate boiling regime.

f) The modes of boiling from an enhanced structure proposed by Nakayama et al. (1982) were unable to explain the boiling curves obtained in this study. This is explained in light of the contribution from the top finned face of the enhanced structure.

CHAPTER 4: POOL BOILING UNDER TOTAL TOP CONFINEMENT

Nucleate pool boiling from top-covered enhanced structures is a particular case of pool boiling potentially useful in cooling electronic devices operating under tight spatial constraints. This situation can occur in applications where there is complete confinement in the vertical direction, for example in next generation three-dimensionally stacked layers of powered electronic chips (Banerjee et al. (2001)). Moreover, the single-layered enhanced structures employed in this study (see Chapter 2) can be potentially used in a stacked configuration to enhance the overall thermal performance. In this case, the bonding between individual layers may require the presence of a thin metallic foil (for instance, gold; see Ramaswamy (1999). Hence the completely covered top situation may be encountered in many practical implementations. The insulated condition is chosen to provide a well-controlled thermal boundary. There is virtually no data on the boiling performance of the single-layered enhanced structures in such closed-top configuration.

The present study seeks to investigate the thermal performance of the enhanced structures in the limiting case of insulated top confinement. Also, the effect of channel width W_t on the thermal performance needs to be clarified. It is expected that this geometric parameter will have a large influence on the boiling phenomena. For a fixed channel pitch P_t, the wider the channel, the larger the area available for boiling heat transfer and the smaller the area exposed to conduction. Understanding the boiling phenomena, as well as identifying the boiling regimes that might establish for the enhanced structures with insulated top is also an objective of this study.

4.1 Boiling heat transfer performance

The boiling curves obtained for copper structures under saturated condition are presented in Figure 4.1. By completely covering the top surface of the structures, the performance decreases considerably in comparison to the open top case. The maximum heat flux attainable (with the wall temperature below 85 ^{o}C) was 10.8 W/cm^2 with the structure C-0.105-0.7 and 9.1 W/cm^2 with the structure C-0.360-0.7. A remarkable fact from Figure 4.1 is that the copper structures perform nearly similarly, for every channel width. The resulting boiling curves are almost linear (in a log-log plot), indicating the presence of a single boiling regime throughout the range of the investigated heat fluxes. Also plotted in Figure 4.1 is the boiling curve obtained with a plain unconfined sample. Within a heat flux range of 1 W/cm^2 < q'' < 4 W/cm^2 the top-insulated enhanced structures show a performance superior to the plain structures with the top open. This behavior is attributable to the prevalence of latent heat transport at low heat fluxes. The enhanced structures have a considerably larger surface area available for heat transfer (see Table 4.1) and therefore can dissipate more heat at the same wall superheat (through the internal evaporation process). As the heat flux increases, the external convection becomes dominant and the plain surface open to the liquid pool performs better.

Figure 2.3 (b) represents the top surface of the heater to which the structure in Figure 2.3 (a) is attached. The black rectangles represent the portions of the heater surface in contact with the fluid, while the white regions represent the portions covered by the structure. The fraction of the heater base surface area on which boiling may occur is therefore $A_b = N \cdot L \cdot W_t$, where N is the number of channels and L is the overall length of the structure.

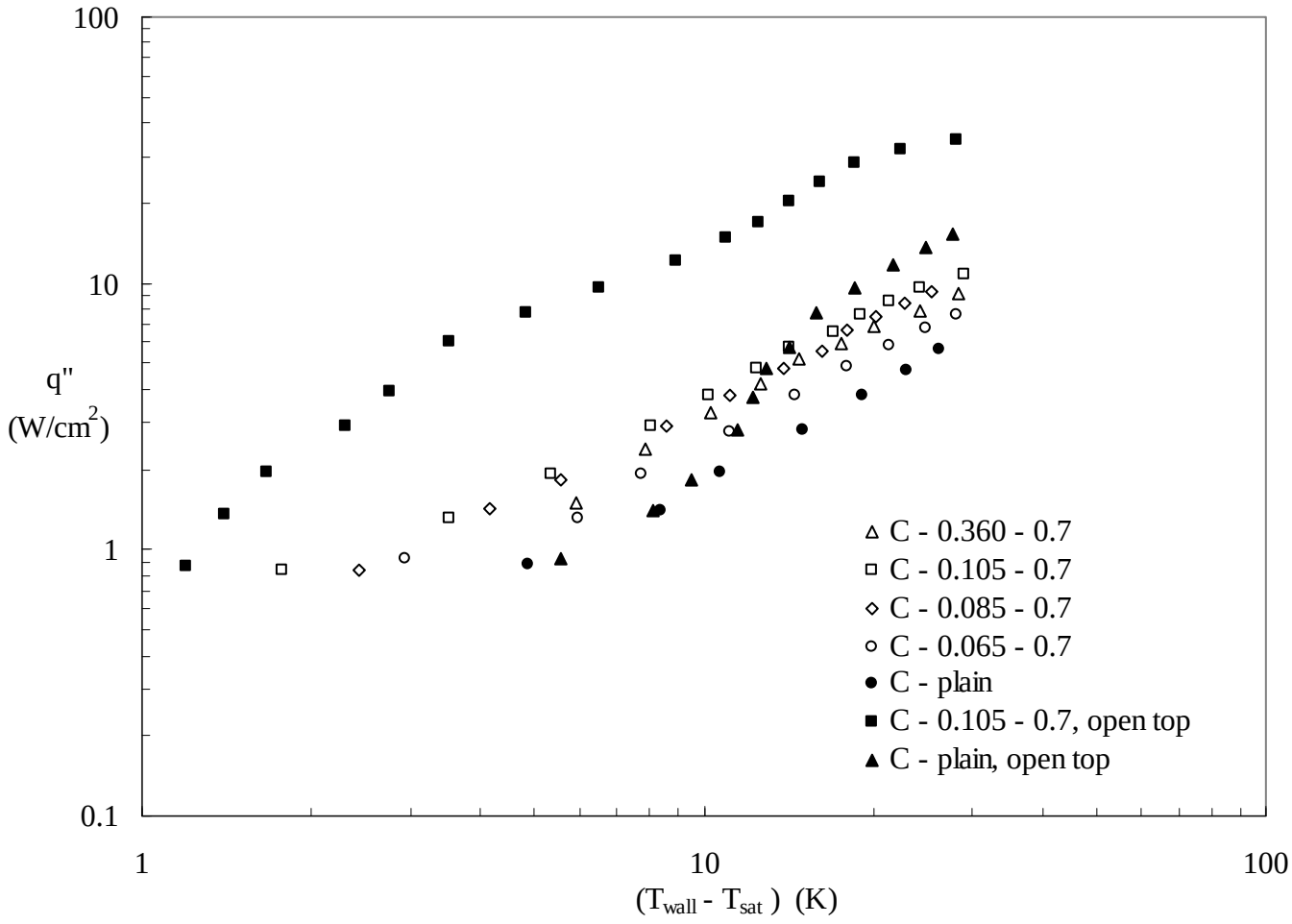

Figure 4.1 Boiling curves at saturation for copper structures.
The maximum uncertainty is ± 0.25 K for (T_{wall}-T_{sat}) and ± 15 % for q"

Table 4.1 Geometrical parameters of the enhanced structures

Structure identification*	Increase in wetted area (A_w / A)	Fraction in contact with the top cover (A_c / A)
C-0.065-0.70	9.1	0.92
C-0.085-0.70	9.2	0.89
C-0.105-0.70	9.3	0.86
C-0.360-0.70	9.6	0.52
Q-0.065-0.70	9.1	0.92
Q-0.105-0.70	9.3	0.86
Q-0.200-0.70	9.5	0.74
Q-0.250-0.70	9.6	0.68

* C denotes copper and Q quartz.

For a constant channel pitch, this area increases with the increase in channel width. The fraction of the base area available for conduction is $A_c = A - A_b$, where A is the area of the heater top surface. For a smaller channel width or a larger channel pitch, more of the heat leaves the heating surface by conduction. The fraction of bottom surface area exposed to conduction ranges from 50 to 90 % (see Table 4.1).

From the heat transfer data obtained with quartz structures (plotted in Figure 4.2) some remarks can be made. The thermal performance is expected to increase with the increase in A_b. However, the heat transfer data presented in Figure 4.2 indicate that the quartz structures perform similarly at all heat inputs. The quartz structures were attached to the heater using a thin layer of thermally conductive epoxy. The thickness of the bonding layer was measured to be around 50μm for all attached samples, so the thermal resistance of the epoxy layer is constant. The conclusion that can be drawn is that the area

participating in heat transfer is much less than the channels bottom area A_b. This can be explained by the fact that the vapor slugs seen in the bottom channels (see Figure 4.7(d)) form an insulating vapor layer close to the heat transfer surface. Heat transfer, therefore, occurs only through the liquid menisci held in the corners. The area occupied by these menisci is similar for all the structures tested, hence the similar performance. It is believed that increase in performance may be achieved by decreasing the channel pitch and thereby increasing the number of menisci.

For an open top configuration, the conducted fraction of the heat leaves the structure by external convection. This fraction of the heat transfer was found (Nakayama et al. (1980a)) to account for only 10 % at a heat flux of 0.1 W/cm^2 and for 70 % at a heat flux of 2 W/cm^2. Thus for the range of heat fluxes of interest in electronics cooling, the majority of heat leaves by external convection. By completely covering the top of the structure the decrease in performance is therefore expected, particularly at higher heat fluxes.

The boiling initiation is sometimes explosive and accompanied by a significant and rapid temperature drop. Marto and Lepere (1982) noticed a similar explosive initiation for a High-Flux surface. Figure 4.3 (a) presents a temperature record for structure C-0.105-0.7 capturing the heat-up process and the boiling incipience. The temperature is measured at a location below the structure bottom surface. The heat flux is stepped up at time t = 20 s to q'' = 0.85 W/cm^2 from the previous power level. Initially, the temperature increases without vapor bubbles being generated.

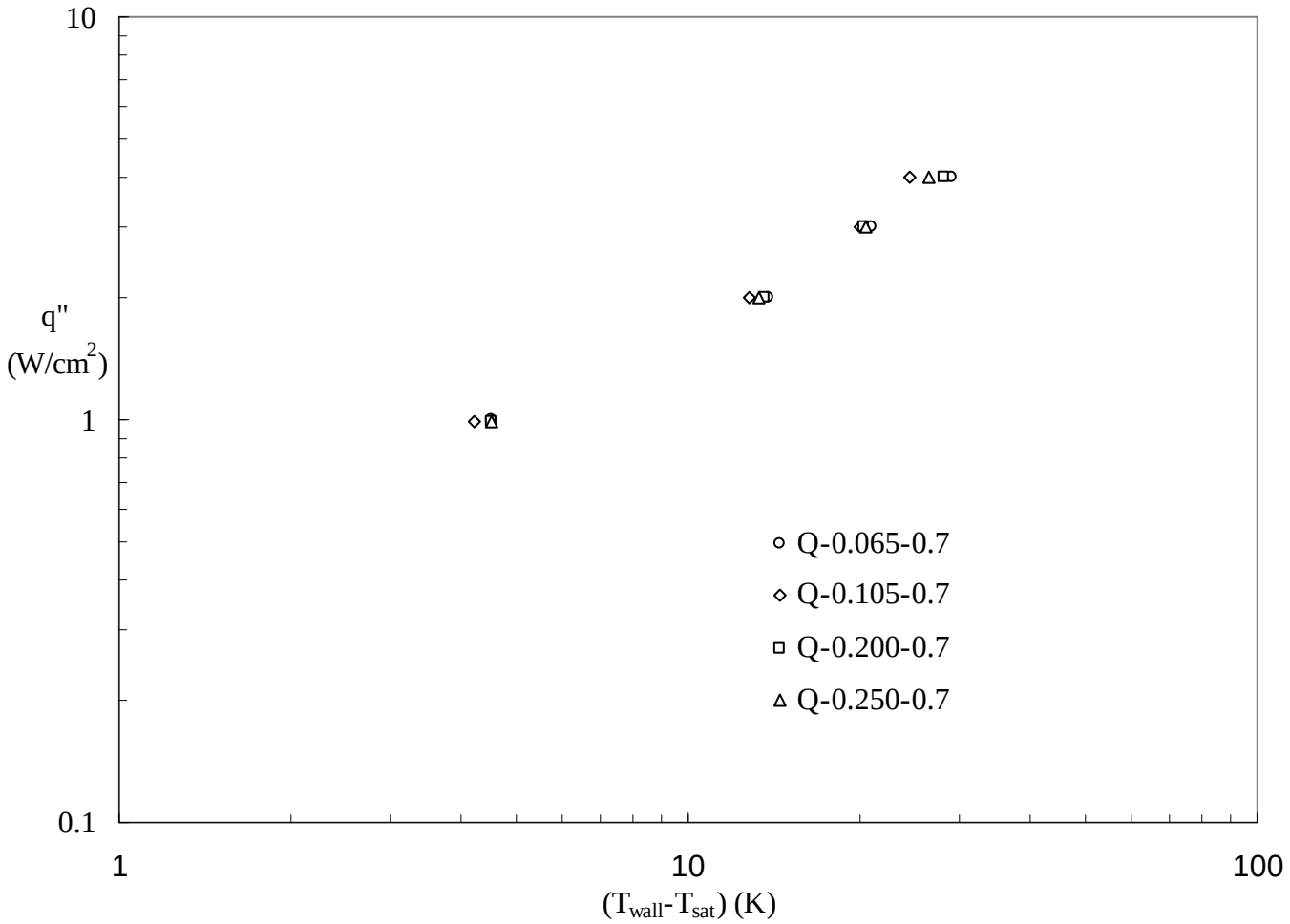

Figure 4.2 Boiling curves at saturation for quartz structures.
The maximum uncertainty is ± 0.25 K for (T_{wall}-T_{sat}) and ± 15 % for q"

As can be seen in Figure 4.3 (a) at time mark t = 283 s the boiling started from top channels. Subsequent activation occurred at t = 353 s. The arrows on the graph indicate these moments. Sudden and large drops in surface temperature accompany the boiling incipience. The steady-state zone of the measured temperature trace, which is considered to start at t = 400 s, is shown on Figure 4.3 (b). The surface temperature oscillations with time under nominally steady conditions are believed to be the effect of the transient bubble forming-releasing process inside the structure.

4.2. Visualizations

In order to better understand the boiling phenomena from the top-covered enhanced structures, high-speed visualizations were performed for both copper and quartz structures. In both cases, a quartz plate covering the top of the structures permitted visualization of liquid-vapor conditions inside the enhanced structure. The visualizations were performed from the top and lateral positions. The results of the photographic observations are presented in detail in the following sections.

4.2.1 Copper structures

For the opaque copper structures, visualizations can provide information only around the exterior envelope. Visualizations from the sides were performed for structures C-0.065-0.7, C-0.105-0.7 and C-0.360-0.7. The power input was applied in incrementing or decrementing steps. Upon addition of heat, vapor starts to form at random nucleation sites inside the structure and, due to buoyancy, accumulates in the top channels.

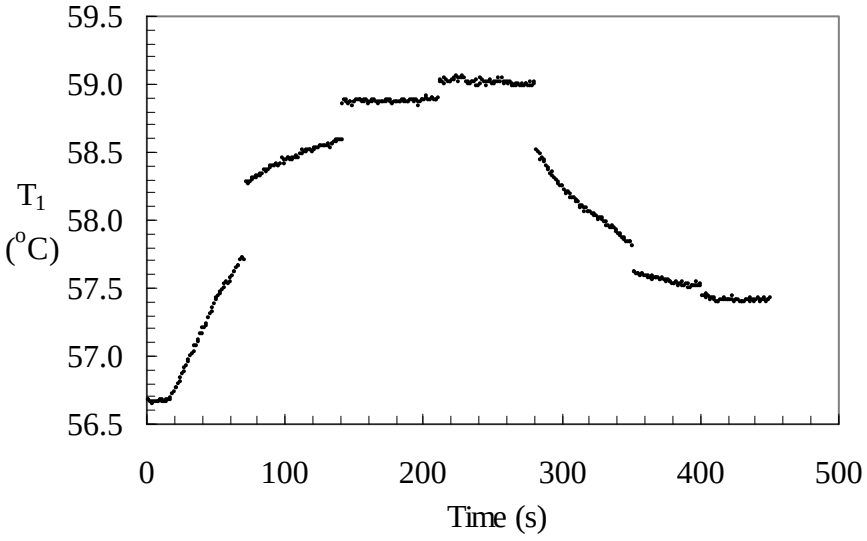

(a)

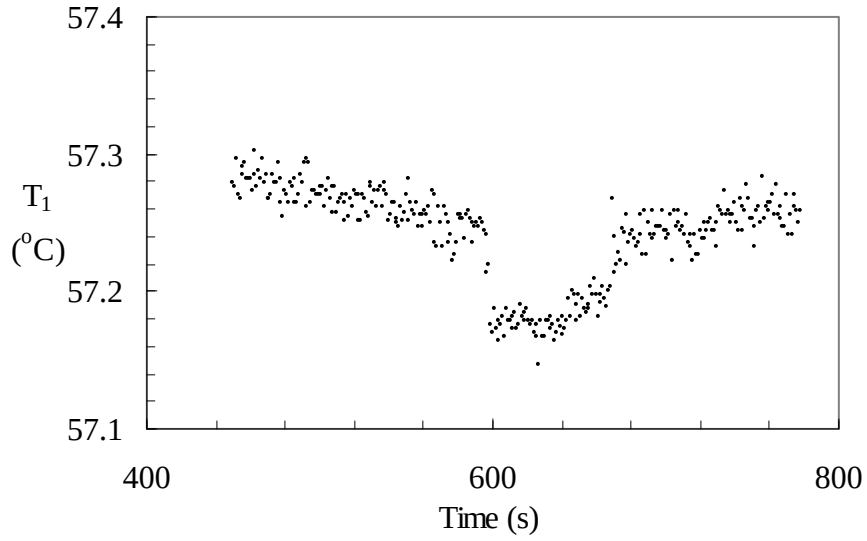

(b)

Figure 4.3 Wall temperature variation (structure C-0.105-0.7, q'' = 0.85 W/cm^2)
(a) temperature trace capturing pre - boiling and boiling inception
(b) steady-state zone of the temperature trace

The vapor formed inside the bottom channels migrates to the top channels through the pores. Due to the constraint exercised by the solid parts of the enhanced structure, the vapor bubbles deform and take the shape of slugs. In general, the significant bubble expulsion process initiates from the top channels. Typical sequences of boiling from structure C-0.065-0.7 are shown in Figure 4.4. The frames show the top channels row and were taken under decreasing heat flux conditions. At the lowest heat flux tested ($q^{"}$ = 0.35 W/cm^2) a few active sites were present. The vapor escaped mainly from the upper ends of the top channels in the shape of small, spherical bubbles. The bubbles maintain their individuality during the release process. At higher heat fluxes, more top channels become active (Figure 4.4 (a)). The bubble departure diameter increases, bubbles becoming elongated. Figure 4.4 (b) at a heat flux $q^{"}$ = 1.8 W/cm^2 shows an increase in the bubble departure diameter. However, the bubbles maintain their individuality. These are emitted from all the channel openings, indicating the extent of the vapor regions in the top channels. Bubbles ejected through the end of the channels act as little pumps allowing the pool liquid to enter the structure. The shape and volume of emitted bubbles change with the heat flux. Large, elongated bubbles are being laterally expelled with a high frequency for heat fluxes in excess of 5 W/cm^2 (Figure 4.4 (c)). Lateral coalescence of bubbles also occurs for heat fluxes in this range. At the highest heat flux tested, all top and the majority of bottom channels were active. Vapor agglomerates laterally in large formations (Figure 4.4 (d)). The process of re-wetting of the channels can be explained in reference to Figure 4.7 (d). When a vapor bubble is ejected from one channel, the liquid from the surrounding pool enters the channel along its corners. This is visually evident by the movement of the liquid menisci existent along the walls of the channel.

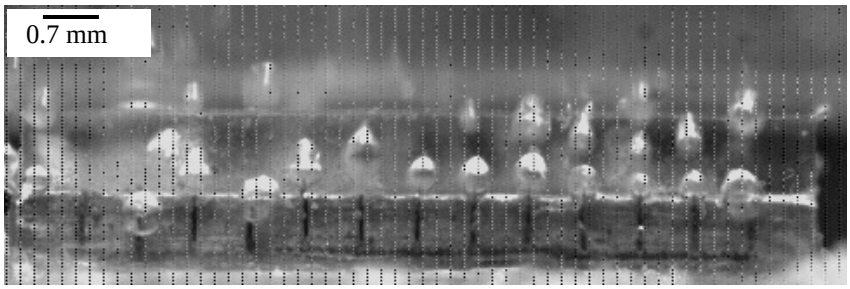

(a)

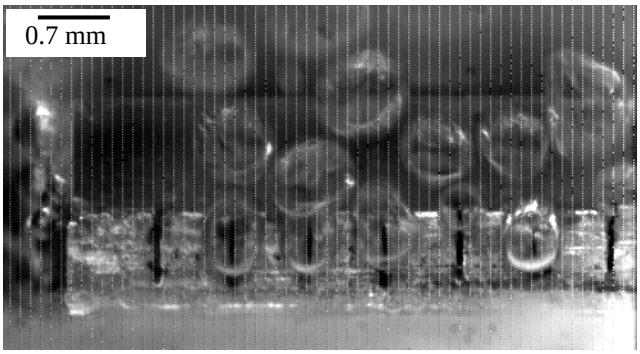

(b)

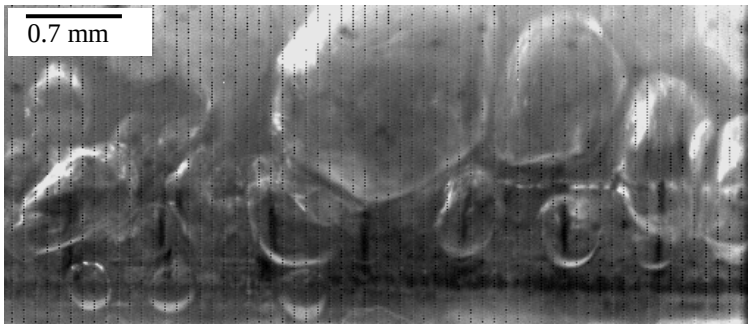

(c)

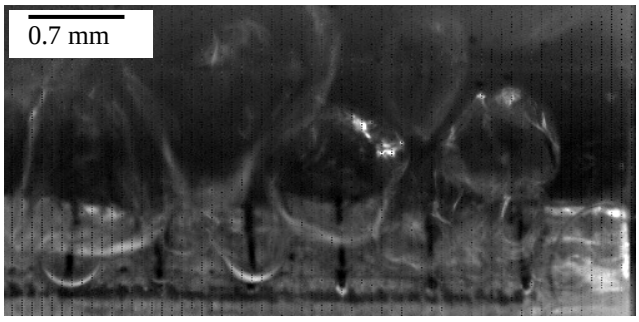

(d)

Figure 4.4 Lateral view of boiling from structure C-0.065-0.7, top channels (a) spherical bubbles are emitted, q'' = 0.8 W/cm^2 (b) larger bubbles are emitted, q'' = 1.8 W/cm^2 (c) big, elongated bubbles are emitted, q'' = 5.8 W/cm^2 (d) vapor bubbles coalesce laterally, q'' = 6.8 W/cm^2

Figure 4.5 presents boiling visualizations for the largest width structure (C-0.360-0.7), with increasing heat flux. Boiling started predominantly from the top channels (Figure 4.5 (a)) at the lowest heat flux tested (q'' = 1.4 W/cm^2). When a nucleation site is close to a bottom channel's end, vapor is seen exiting from the bottom (Figure 4.5 (b)). A nucleation site other than channel ends can also be observed in Figure 4.5 (b). With the increase in heat flux the number of active top (Figure 4.5 (c)) and bottom (Figure 4.5 (d)) channels increases. At even higher heat fluxes, lateral coalescence of bubbles occurs (Figure 4.5 (e), (f), (g)). Vapor agglomerates with a mushroom–like shape vertically (Figure 4.5 (h)) at the highest heat flux (q'' = 7.8 W/cm^2).

4.2.2 Quartz structures

A clearer image of the two-phase phenomena occurring inside an enhanced structure can be obtained through visualizations performed with structures made of transparent materials. For the present study, the material of choice was quartz. Table 2.1 summarizes the geometrical dimensions of the quartz structures employed in the current study. The parameters investigated were channel width and heat flux. Due to the low thermal conductivity of quartz (k = 1.2 W/m·K) the top boundary can be considered as nearly adiabatic, with the entire structure being held at saturation temperature (immersed in saturated PF 5060). The heat flux was increased stepwise until the wall temperature reached 85 ^{o}C, corresponding to a maximum heat flux of ~ 4 W/cm^2. The observed phenomena are graphically illustrated in Figure 4.6 and Figure 4.7 as plan views. Relative to Figure 2.2 (b), in the presented figures the top channels are oriented in the x direction whereas the bottom channels are oriented in the y direction.

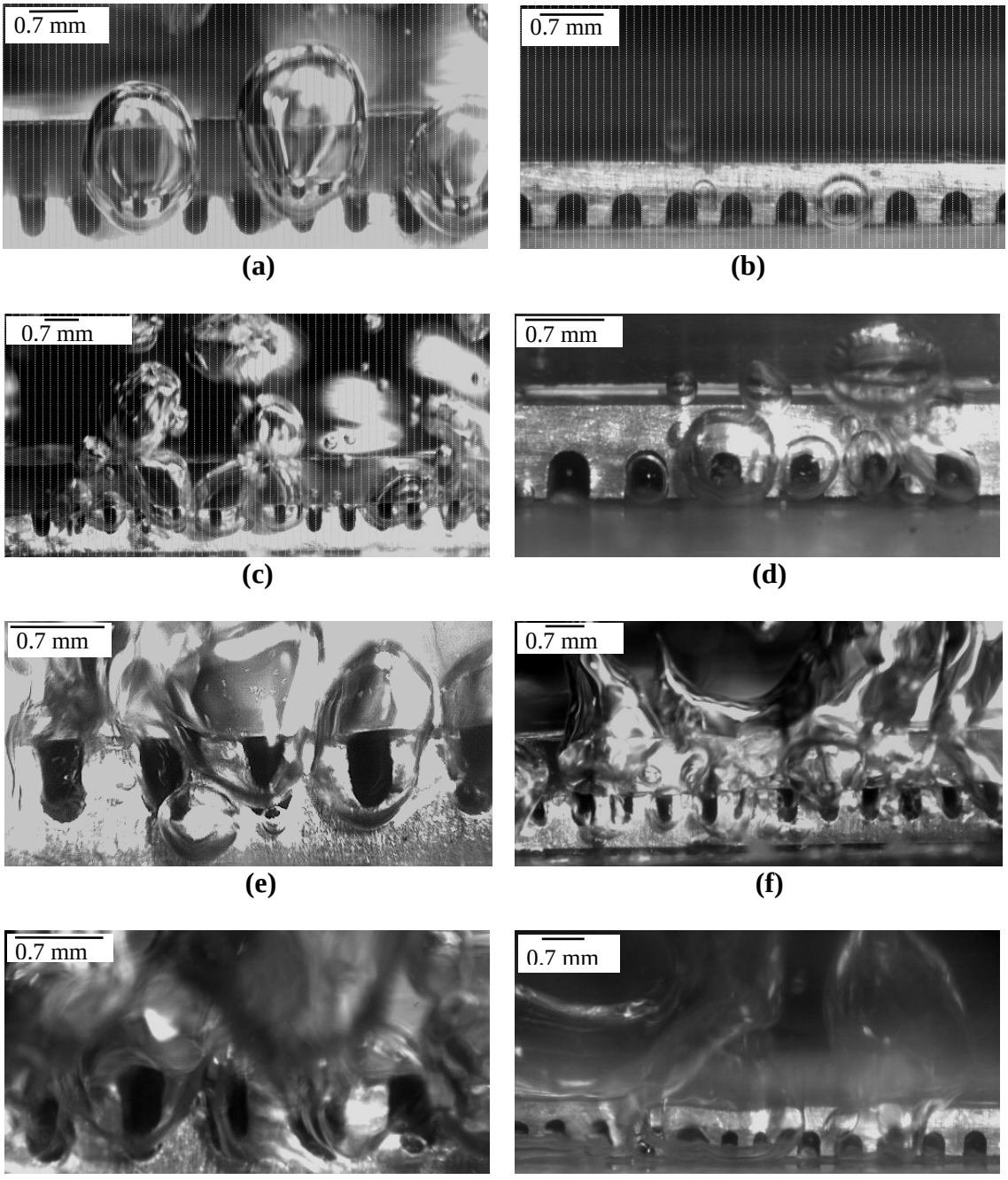

Figure 4.5 Lateral view of boiling from structure C-0.360-0.7, top channels (a) single bubble expulsion, top channels, q'' = 1.4 W/cm^2 (b) single bubble expulsion, bottom channels, q'' = 1.4 W/cm^2 (c) more top channels activate, q'' = 3.3 W/cm^2 (d) more bottom channels activate, q'' = 3.3 W/cm^2 (e) lateral coalescence, top channels, q'' = 6 W/cm^2 (f) lateral coalescence, top channels, lower magnification, q'' = 6 W/cm^2 (g) vapor mushrooms, top channels, q'' = 7.8 W/cm^2 (h) vapor mushrooms, bottom channels, q'' = 7.8 W/cm^2

Figure 4.6 presents pictures taken with increasing heat flux during boiling from structure Q-0.105-0.7. Prior to the heat addition, small portions of vapor were observed in the bottom channels (Figure 4.6 (a)). As the heat was added, extended vapor slugs (shown as black in accompanying cartoons) could be seen forming in the bottom and top channels (Figure 4.6 (b)). The slugs exhibit an oscillatory motion (with an average frequency of about 100 Hz); especially those formed in the top channels; when a vapor slug reaches the end of a channel, bubbles are expelled in the surrounding liquid pool. Upon further increase of heat flux, the bubble emission intensifies, as more channels become active. Due to the pumping action exercised by the bubbles, liquid plugs are observed forming in the top channels (Figure 4. 6 (c)). At the highest heat flux tested (q'' = 3.8 W/cm^2) almost all channels expel vapor bubbles (Figure 4.6 (d)) and liquid plugs occupy portions of the top channels.

Characteristics of boiling pertaining to structure Q-0.250-0.7 are presented in Figure 4.7. The pictures are selected from movies made at steady-state conditions with increasing heat flux. At low heat fluxes (q'' < 1.5 W/cm^2) the majority of top and bottom channels are already filled with vapor slugs (Figure 4.7 (a)). The vapor slugs show an oscillatory move towards the edges of the structure. There is no lateral vapor release. With increase in the heat flux, the oscillations intensify and vapor is expelled from the sides. Some of the vapor slugs present in the top channels display fragmentation (Figure 4.7 (b)). Due to the pumping action of the departing bubbles, liquid from the outside pool enters the channels forming plugs. These liquid regions can be clearly seen on central parts of some top channels (Figure 4.7 (c), q'' = 3.8 W/cm^2)).

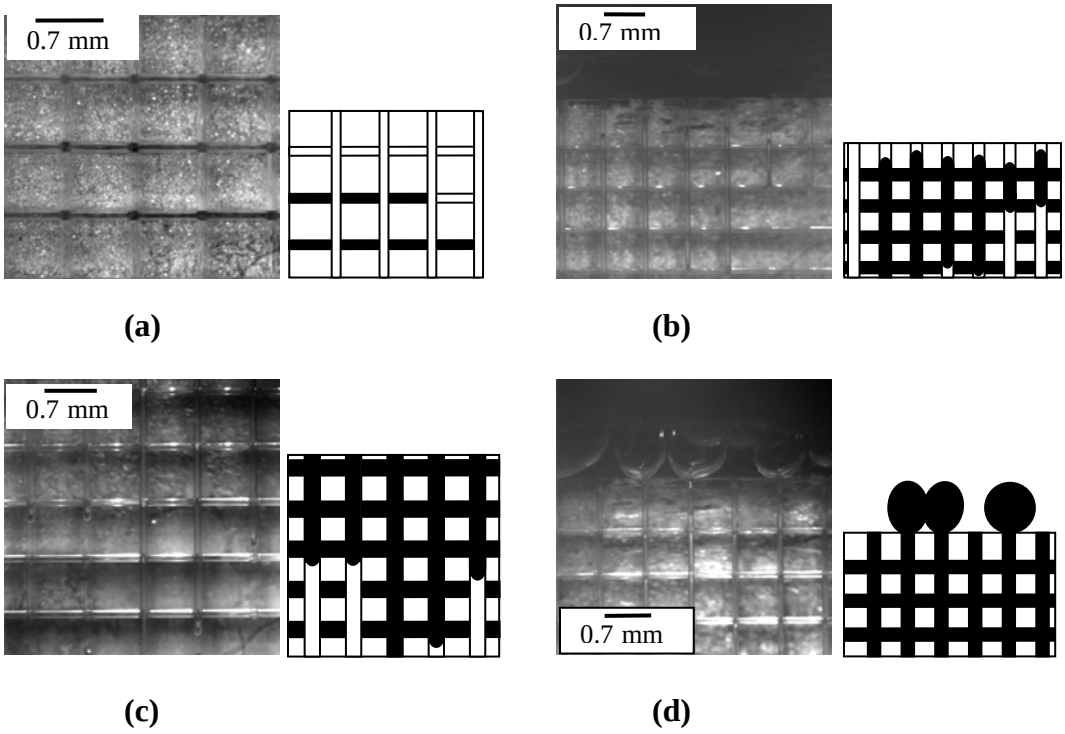

Figure 4.6 Boiling from structure Q-0.105-0.7
(a) unheated state, q'' = 0 W/cm^2
(b) vapor slugs in the top and bottom channels, q'' = 0.8 W/cm^2
(c) liquid plugs in the top channels, q'' = 1.8 W/cm^2
(d) intensified bubble expulsion, q'' = 3.8 W/cm^2

Figure 4.7 (d) (corresponding to the highest heat flux ($q^{"}$ = 3.8 W/cm^2)) presents a magnified view of a region of the structure near the edge. Vapor slugs can be seen in the bottom channels with thin liquid films existing between vapor and walls. In one of the top channels a discontinuity in the vapor slug (filled by a liquid plug) can be observed.

Summarizing, the following events were commonly observed for the channel widths investigated:

a) After degassing and cooling off, small portions of gas were seen in the bottom channels. This can be due to air entrapment during charging.

b) Vapor formation started at 0.8 W/cm^2 from nucleation sites located on the heated surface (bottom channels). The produced vapor migrated to the top channels through the pores and coalesced forming slugs. Upon reaching steady state, most of the top channels were filled with vapor. The vapor slugs showed an oscillatory move. At low heat fluxes the slugs do not reach the sides of the structure, oscillating inside. In some instances the vapor slugs in the top channels expand towards the bottom channels through the pores. The oscillatory move of the vapor slugs is a proof of the intermittent vapor formation, at discrete points on the heating surface. Liquid films were observed in the channels along the edges.

c) The increase in the heat flux does not change the phenomena described above; it increases the frequency of vapor slug oscillation and the number of expulsion sites. The slugs expand and vapor expulsion activity intensifies from the sides. As a result, lateral coalescence occurs. When a bubble departs, the pressure inside the vapor slug decreases and the slug retreats. At this moment liquid from the pool enters the channel.

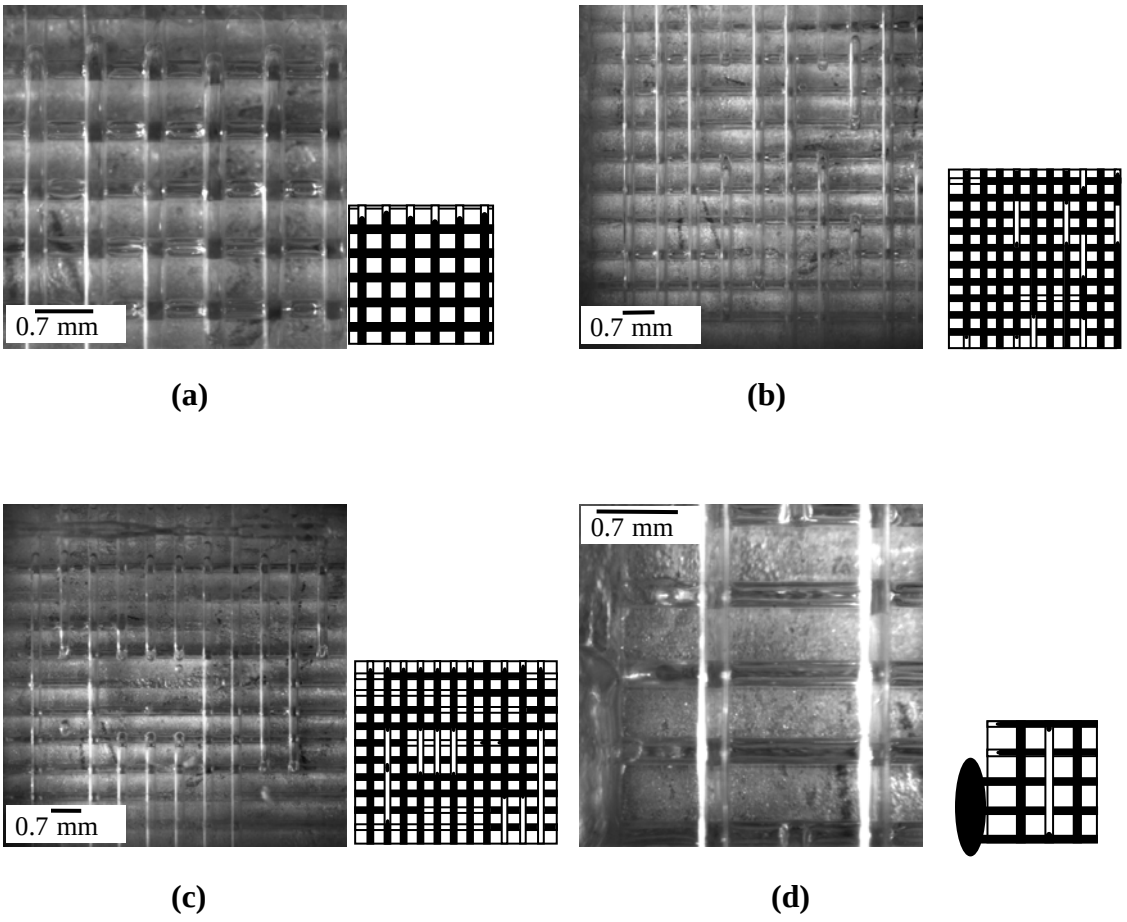

Figure 4.7 Boiling from structure Q-0.250-0.7
(a) vapor slugs form at lowest heat flux, q'' = 0.8 W/cm^2
(b) some vapor slugs become discontinuous, q'' = 2.8 W/cm^2
(c) liquid plugs in top channels, q'' = 3.8 W/cm^2
(d) magnified view of a liquid plug, q'' = 3.8 W/cm^2

When the bubbling activity intensifies, liquid plugs were seen in the top and bottom channels. This phenomenon happens at heat fluxes $q'' \geq 2$ W/cm^2.

4.3 Comparison between copper and quartz structures

For the same geometry, along with the expected decrease in performance indicated by the boiling curves, several dissimilarities between boiling from copper and quartz structures are present. At the same heat flux, more nucleation sites form on the internal and external surfaces of the copper structures. The formation of extra nucleation sites is driven partly by the larger wall temperature available in the copper case. As a result, the evaporation process is intensified. Vapor is released in the form of bubbles having significantly different departure diameters (Figure 4.5 (c), (d)).

Despite the large difference in thermal conductivity between copper and quartz, it is believed that the visualizations employing transparent structures capture the essential characteristics of boiling under complete confinement. The oscillatory movement of the vapor slugs, vapor expulsion followed by slug retreat and liquid entering the channels, as well as first activation of top channels are phenomena observed in the visualizations experiments with both types of structures.

4.4 Summary

The present study investigates the nucleate pool boiling from enhanced structures under total confinement. Through heat transfer measurements and high-speed visualization the underlying phenomena are illuminated. The study establishes the oscillatory move of the vapor/liquid interfaces as the main characteristic of the

liquid/vapor dynamics inside the enhanced structure, regardless of geometric parameters. This confirms the dynamic nature of the boiling process. Additionally, the following conclusions are drawn from the study:

a) The heat transfer performance of the enhanced structures with insulated top decreases significantly in comparison to the open top situation. However, there is a certain range of heat fluxes (1 W/cm^2 < q'' < 4 W/cm^2) for which the top-covered structure outperforms a plain structure with the top open.

b) The heat transfer performance of the enhanced structure with insulated top has only a marginal dependence on the channel width. It is hypothesized that the channel pitch may have a bigger influence through the number of menisci created inside the channels.

c) The boiling curves obtained with enhanced structures completely confined show no change in slope over the tested heat flux range; however, the visualizations indicate the presence of two boiling regimes: slug predominance regime and slugs and plugs regime.

d) The internal evaporation process is an important heat transfer mechanism; its contribution to the total dissipated heat is significant, especially at low heat fluxes.

e) Vapor slugs exist in the top and bottom channels even for the lowest heat fluxes and exhibit an oscillatory movement. This is believed to be an effect of the transient nature of internal evaporation.

CHAPTER 5: POOL BOILING UNDER TOP CONFINEMENT

Nucleate pool boiling, a very efficient way of transferring heat from a surface to a stationary bulk liquid, can be further intensified using enhanced structures. This has been proved extensively in literature as well as in the present study (see Chapter 3). Most of the published studies on this topic have treated only the unconfined case. That is, the movement of vapor/liquid was unrestricted around the structure. Pool boiling in confined spaces has applications in electronics cooling, where the available space is at a premium. Thus the assessment of boiling heat transfer under tight spatial constraint conditions and its comparison with the open top case is of significant importance.

The present study intends to clarify the influence of top confinement on boiling heat transfer from enhanced structures. The boiling is characterized by identifying the regimes (modes) established for different top gaps and heat flux levels. The gap between the enhanced structure and the confinement plate constitutes the main geometrical parameter varied in several steps. Boiling curves and high-speed visualizations of the boiling at maximum frame rate of 2,100 frames/s were obtained to elucidate the complicated boiling phenomena.

5.1 Boiling curves

The boiling curves obtained for various top gaps for the copper structure C-0.105-0.7 are presented in Figure 5.1. The presence of a confining plate at a certain distance above the top surface of the enhanced structures changes the shape of the boiling curve relative to the open top case. The plate restricts the vapor/liquid movement above the

structure; it is therefore expected that the boiling phenomena will differ from the open top case. For an open case configuration, the vapor rises unrestricted towards the free surface of the liquid pool. With a confining plate, the vapor accumulates at the top quartz surface prior to leaving laterally.

The shift to the left of the boiling curves with increasing S indicates improvement in heat transfer performance, nearly approaching the unconfined pool boiling performance for S = 13 mm. Two features are particularly remarkable from the examination of the boiling curves. First, the enhancement of heat transfer over the open case at low heat fluxes is no more present. This result is in contrast with the data reported for plain surfaces (Katto and Yokoya (1966), Katto et al. (1977)), but similar to the findings of previous investigations involving enhanced structures (Nowell et al. (1995), Chien and Chen (2001)). The particularity of boiling from enhanced structures is the generation of vapor primarily inside the structure, followed by its ejection into the surrounding pool of liquid. The bubble nucleation is therefore replaced by vapor expulsion from specific locations. A possible explanation for the lack of enhancement is based on the fact that enhanced evaporation is already taking place inside the structure. The nature of the working fluid employed also plays a significant role. For PF 5060, the latent heat of vaporization is very low (h_{fg} = 88 kJ/kg at atmospheric pressure) compared to coolants such as water; used by Katto and Yokoya (1966), for instance.

The second characteristic feature in Figure 5.1 is the decrease in performance with decreasing S at high heat fluxes. The largest heat flux attainable (with the wall temperature maintained below 85 ^{o}C) increased with the increase of the top spacing.

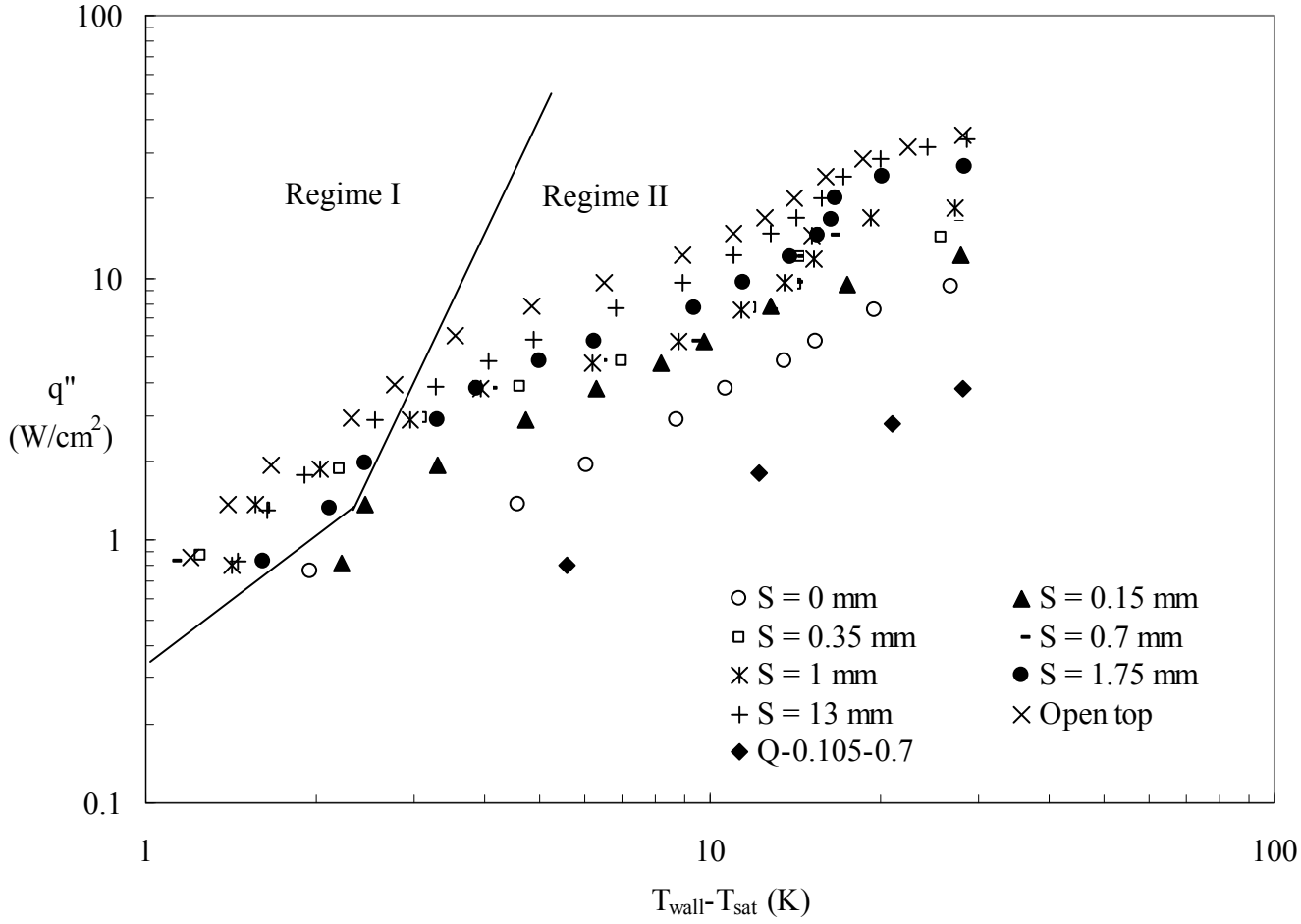

Figure 5.1 Boiling curves for various top gaps. The lines delineate the observed flow regimes. The maximum uncertainty is ± 0.23 K for (T_{wall}-T_{sat}) and ± 14 % for q"

This value was not known a priori; therefore a trial and error method was applied to arrive at the highest value of q'' with the maximum surface temperature of 85 ^{o}C. For S = 0.15 mm, the highest heat flux is q'' = 12.2 W/cm^2. This value increase to q'' = 26.6 W/cm^2 for S = 1.75 mm. A top space of 13 mm ensures a similar performance at high heat fluxes as for open top.

The shapes of the boiling curves plotted in Figure 5.1 reflect the effect of confinement on the boiling from enhanced structures. For S = 0 mm (completely closed top) the curve is almost linear (in log-log coordinates). This case has been treated in detail in Chapter 4. As the top gap increases, the corresponding boiling curves deviate from the linearity. A common characteristic of curves for S = 0.35-1.75 mm is their S shape. At low heat fluxes the curves are almost linear with a steep slope yielding a high heat transfer coefficient. For the intermediate range of heat fluxes the curves become concave. The slope of the curve decreases corresponding to a decrease in performance. This decrease in performance can be attributed to a change in the liquid/vapor conditions in the space above the enhanced structure. The increase in vapor production is not doubled by a corresponding increase in the vapor release capability. This creates an almost stationary vapor blanket on top of the enhanced structure, as seen in the visualizations later. An almost vertical region follows the concave portion of the boiling curve. It is believed that a very efficient (high heat transfer coefficient) mode of boiling, valid for a narrow range of heat fluxes and top gaps, is established. Finally, the curves take a convex, descendent form.

Figure 5.1 also includes a boiling curve for structure Q-0.105-0.7. The results correspond to a top gap S = 0.5 mm. The curve displays the expected decrease in thermal

performance due to the additional thermal resistance of the transparent enhanced structure.

A comparison of the present boiling data and the results of Chien and Chen (2001) is presented in Figure 5.2. A set of data from the current investigation (for S = 0.6 mm) is plotted along with a boiling curve from their study (for S = 0.5 mm). The authors did not report data for heat fluxes $q'' \leq 3$ W/cm^2. For intermediate heat fluxes (4 W/cm^2 $\leq$ q'' $\leq$ 14 W/cm^2) their enhanced structures exhibited a much better heat transfer performance. The two curves intersect at higher heat fluxes ($q'' \geq 14$ W/cm^2). Several differences in the experimental conditions should be mentioned: the Chien and Chen (2001) data are obtained with cross-grooved enhanced structures placed vertically in a pool of HFC4310 at saturation (T_{sat} = 75.5 ^{o}C at atmospheric pressure). The vertical configuration may have a beneficial effect on the heat transfer performance, due to buoyancy induced circulation. The data from Chien and Chen (2001) were used for comparison in the present study as the closest match in experimental conditions that could be found in the literature.

The steady-state temperature measurements show interesting characteristics. A sufficiently long time (1 hour nominally) was allowed to pass between the application of power level and the start of data collection. Figure 5.3 presents several temperature records for q'' = 12 W/cm^2, each corresponding to a different top gap S. Figure 5.3 (a) (S = 0.35 mm) shows a fairly smooth temperature profile, with one spike of ~ 1 ^{o}C.

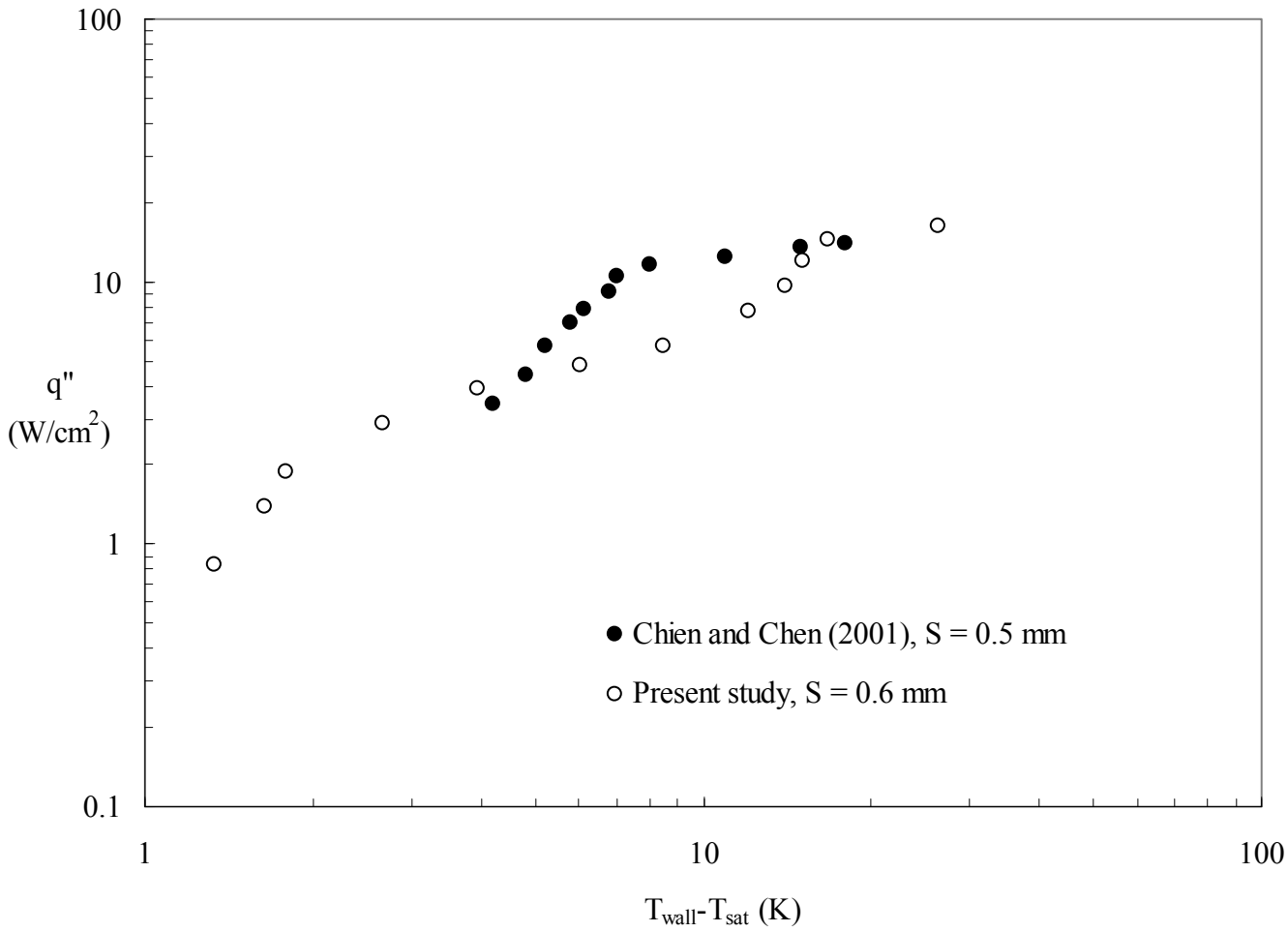

Figure 5.2 Comparison between present data and Chien and Chen (2001) data
The maximum uncertainty is ± 0.23 K for (T_{wall}-T_{sat}) and ± 14 % for q"

The dominant frequency obtained using a Fast Fourier Transform is 0.01 Hz. A considerable difference between the maximum and minimum recorded temperatures (~ 1.5 ^{o}C) characterize the temperature recording for S = 1 mm (Figure 5.3 (b)). As the top gap increases, the temperature trace presents oscillations of lesser amplitude (1.2 ^{o}C) (Figure 5.3 (c), S = 1.75 mm). This is probably the effect of the decreasing influence of the confining plate on the boiling phenomena with increasing top gap S .Figure 5.3 (d) (recorded for a maximum top gap tested S = 13 mm) displays a temperature profile with minimum/maximum values within 0.5 ^{o}C. For this last case, the dominant frequency is higher (0.04 Hz). It can be inferred that as top gap increases, the vapor formations depart easier from the space above the structure. This fact is reflected in the dominant frequency captured in the FFT.

5.2 Visualizations

High-speed visualizations were performed from the top and sides of enhanced structures made of both copper and quartz. The quartz plate placed parallel to the top surface of the structure (Figure 2 (b)) permitted visualization of liquid-vapor conditions above the enhanced structure. The acquired data consisted of movies and still pictures. The photographic observations are described in the following sections.

5.2.1 Copper structure

The enhanced structure C-0.105-0.7 was employed for both heat transfer measurements and flow visualizations. A frontal top view of the structure is presented in Figure 2.1 (a). Figures 5.4 through 5.7 present the boiling phenomena for selected top gaps.

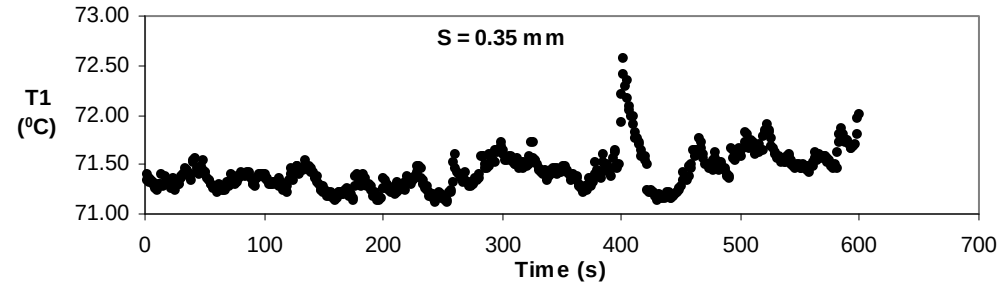

(a)

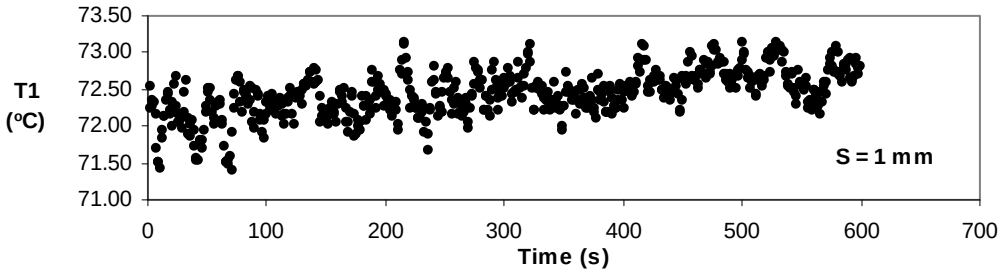

(b)

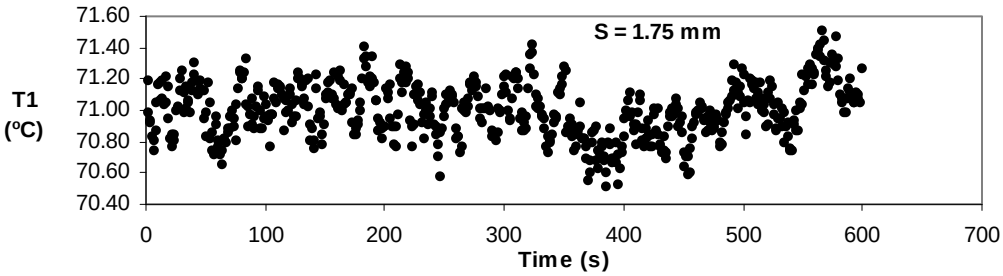

(c)

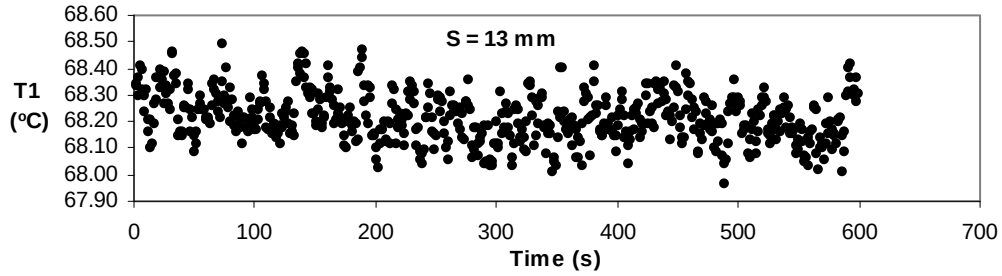

(d)

Figure 5.3 Temperature traces at steady state condition (structure C-0.105-0.7, q'' = 12 W/cm^2)
(a) S = 0.35 mm (b) S = 1 mm
(c) S = 1.75 mm (d) S = 13 mm

a) S = 1.75 mm

Figure 5.4 captures representative instances of boiling for top gap S = 1.75 mm. The influence of the confining plate is weakly felt for the low heat fluxes. Since the distance between the confining plate and the structure is quite large, the bubbles could be observed forming and emerging from the structure at low heat fluxes. Figure 5.4 (a) presents the boiling phenomena at the lowest heat flux tested (q'' = 0.8 W/cm^2). Bubbles can be seen emerging from the sub-surface pores and feeding larger vapor formations at the top surface. The inactive pores (the shining spots on the left side of the structure) can also be noticed. No bubble nucleation from the top surface of the structure was observed. With the increase in heat flux, the vapor fills almost entirely the space above the structure (Figure 5.4 (b), q'' = 5.7 W/cm^2). However, the vapor formations maintain their individuality. An even higher level of heat flux brings about more dynamic vapor behavior: the vapor masses coalesced almost entirely, and the upper vapor/liquid interface becomes wavy. As a result, the top surface of the enhanced structure cannot be seen clearly anymore (Figure 5.4 (c), q'' = 14.5 W/cm^2). The last picture of this set shows a single vapor cluster above the structure, with a wavy interface (Figure 5.4 (d), q'' = 24.4 W/cm^2).

b) S = 1 mm

Starting at the lowest tested heat flux (q'' = 0.9 W/cm^2) vapor formations could be seen accumulating at the top of the structure. These vapor masses are the result of the coalescence of small bubbles emerging from the pores (Figure 5.5 (a)). With the increase in heat flux, the fraction of the top surface filled with vapor formations increases.

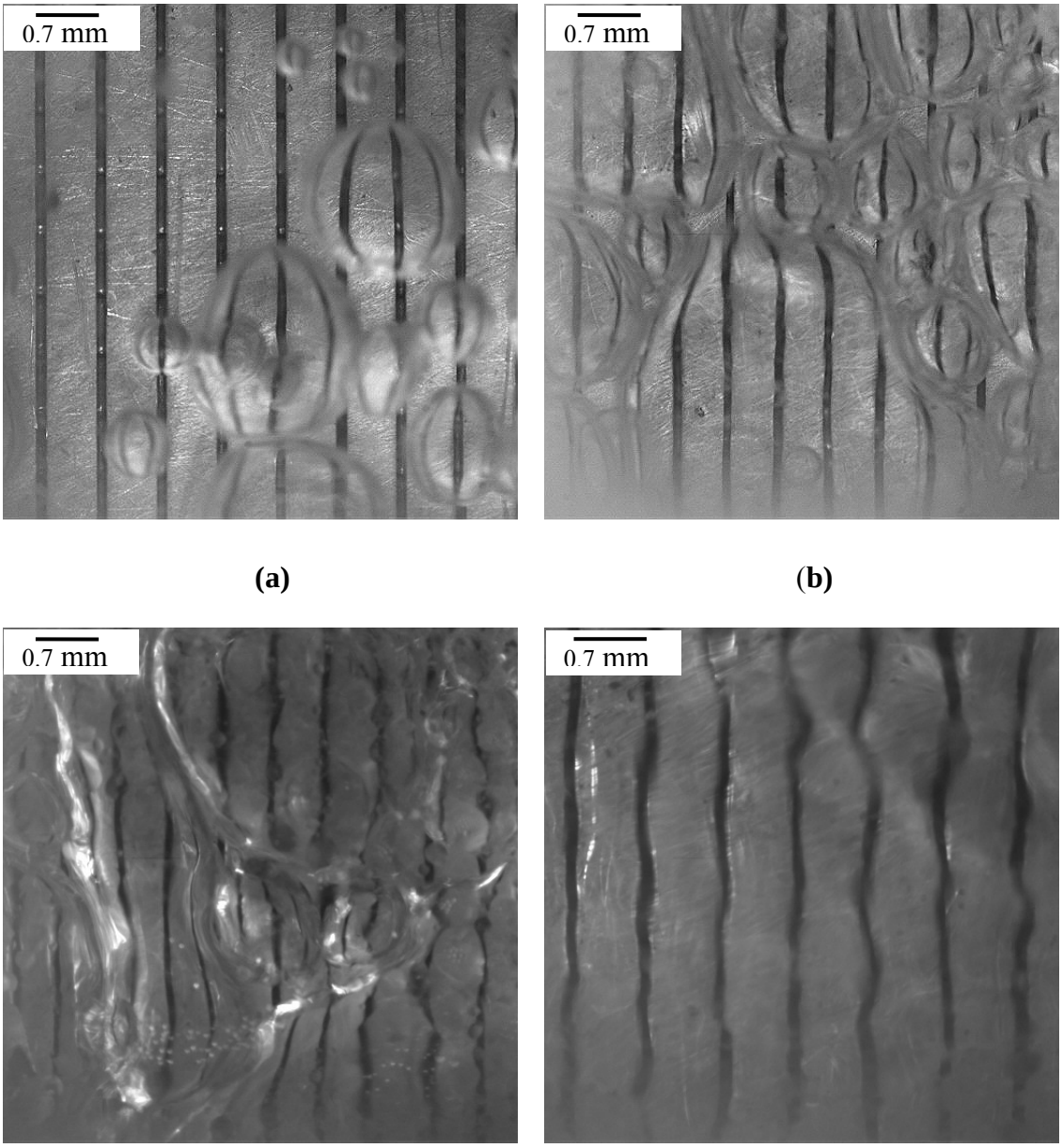

Figure 5.4 Visualization of boiling for top gap S = 1.75 mm
(a) individual bubbles are present, q'' = 0.8 W/cm^2
(b) coalescence occurs producing bubble clusters, q'' = 5.7 W/cm^2
(c) almost entire space is filled with vapor, q'' = 14.5 W/cm^2
(d) vapor filled space with a wavy interface, q'' = 24.4 W/cm^2

In Figure 5.5 (b) (q'' = 5.6 W/cm^2) several individual bubbles feeding the coalesced vapor regions from underneath (top right corner) are noticeable. A higher magnification is used to illustrate specific vapor formations occurring at a higher heat flux (Figure 5.5 (c), q'' = 14.5 W/cm^2). Liquid droplets start to adhere to the lower surface of the confining quartz plate. Some of the events occurring at the highest heat flux tested are shown in Figure 5.5 (d). Remarkable are the wavy interface and the liquid encapsulated in elongated slugs. Due to the wavy liquid/vapor interface, the individual bubble feeding could not be observed for this level of heat flux.

c) S = 0.7 mm

Further decreasing the top gap makes the confinement influence more pronounced. Figure 5.6 (a) presents a side view of phenomena occurring at q'' = 0.8 W/cm^2. This lateral view shows two bubbles emerging from the structure and feeding the vapor space above. The bubbles are bell-shaped. For better visibility, these are marked with black lines. At a higher heat flux (q'' = 3.8 W/cm^2) vapor formations occupy the majority of the top space, with some individual bubbles still visible (Figure 5.6 (b)). At higher heat flux (q'' = 7.6 W/cm^2) the upper liquid/vapor interface becomes wavy, with some liquid droplets residing on the surface of quartz plate facing the enhanced structure (Figure 5.6 (c)). At a much higher heat flux, liquid portions taking the shape of slugs entrapped in the vapor mass are noticed (Figure 5.6 (d)). (q'' = 16.5 W/cm^2).

d) S = 0.35 mm

A sequence of 8 frames captured at a rate of 500 frames/s is presented in Figure 5.7 (a). It shows the growth and coalescence of two individual flattened bubbles for q'' = 0.9 W/cm^2.

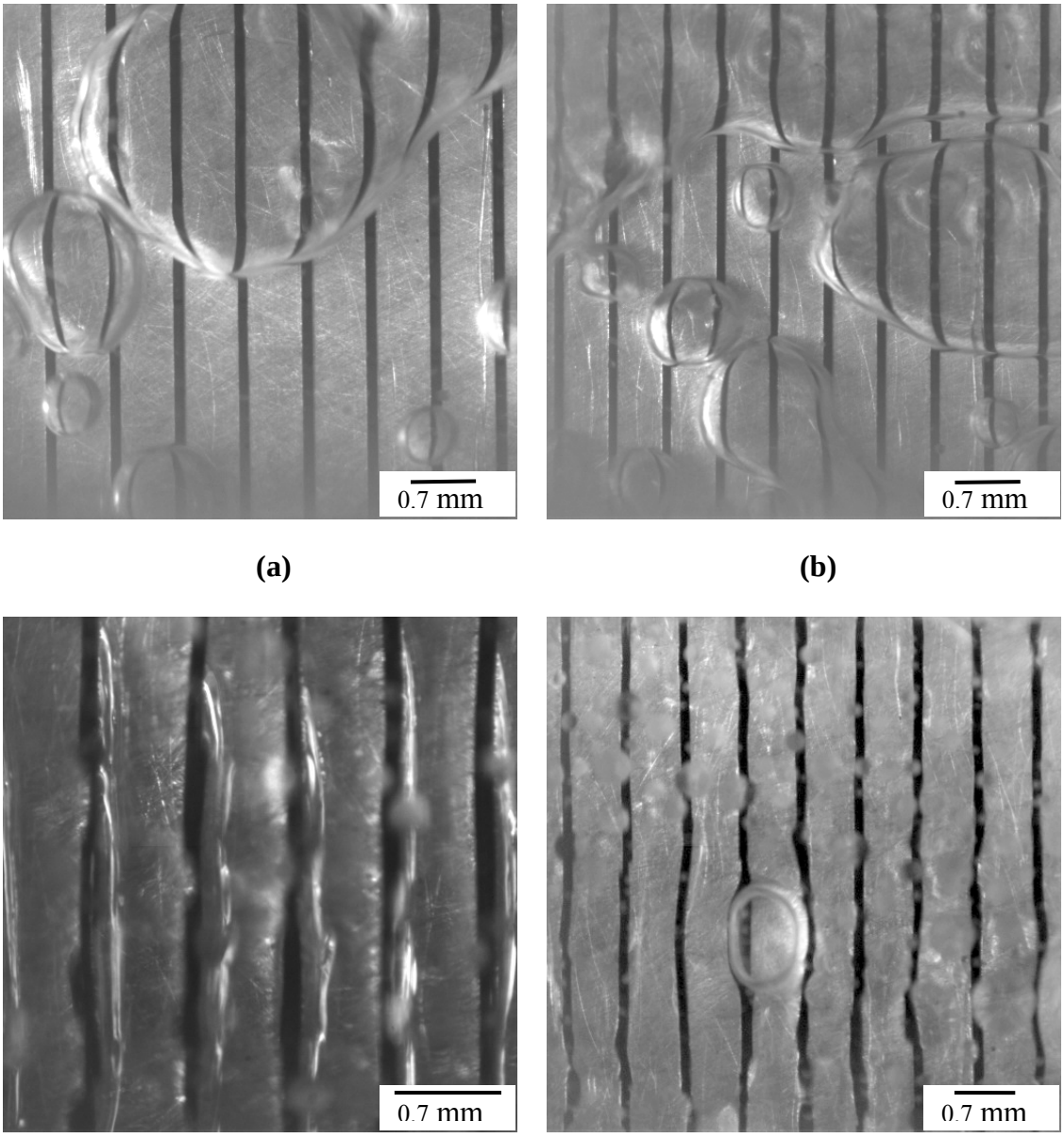

Figure 5.5 Visualization of boiling for top gap S = 1 mm
(a) vapor covers portions of the top surface, q'' = 0.9 W/cm^2
(b) individual bubbles are feeding the vapor formations from below, q'' = 5.6 W/cm^2
(c) higher magnification view of the top channels, q'' = 14.5 W/cm^2
(d) boiling phenomena at the highest tested heat flux, q'' = 18.3 W/cm^2

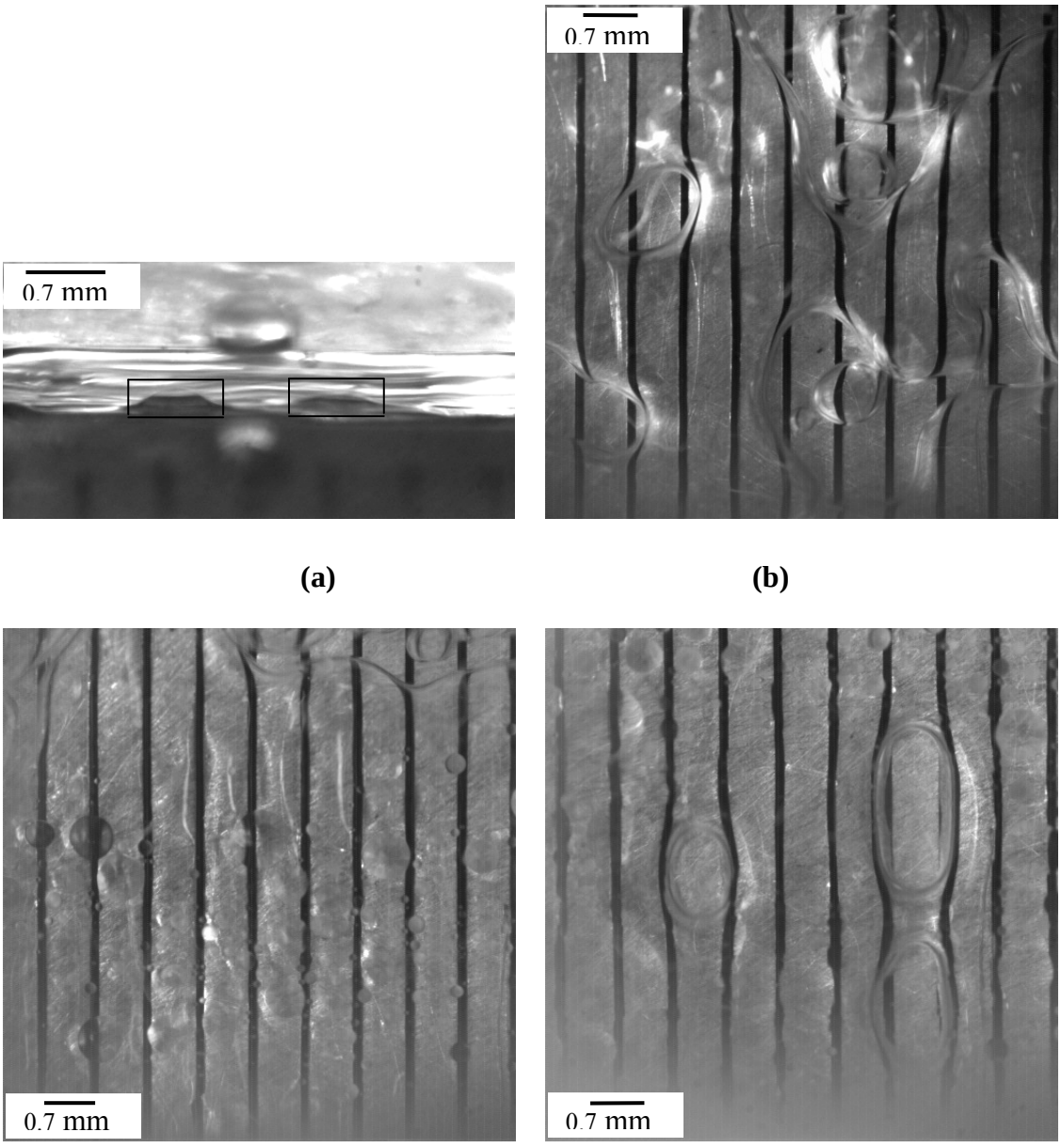

(a) **(b)**

(c) **(d)**

Figure 5.6 Visualization of boiling for top gap S = 0.7 mm
(a) lateral view of two bubbles entering the vapor mass, q'' = 0.8 W/cm^2
(b) coalesced vapor formations occupy much of the top space, q'' = 3.8 W/cm^2
(c) wavy interface, droplets on top surface, q'' = 7.6 W/cm^2
(d) liquid plugs entrapped in the vapor mass, q'' = 16.5 W/cm^2

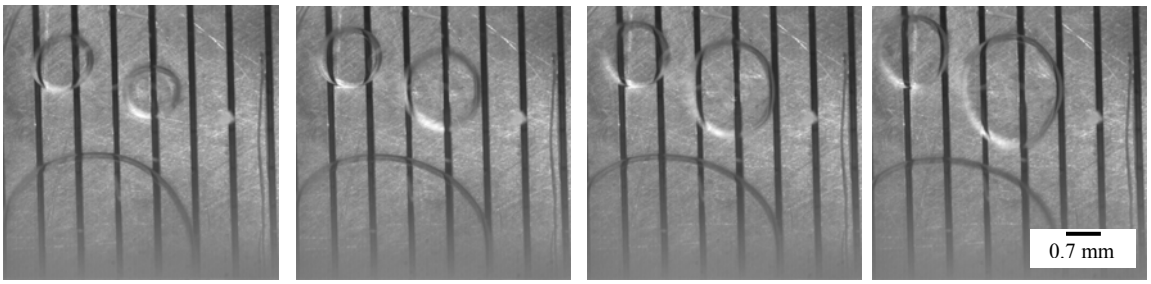

t = 0 ms **t = 4 ms** **t = 8 ms** **t = 12 ms**

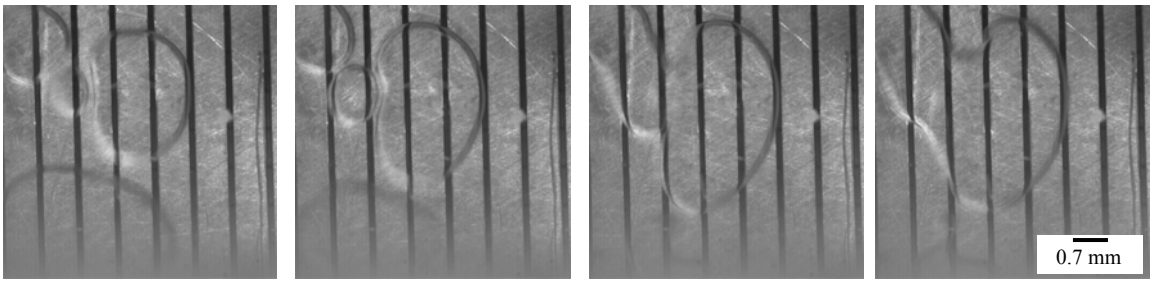

t = 16 ms **t = 20 ms** **t = 24 ms** **t = 26 ms**

(a)

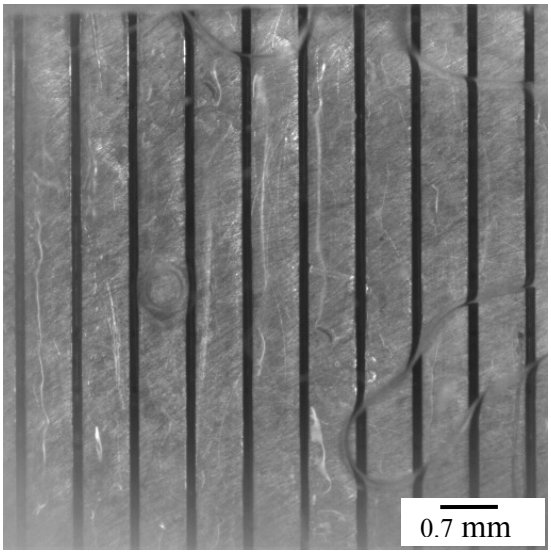

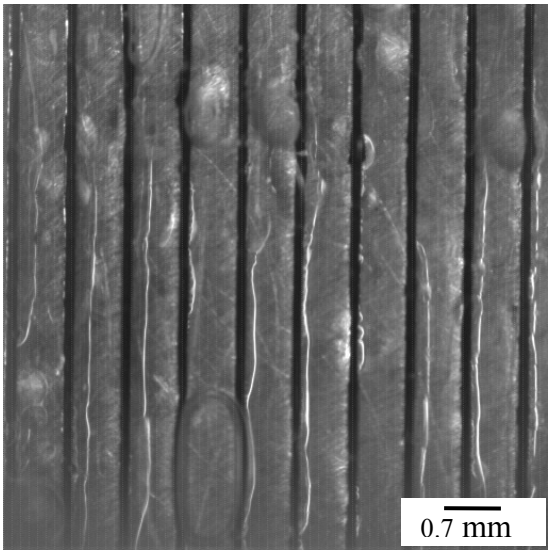

(b) **(c)**

Figure 5.7 Visualization of boiling for top gap S = 0.35 mm
(a) growth and coalescence of two individual bubbles, q'' = 0.9 W/cm^2
(b) thin liquid films forming on the top surface, q'' = 5.8 W/cm^2
(c) thin liquid film edges and liquid plugs, q'' = 14.3 W/cm^2

The frames presented are 4 ms apart; except the last two which are 2 ms apart. The limited space available above the structure forces the bubbles to grow laterally. At some point, coalescence occurs and larger vapor clusters form. Another feature revealed by the visualizations was the existence of thin liquid films between the top surface of the structure and the vapor mass (Figure 5.7 (b), q'' = 5.8 W/cm^2). The edges of the films are more clearly seen in Figure 5.7 (c) (q'' = 14.3 W/cm^2). Liquid entrapment in the form of slugs takes place; such a formation is visible at the bottom of the image.

5.2.2 Quartz structures

Intrinsic limitations restrict the amount of information offered by visualizations from the copper enhanced structure. The accessible regions are the envelope surfaces of the structure and partially the top channels. The use of a transparent material for the enhanced structures can extend the field of view and lead to a qualitative understanding of the two-phase phenomena occurring in the interior of the structure. Quartz was chosen for the current investigation due to its easy manufacturability. The detailed geometrical dimensions for the quartz structures employed in the current study are included in Table 2.2. Figures 2.1 (d) and (e) illustrate magnified lateral and frontal views of two top channels. The visualizations, performed from above the structure, provide useful insights. Due to the transparent nature of quartz, the bottom channels are available for optical investigation. In Figure 5.8, S = 0.5 mm, the top channels are oriented vertically and the bottom channels horizontally.

Boiling started at discrete sites located on the heated surface of the bottom channels. Once a nucleation site becomes active, the vapor bubble, bounded by the channels walls, expands laterally and towards the top channels through the pores. The vapor takes the shape of an elongated slug, which advances and retreats periodically. The region above the structure is only partially occupied by flattened vapor bubbles (Figure 5.8 (a), $q^{"}$ = 1.8 W/cm^2). No vapor formation can be seen in most of the channels. Maintaining the same heat flux, a higher magnification view (Figure 5.8 (b)) allows the observation of liquid films formed between the advancing vapor slug and solid walls. The slug forms below a vapor formation situated in the top gap formed between the enhanced structure and the confining quartz plate. The increase in heat flux increases the quantity of vapor produced in the bottom channels and released towards the top of the structure. Figure 5.8 (c) ($q^{"}$ = 3.8 W/cm^2) presents a few top channels being supplied with vapor from the bottom channels. This vapor advection takes place through the pores. The vapor takes an elongated form, expanding laterally prior to joining the vapor mass residing above the structure. For the highest heat flux tested with the quartz structure (Figure 5.8 (d), $q^{"}$ = 4.8 W/cm^2), vapor fills the entire top gap, with a few liquid portions towards the edges of the structure. Vapor slugs of various lengths, emerging from the pores, can be seen in the top channels.

The advancing/receding vapor slugs constitute the main feature of boiling from enhanced structures. With the increase in the heat input, more vapor slugs are forming. They are moving faster along the channels; their lifetime decreases considerably. Coalescence/breakage occurs at a higher rate.

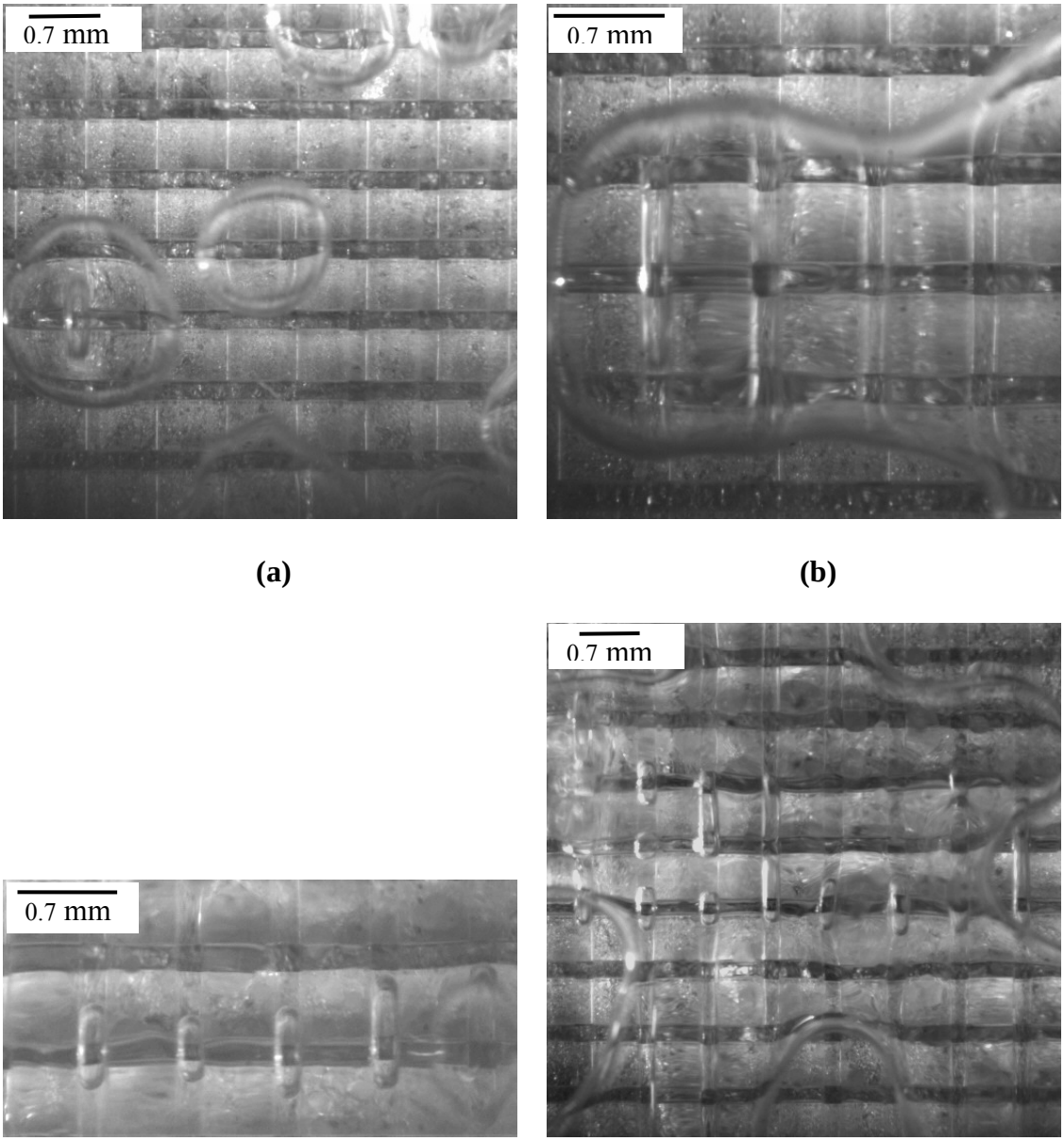

Fig. 5.8 Visualization of boiling for structure Q-0.200-0.7
(a) a few flattened vapor bubbles rise above the structure, q'' = 1.8 W/cm^2
(b) vapor slug forming inside a bottom channel, q'' = 1.8 W/cm^2
(c) deformed vapor bubbles reside in the top channels, q'' = 3.8 W/cm^2
(d) vapor fills the entire gap space, q'' = 4.8 W/cm^2

5.3 Discussion

Despite the fact that two orders of magnitude separate the values of copper and quartz thermal conductivity, the visualizations performed with transparent structures provide useful information about the specifics of boiling from enhanced structures in general. These observations can be extrapolated to the phenomena occurring with copper structures. It is assumed that the mechanism of vapor formation and coalescence in the bottom channels, followed by migration to the top channels through the pores, is similar. This conjecture is supported by several boiling events observed for structure C-0.105-0.7.At low heat fluxes, the vapor is formed in the bottom channels and ejected through the pores into the liquid pool. Another remarkable phenomenon is the lack of nucleation sites on top channels.

The data collected for different top gap spaces S and over a large range of heat fluxes allow a division of the nucleate boiling curve into sub-regimes. This division is marked with solid line segments in Figure 5.1.The regimes are the *isolated flattened bubbles* regime (Regime I in Figure 5.1) occurring at low heat fluxes and large top gaps and the *coalesced bubbles* regime (Regime II in Figure 5.1) for high heat fluxes or low heat fluxes and small top gaps. Characteristics of the *isolated flattened bubbles* regime are: individual bubbles are ejected from the top channels and feed the vapor clusters from below. The heat transfer coefficient is the highest for this regime. The *coalesced bubbles* regime implies the existence of a hovering vapor mass covering almost entirely and permanently the top surface of the structure. This vapor cluster presents a wavy upper liquid/vapor interface. Liquid is entrapped as slugs inside the vapor cluster.

The proposed division of the boiling curve into two sub-regimes is applicable for boiling from structures made of high thermal conductivity materials. However, its validity may be extended to enhanced structures made of low thermal conductivity materials, but for a different range of heat fluxes.

5.4 Summary

A flow visualization study was conducted to assess the influence of top confinement on boiling heat transfer from enhanced structures. Below are the conclusions resulted from the study:

a) The heat transfer performance of the enhanced structures in nucleate pool boiling under top-confined conditions depends significantly on the top gap parameter S. The enhancement observed for plain surfaces in the low heat flux regime is not present for the present enhanced structure. The maximum heat flux dissipated increased with the increase of the top spacing, similar to the plain surface case.

b) The vapor is generated primarily inside the bottom channels. It is ejected through the pores as bubbles toward the top channels. Here the vapor deforms, taking the shape of elongated slugs extending laterally prior to detachment and accumulation into a vapor mass at the bottom surface of the confining plate.

c) The nucleate boiling region of the boiling curve can be broadly divided into the regimes of *isolated flattened bubbles* and *coalesced bubbles*.

CHAPTER 6: SEMI-ANALYTICAL MODEL FOR BOILING FROM ENHANCED STRUCTURES UNDER TOP CONFINEMENT

The employment of enhanced structures proved to be beneficial for boiling heat transfer. However, as mentioned in the introductory chapter, much needs to be done on modeling boiling from enhanced structures in confined geometries. This chapter aims at simulating the process of boiling under confinement from an enhanced structure using a semi-analytical model. For unconfined pool boiling from structured surfaces, Nakayama et al. (1980b) developed the first dynamic model. Chien (1996) used a similar framework and refined the analysis of Nakayama to reduce the number of empirical constants.

Katto and Yokoya (1966) developed a model for boiling from horizontally oriented plain surfaces under top confinement. The model does not take the top gap distance s into account as a geometrical parameter, being developed for S = 0.4 mm only. Fujita et al. (1988) constructed a predictive model for boiling water in a confined space from a plain rectangular surface oriented vertically. For a top gap S = 2 mm, the agreement between prediction and experiment was good. The prediction was higher than the measurement for S = 0.6 mm indicating the drying of the heating surface at some locations.

The current model uses Katto and Yokoya's (1966) analysis and predicts heat transfer from the enhanced structures under top-confined conditions. The evaporation process is assumed to be similar to that proposed by Katto and Yokoya (1966), with the exception that the majority of the vapor is generated inside the enhanced structure and

injected in the space between the structure and the top confining plate. The vapor takes the shape of a flattened bubble spreading laterally towards the edges of the structure. Once the vapor reaches an edge of the structure, it is released in the surrounding liquid pool. A new bubble starts forming from the active nucleate site. This process is illustrated in Figure 6.1. In unconfined pool boiling, there are four essential parameters used in quantifying the boiling process: bubble departure diameter (D_d), frequency (f), nucleate site density (n_s) and the heat flux (q''). The heat flux is averaged over a period of one bubble cycle (Chien (1996), Ramaswamy (1999)). In the presence of confinement, the boiling phenomenon has to be analyzed using a different framework. A flattened bubble cycle consists of two periods: vapor period (Δt_v) and liquid period (Δt_l). During the vapor period the bubble spreads lateraly and evaporation takes place. The space above the enhanced structure is mostly filled with vapor.The liquid period starts immediately after the vapor is release into the liquid pool. Using the movie clips obtained during boiling (Chapter 5) it was determined that the liquid intake period is much shorter than the evaporation period. Therefore, it was neglected in the following analysis and the heat flux was averaged over the evaporation period.

For an enhanced structure, the total dissipated heat flux is made up of two parts, internal heat flux (q''_t) and external heat flux (q''_{ex}). The internal heat transfer can be subdivided into internal evaporation and internal convection to the liquid. Due to the small liquid mass involved the internal convection is neglected in the present analysis. The external heat transfer is composed of external evaporation and external sensible heat transfer (convection). The presence of a confining plate in the close proximity of

the top surface of the enhanced structure diminishes the importance of external convection. This component of the heat flux is also neglected in the present study.

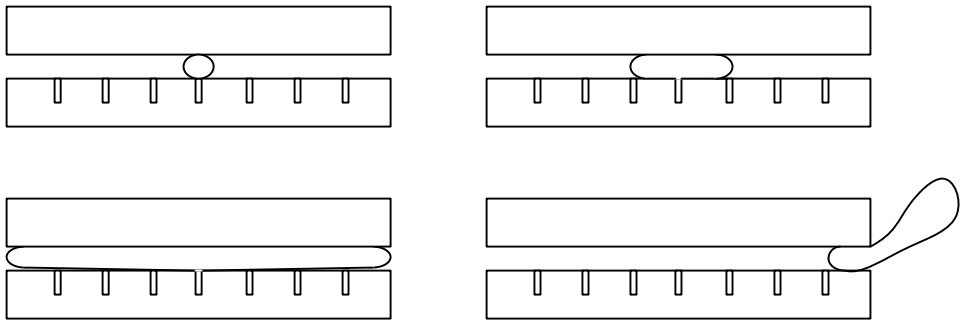

Figure 6.1 Vapor bubble inception, growth and ejection

6.1 Modeling internal heat transfer

Nakayama et al. (1980b) modeled the tunnel heat transfer using empirical constants determined from their experimental data for R-11 at a reference state ($\Delta T_{wall} = 1K$). Using an enhanced structure similar to the ones used in the present study, Ramaswamy (1999) assumed that the evaporation takes place from thin liquid films across the menisci located along the corners of the tunnel. This assumption makes the model unusable for boiling from enhanced structures with circular sub-surface tunnels, which exhibit enhancement as well. The present study takes a simpler approach and assumes, similar with Nakayama et al. (1980a), that the dissipated heat is proportional to the liquid thermal conductivity (k_l) and the wall superheat $\left(T_{wall} - T_{sat}\right)$. Nakayama et al. (1980a) showed that, for the type of structured surfaces utilized in their study, the contribution of latent heat flux to the total heat flux is below 25 % for heat fluxes $q_t'' \geq 3W/cm^2$. This observation is also supported by Bhavnani et al. (2001).

Since the heat flux levels encountered in electronics cooling are well above this value, the latent heat flux will represent a small fraction of the total heat flux. Additionally, the working fluid used in this study (PF 5060) has a very low heat of vaporization ($h_{fg} = 88kJ/kg$). It is also assumed there is negligible convection within the liquid present inside the tunnels. The tunnel heat transfer is expressed as:

$$q_t'' = C_1 k_l \left(T_{wall} - T_{sat} \right) \tag{6.1}$$

where T_{sat} is the local saturation temperature of the liquid, assumed to be same as the bulk saturation temperature. The empirical constant C_1 is considered independent of time and is determined based of the experimental data presented in Chapter 4.

6.2 Modeling external heat transfer

As mentioned in the introductory part of this chapter, Katto and Yokoya (1966) were apparently the first to develop a model for boiling from a plain surface under confined conditions. They assumed that as a flattened bubble spreads with the velocity of the boundary v_s, a thin liquid film is created and partially evaporated. The high heat transfer rates achieved during boiling were attributed to the mechanism of thin film evaporation. If a dried-up zone of radius r' is created in a time t', the mean heat flux from a circular surface of radius r_0 and during the dried-up period can be expressed as (Katto and Yokoya(1966)):

$$q'' = \frac{8}{5} \frac{c_{pl}\left(T_w - T_{sat}\right)}{h_{fg}} \left(\frac{\rho_l \mu_l h_{fg}}{M \sqrt{r_0}} \right) \left(\frac{r_0}{r'} \right) \left[1 - \left(1 - \frac{r'}{r_0} \right)^{\frac{5}{2}} - \frac{5}{3} \left(\frac{r'}{r_0} \right) \left(1 - \frac{r'}{r_0} \right)^{\frac{3}{2}} \right] \tag{6.2}$$

where M is expressed in $m^{0.5}$.

For boiling water under a top confinement $S = 0.4$ mm, the heat flux predicted using equation (6.2) was larger by 57% for a value of heat flux $q'' = 18.6\ W/cm^2$ and a value $\frac{r'}{r_0} = 0.5$. Thin film evaporation constitutes the main mechanism of heat transfer, accounting to about 67 % of the total heat transfer. The model has been developed for the isolated bubble regime of nucleate boiling from plain surfaces.

The present model uses the Kato and Yokoya (1966) analysis adapted for the case of enhanced structures. The top surface of the enhanced structure is alternately covered by vapor and liquid. Heat is assumed to be primarily transferred as latent heat.

6.2.1 Modeling latent heat transfer

Let us consider a vapor bubble ejected through a pore towards the top surface. In order to simplify the analysis, let us assume the vapor generating pore situated in the center of the enhanced structure. For a small enough top gap s,the bubble flattenes and spreads laterally vith a velocity of the boundary v_s. The spreading of the dried-up area on the heating surface, a phenomenon considerably slower than the spreading of bubbles, can be expressed by the empirical formula (Katto and Yokoya(1966)):

$$\Delta t = C_2 r \qquad (6.3)$$

where Δt is the time consumed for drying up an are of radius r and C_2 is an empirical constant expressed in s/m. C_2 can be obtained using high-speed photography. Figure 6.2 shows a dried area of radius r formed underneath the bubble.

Let us also consider a liquid film on a heating surface of temperature T_w with the evaporation taking place from the upper surface of liquid of temperature T_{sat} .Instantenous thickness of the film can be expressed as (Katto and Yokoya(1966)):

$$\frac{\delta}{\delta_0} = \sqrt{1 - 2\frac{k_l(T_w - T_{sat})}{h_{fg}}\frac{t}{{\delta_0}^2}} \tag{6.4}$$

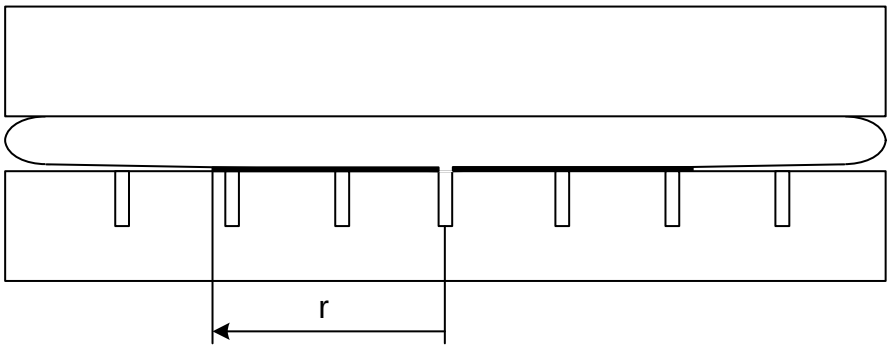

Figure 6.2 Dried up area of radius r underneath a flattened bubble

Where δ_0 is δ at t=0. If we make δ=0 in equation 6.4, the drying up time is:

$$\Delta t = \frac{1}{2}\frac{{\delta_0}^2}{k_l}\frac{\rho_l h_{fg}}{(T_w - T_{sat})} \tag{6.5}$$

This derivation follows that of Katto and Yokoya (1966). As previously mentioned, the gap s is not taken into account in the expression for the initial thickness of the liquid film. An attempt is made here to take S into account. Fujita et al.(1988) performed an experiment to measure the thickness of a liquid film formed between a non-heating surface and an air bubble rising in a narrow gap filled with water. They found the thickness to be $\delta = 34\mu m$ for a gap $S = 2mm$ and $\delta = 9\mu m$ for a gap $S = 0.6mm$. The authors considered that these results are applicable to the case of

boiling. For this study, we will assume that the initial thickness of the liquid films varies direct proportionally with S. The proportionality constant is dimensional $\left(m^{-1}\right)$ and accounts for the differences in orders of magnitude between the two dimensions. Combining equations 6.3 and 6.5 and the above considerations gives the distribution of the initial thickness of the liquid film:

$$\delta_0 = C_3 SM\sqrt{r} \tag{6.6}$$

where M depends of $\left(T_w - T_s\right)$ in the following manner:

$$M = \sqrt{2C_2 \frac{k_l\left(T_w - T_{sat}\right)}{\rho_l h_{fg}}} \tag{6.7}$$

The heat flux resulting from the evaporation of a thin liquid film can be calculated now. Assume a liquid film has the initial thickness distribution expressed by equation (6.6). If a dried-up area of radius r' is produced in a period of time Δt_v, the expressions for Δt_v and the thickness of non-evaporated liquid film δ' are:

$$\Delta t_v = \frac{1}{2k_l}\frac{\rho_l h_{fg}}{\left(T_w - T_{sat}\right)} C_3^2 S^2 M^2 r' \tag{6.8}$$

$$\delta' = C_3 SM\sqrt{r - r'} \tag{6.9}$$

With this we can calculate the quantity of liquid vaporized and the heat dissipated at the base of one flattened bubble. Dividing this value by Δt_v and by the projected surface aria of the enhanced structure gives the time averaged heat flux:

$$q_v'' = \frac{8}{5}\frac{c_{pl}\left(T_w - T_{sat}\right)}{h_{fg}}\left(\frac{\rho_l \mu_l h_{fg}}{C_3 \cdot S \cdot M \cdot \sqrt{r}}\right)\pi r^2 \frac{1}{L^2}\left(\frac{r}{r'}\right)\left[1 - \left(1 - \frac{r'}{r}\right)^{\frac{5}{2}} - \frac{5}{3}\left(\frac{r'}{r}\right)\left(1 - \frac{r'}{r}\right)^{\frac{3}{2}}\right] \tag{6.10}$$

where r is the radius of the bubble at the end of the evaporation period and L is the length of the structure. The full derivation of equation (6.10) is presented in Appendix B.

Replacing M with the corresponding expression yields:

$$q_v'' = \frac{8}{5}(T_w - T_{sat})^{0.5}\left(\frac{1}{C_3 \cdot S}\right)\left(\sqrt{\frac{h_{fg}\rho_l k_l}{2C_2}}\right)\left(\frac{\pi r^2}{\sqrt{r}}\right)\frac{1}{L^2}\left(\frac{r}{r'}\right)\left[1-\left(1-\frac{r'}{r}\right)^{\frac{5}{2}} - \frac{5}{3}\left(\frac{r'}{r}\right)\left(1-\frac{r'}{r}\right)^{\frac{3}{2}}\right]$$

(6.11)

The ratio $\frac{r'}{r}$ can take different values less than 1. The bubble radius at the end of evaporation period (r) can take a maximum value of $L/2$.

The conduction thermal resistance introduced by the enhanced structure itself should be taken into account in equation (6.11). This resistance depends on the geometry of the structure as well as on its constituent material. In this study, a simple one-resistance network is proposed as illustrated in Figure 6.3.

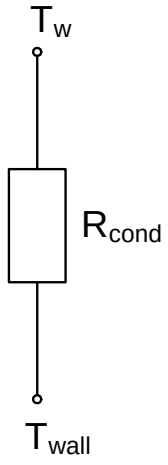

Figure 6.3 Conduction thermal resistance introduced by the enhanced structure

In Figure 6.3, T_w is the temperature at the top surface of the enhanced structure and T_{wall} is the temperature at the base of the enhanced structure. Since the enhanced structure used for the modeling work (C-0.105-0.7) is made of copper, has an overall height of only 1 mm and has a low porosity, the conduction resistance can be neglected Therefore, $T_w \cong T_{wall}$.

6.3 Modeling total heat flux

The external heat flux can now be calculated using equations (6.11) assuming that no heat transfer mechanisms other than thin film evaporation have a significant contribution to the heat removal through the top surface:

$$q_{ex}^{"} = q_v^{"} \tag{6.12}$$

The total heat flux can now be calculated using equations (6.1) and (6.12):

$$q^{"} = q_t'' + q_{ex}^{"} \tag{6.13}$$

6.4 Determination of empirical constants

For the determination of C_1, heat transfer data obtained for boiling under total confinement (Chapter 4) were used. For the completely covered top surface, it can be assumed that the entire heat is dissipated as latent heat. A power –law curve fit of the data for the enhanced structure C-0.105-0.7 yields:

$$q_l^{"} = C_1^{'} \Delta T_{wall}^{n} \tag{6.15}$$

where $C_1^{'} = 0.3346\ (W / cm^2 \cdot K^{-n})$ and $n = 1.019$.

We can assume $n \approx 1$, so the internal heat transfer can be expressed as:

$$q_t^{"} = C_1 k_l (T_{wall} - T_{sat}) = C_1^{'} \Delta T_{wall}^n = 0.3346 \Delta T_{wall} \quad (6.16)$$

with the dimensional constant is expressed in $\left(W / cm^2\right) K^{-1}$.

The empirical constant used in calculting the speed of evaporation (C_2) is the most important constant introduced in this analysis. It controls the evaporation rate. From the analysis of movie clips, Katto and Yokoya (1966) determined a value $C_2 = 13.33 s \cdot m^{-1}$ for boiling water under a top confinement $s = 0.4 mm$. In this study, C_2 was assumed to depend on S. With the increase of top spacing, the process of evaporation becomes slower, therefore C_2 decreases in magnitude.

The value of C_3 was estimated based on Fujita et al.(1988).For the current study, a value of 1000 was used for all predictions yielding good results.

6.5 Prediction procedure

Based on the equations outlined above a prediction procedure employing the semi-analytical model was developed. The steps in predicting the heat flux are as follows:

1) Calculate the tunnel heat flux ($q^{"}_t$) using equation (6.1)
2) Calculate the external convective heat flux ($q^{"}_{ex}$) using equation (6.12)
3) The total heat flux is calculated as $q'' = q^{"}_t + q^{"}_{ex}$

The stages of the model and the calculation flowchart are presented in Figure 6.4. The diagram shows various components of the model and their interdependence.

6.6 Predictions using the model

The model outlined in the preceding sections was used to predict the boiling data obtained in the case of top confinement. The experimental results used for comparison were included in Chapter 5. In equation (6.11), the expression:

$$\left(\frac{r}{r'}\right)\left[1-\left(1-\frac{r'}{r}\right)^{\frac{5}{2}}-\frac{5}{3}\left(\frac{r'}{r}\right)\left(1-\frac{r'}{r}\right)^{\frac{3}{2}}\right] \qquad (6.17)$$

was evaluated for different values of the ratio $\frac{r'}{r}$ .The results were included in Appendix B. For a ratio $\frac{r'}{r}=0.1$ the value of the expresion (6.16) is 0893 and for $\frac{r'}{r}=0.7$ the value is 1.084.

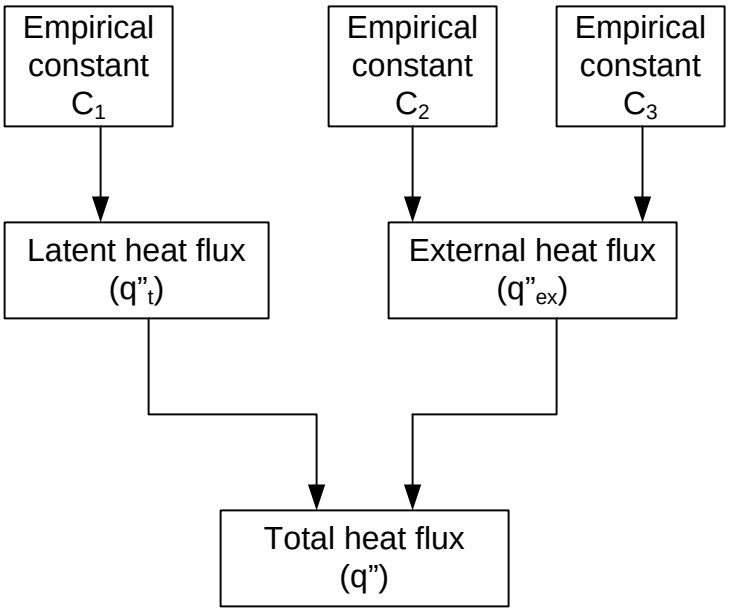

Figure 6.4 Calculation flowchart for the proposed model

6.6.1 Predictions for $S = 0.15mm$

The results for the smallest gap spacing are presented in Figure 6.5. The two sets of predicted data are obtained for the minimum, respectively maximum value of expression (6.17). A value of $C_2 = 2000s \cdot m^{-1}$ best fits the data and was used for the calculation. The model captures the trend of the boiling curve well. The predicted data is within ±20% of the experimental results for all the data points except for the lowest heat flux measured.

6.6.2 Predictions for $S = 0.35mm$

Figure 6.6 shows the comparison for this gap spacing. A value $C_2 = 100s \cdot m^{-1}$ was employed. Again the predicted heat flux is within ±20% of the experimental results with two exceptions: the lowest heat flux and the kink in the boiling curve occuring at $q'' = 12W / cm^2$.

6.6.3 Predictions for $S = 0.7mm$

The results for $S = 0.7mm$ are presented in Figure 6.7. The trend of the boiling curve is captured fairly well,with the exception of the "hump" starting at $\Delta T_{wall} = 14.3K$. With the exception of the smallest heat flux, all the data is within a band of ±30% of the measured values. For this case, $C_2 = 20s \cdot m^{-1}$.

6.6.4 Predictions for $S = 1mm$

For further increse in the top gap, the results in Figure 6.8. General observations for $S = 0.7mm$ are true in this case also. The lowest heat flux and two other data points

are ouside of the ±30% interval around the measured data. $C_2 = 15s \cdot m^{-1}$ was selected for this gap.

6.6.5 Predictions for $S = 1.75mm$

The results for the largest gap spacing are presented in Figure 6.9. The model underpredicts the data by as much as 50% for almost the entire measured boiling curve. This can be interpreted as a result of the fact that the proposed thin film evaporation mechanism ceases to play an important role as the gap distance increases. Further refinement of the analysis is required by incorporating of a term accounting for the sensible heat transfer.A value $C_2 = 5s \cdot m^{-1}$ was selected for this gap.

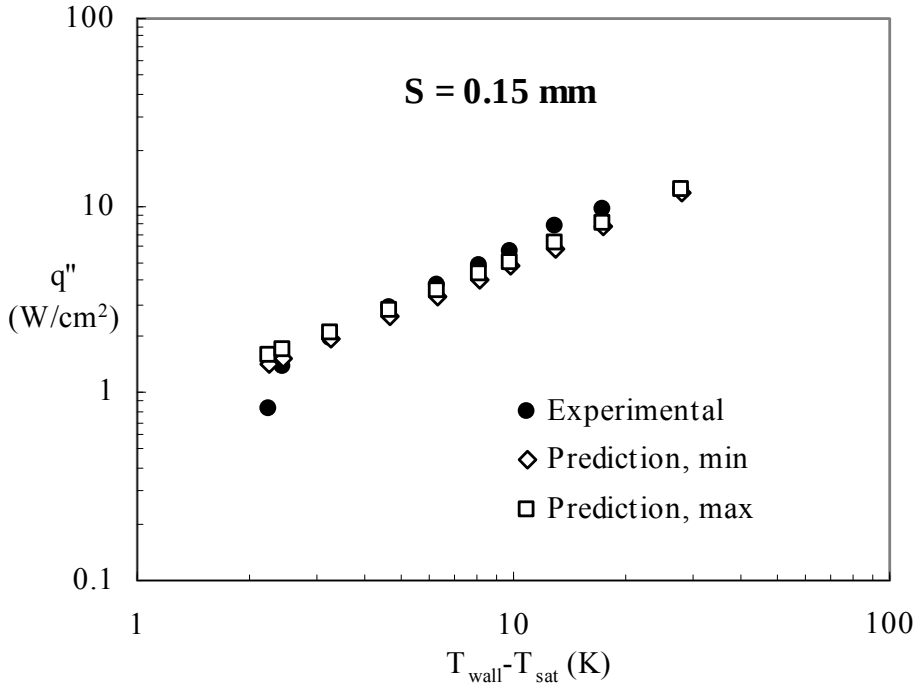

Figure 6.5 Comparison between measured and predicted heat flux for $S = 0.15mm$

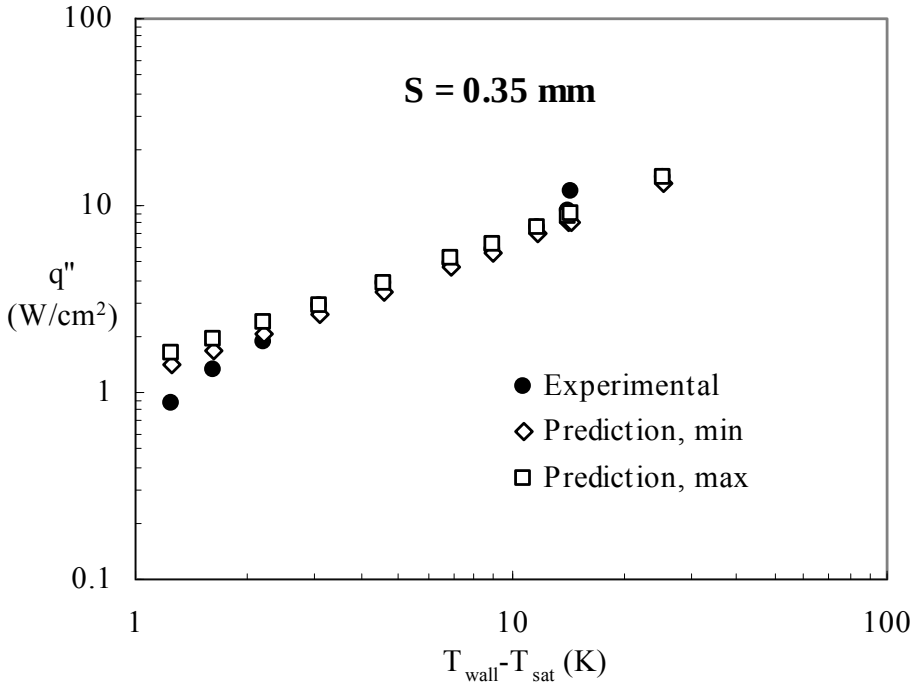

Figure 6.6 Comparison between measured and predicted heat flux for $S = 0.35mm$

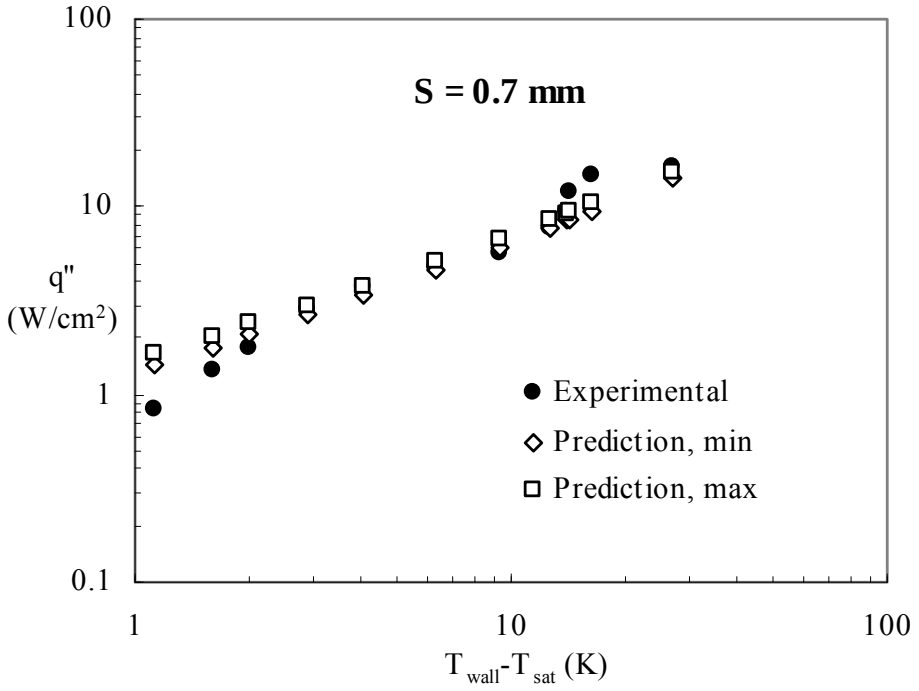

Figure 6.7 Comparison between measured and predicted heat flux for $S = 0.7mm$

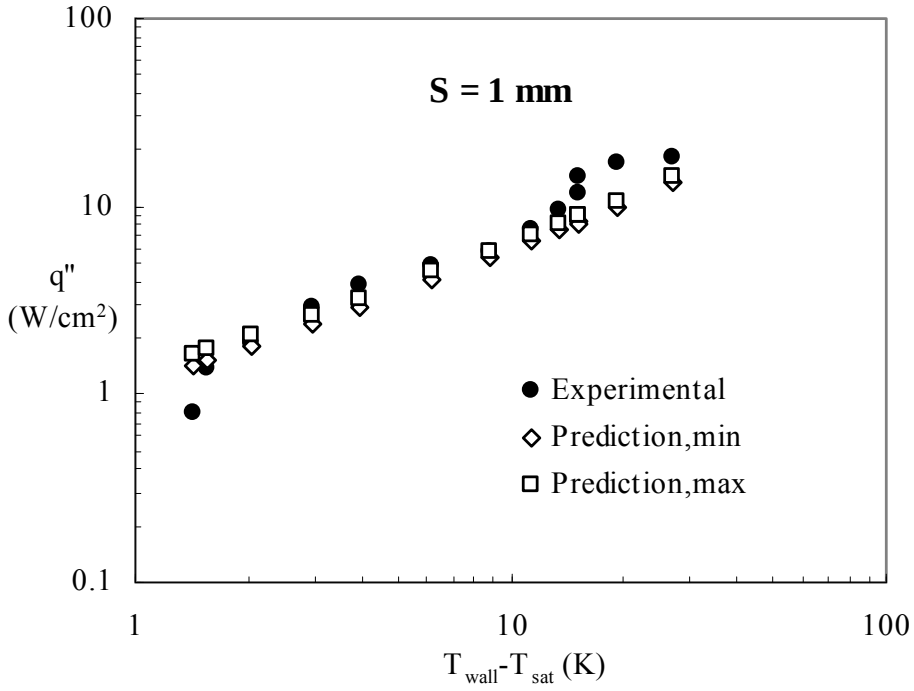

Figure 6.8 Comparison between measured and predicted heat flux for $S = 1mm$

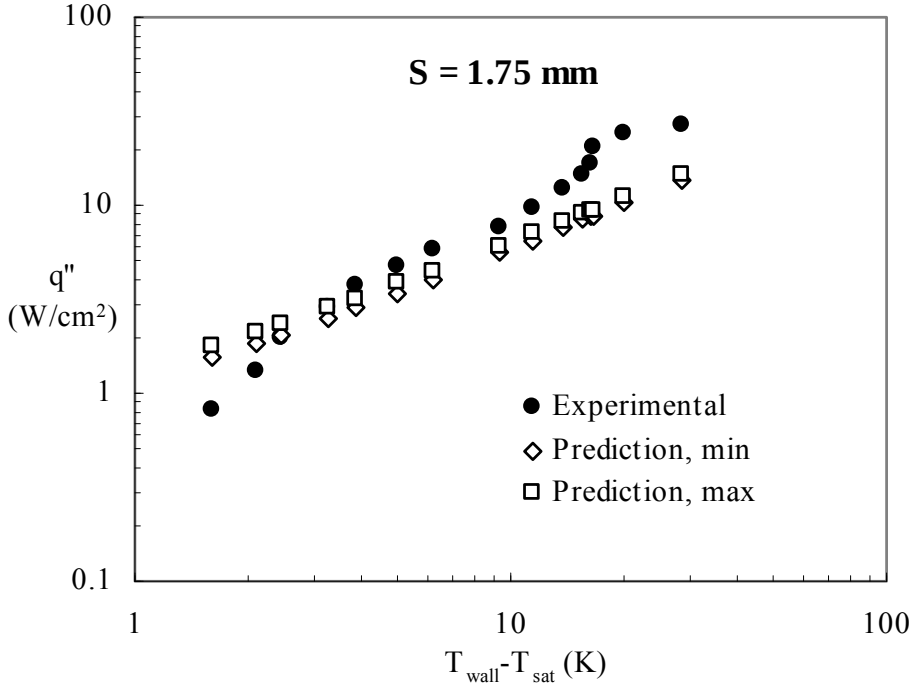

Figure 6.9 Comparison between measured and predicted heat flux for $S = 1.75mm$

6.7 Summary

A semi-analytical model that predicts the total heat flux dissipated in confined pool boiling from enhanced structures has been constructed. The model builds on existing models developed for plain surfaces. The novel features of the model are:

a) To the author's knowledge, this is the first analytical model applicable to confined pool boiling from enhanced structures.

b) A simplified method of estimating the tunnel heat transfer is proposed. It eliminates the complexity of the previous proposed model, requiring only one boiling curve.

c) The main heat transfer mechanism is considered to be thin film evaporation above the structure. As the flattened bubble spreads laterally, a thin liquid film forms and subsequentely evaporates.

d) C_2 decreases in magnitude with the increase of the top gap S. For the current study, a constant value of C_3=1000 was used for all predictions yielding good results.

e) The model captures well the trends in heat dissipation.

CHAPTER 7: SUMMARY, CONCLUSIONS, APPLICATIONS AND RECOMMENDATIONS FOR FUTURE WORK

7.1 Summary

The advantages of two-phase liquid cooling were presented along with a detailed literature review section (Chapter 1). A special designed enhanced structure was identified as the best candidate for improving the performance of the evaporator section of a two chamber thermosyphon.

The enhanced structures were fabricated (Chapter 2), included in a thermosyphon loop and tested. The effect of reduction in the geometrical dimensions on the boiling heat transfer performance is assessed in Chapter 3. Predictive correlations for the nucleate boiling regime are proposed for the proper design and employment of the enhanced structures. The effect of confinement on the thermal performance of the enhanced structures in analyzed in Chapter 4 (total top confinement) and Chapter 5 (partial top confinement). The boiling is characterized by identifying the regimes (modes) established for different top gaps and heat flux levels. The gap between the enhanced structure and the confinement plate constitutes the main geometrical parameter varied in several steps. A semi-analytical model intended to simulate the boiling under confinement was proposed. The model assumes that the main heat transfer mechanism is the evaporation of a thin liquid film form between the top surface of the structure and the confining plate.

7.2 Conclusions

a) The enhanced structures employed in this study show superior heat transfer performance in comparison with the plain surface. The structures are highly efficient in promoting boiling heat transfer over the entire nucleate boiling curve. The maximum dissipated heat flux was q'' = 43 W/cm^2. In the low heat fluxes range (q'' = 1-8 W/cm^2), the superheat required to transfer a certain heat flux is reduced to nearly one fifth, at best.

b) In general, the performance of the enhanced structure increases with the increase of the channel width. This effect is more pronounced in the low to intermediate heat fluxes range (1-10 W/cm^2). At higher heat flux levels (more than 15 W/cm^2) this effect diminishes, ultimately disappearing.

c) The channel pitch has a large influence on the boiling performance of the enhanced structures. For the 65 μm channel width, the pitch reduction improves the performance at all heat fluxes (except the maximum). For the 105 μm channel width, the improvement is significant only beyond q'' ~ 25 W/cm^2.

d) The best thermal performance is obtained with structure C-0.065-0.2 for q'' < 30 W/cm^2 and with structure C-0.105-0.35 for q'' > 30 W/cm^2.

e) Simple multi-line curve fits are provided as empirical predictive correlations for boiling using enhanced structures. The present curve fits are intended to serve as quick dimensioning tools for the designer of cooling systems and represent the thermal performance of the enhanced structure over the entire nucleate boiling regime.

f) The modes of boiling from an enhanced structure proposed by Nakayama et al. (1982) were unable to explain the boiling curves obtained in this study. This is explained in light of the contribution from the top finned face of the enhanced structure.

g) The heat transfer performance of the enhanced structures with insulated top decreases significantly in comparison to the open top situation. However, there is a certain range of heat fluxes (1 W/cm^2 < q'' < 4 W/cm^2) for which the top-covered structure outperforms a plain structure with the top open.

h) The heat transfer performance of the enhanced structure with insulated top has only a marginal dependence on the channel width. It is hypothesized that the channel pitch may have a bigger influence through the number of menisci created inside the channels.

i) The boiling curves obtained with enhanced structures completely confined show no change in slope over the tested heat flux range; however, the visualizations indicate the presence of two boiling regimes: slug predominance regime and slugs and plugs regime. The internal evaporation process is an important heat transfer mechanism; its contribution to the total dissipated heat is significant, especially at low heat fluxes. Vapor slugs exist in the top and bottom channels even for the lowest heat fluxes and exhibit an oscillatory movement. This is believed to be an effect of the transient nature of internal evaporation.

j) The heat transfer performance of the enhanced structures in nucleate pool boiling under top-confined conditions depends significantly on the top gap parameter S. The enhancement observed for plain surfaces in the low heat flux regime is not present

for the present enhanced structure. The maximum heat flux dissipated increased with the increase of the top spacing, similar to the plain surface case. The nucleate boiling region of the boiling curve can be broadly divided into the regimes of *isolated flattened bubbles* and *coalesced bubbles*.

k) A semi-analytical model that predicts the total heat flux dissipated in confined pool boiling from enhanced structures has been constructed. The model builds on existing models developed for plain surfaces. To the author's knowledge, this is the first analytical model applicable to confined pool boiling from enhanced structures. A simplified method of estimating the tunnel heat transfer is proposed. It eliminates the complexity of the previous proposed model, requiring only one boiling curve.The main heat transfer mechanism is considered to be thin film evaporation above the structure.The model captures well the trends in heat dissipation.

7.3 Applications of confined boiling in electronics cooling

Confined nucleate pool boiling from enhanced structures is a particular case of pool boiling potentially useful in cooling electronic devices operating under tight spatial constraints.

One application for this type of boiling could be in next generation three-dimensionally stacked layers of powered electronic chips (Banerjee et al. (2001)). The thin enhanced structure could act as a thermal management layer between two active layers vertically integrated.

Another potential use of confined boiling from single-layered enhanced structures can be in a stacked configuration. In this case, the bonding between

individual layers may require the presence of a thin metallic foil (for instance, gold; see Ramaswamy (1999).

For portable electronic devices with space confinement (laptop computers in special), the use of boiling from enhanced structures could become a thermal management solution when the heat removal capability of heat pipes is exceeded. For instance, a maximum heat flux $q^{"}$ = 11 W/cm^2 can be reached in a total confinement configuration (top surface of the enhances structure covered with a insulating plate). A top gap of only 1 mm increases this value to $q^{"}$ = 18 W/cm^2. Nevertheless, the thermal designer must take into account several factors for a sucesful implementation. First, if the enhanced structures will be used in a thermosyphon loop, the difference in elevation between the condenser and the evaporator, essential for the functioning of a thermosyphon, needs to be present. This can be achieved,for instance, by placing the condenser on the backside of the display screen. If needed,a micropump can be added to the loop. Second, the thermal management device employing the enhanced structures should be orientation independent. A flat two-phase heat spreader plate recently developed (Murthy (2004)) met such demand. The orientation independence of the device is achieved by carefully designing the enclosure containing the liquid. Single-layer enhanced structures placed in the evaporator section significantly improved the spreader heat transfer performance. For such an application, the single line curve fits presented in Table 3.6 could serve as quick dimensioning tools for choosing the optimal enhanced structure.

7.4 Recommendations for future work

The present study was performed for a range of geometrical parameters that affect the thermal performance of the enhanced structure significantly. However, further investigations are needed to shed more light on the complex boiling phenomena. The recommandations for future work are:

a) The critical heat flux was not measured in the present study. Since this is an important point on the pool boiling curve, the current investigation should be extended to quantify the maximum heat flux attainable by employing enhanced structures.

b) The effect of structure thermal conductivity needs to be explored further with enhanced structures fabricated in materials different from copper or quartz.

c) The effect of varying the channel pitch on heat transfer performance was investigated for the conventional (open top) case only. The investigation needs to be extended to the isolated total confined case since it is likely that such configuration will play a role in future space constrained applications.

d) The evaporation process inside the channels need to be modeled more accurately and the results incorporated into the analysis.

e) The semi-analytical model can be improved by taking the geometrical parameters of the enhanced structure into account. Also, additional high speed visualization studies are needed for a more accurate determination of empirical constants C_2 and C_3.

APPENDIX A: UNCERTAINTY ANALYSIS

Based on the method proposed by Kline and McClintock (1953), the uncertainties in the measured quantities were used to evaluate those in the derived quantities. For a derived quantity, Y which is a function of n independent variables, x_i, the uncertainty w_y can be expressed as:

$$w_y = \left[\left(\frac{\partial Y}{\partial x_1} w_{x_1} \right)^2 + \left(\frac{\partial Y}{\partial x_2} w_{x_2} \right)^2 + \cdots\cdots + \left(\frac{\partial Y}{\partial x_n} w_{x_n} \right)^2 \right]^{0.5} \qquad \text{A.1}$$

where w_{x_i} is the maximum uncertainty in the ith independent variable.

For the heat transfer experiments, the independent variables were temperature, voltage and spacing of the thermocouples. The uncertainties associated with these quantities are given in Chapter 2 (section 2.4). The two main derived quantities for these experiments were the heat flux q'' and the wall superheat (ΔT_{wall}). As mentioned in the experimental procedure section (2.3), the heat input was calculated using a one-dimensional analysis and can be expressed as:

$$q = kA_h \frac{\Delta T}{\Delta x} \qquad \text{A.2}$$

The term $\Delta T/\Delta x$ is the slope calculated using a linear curve-fit to the in-line thermocouple data. The uncertainty in the temperature data and the placement of thermocouples will lead to an uncertainty in the calculated slope.

As an example, a calculation will be performed for two heat input values, one low and one high. First, the uncertainty in the slope (w_{slope}) calculated.

For q = 5 W, *slope* = 155 ± 20 ^{o}C/m, so w_{slope}=± 20 ^{o}C/m

For q = 32.4 W, *slope* = 1002.5 ± 50 ^{o}C/m, so w_{slope}=± 50 ^{o}C/m

Using equations A.1 and A.2, the uncertainty in q can be expressed as

$$w_q = \left[\left(kA_h w_{slope}\right)^2 + \left(k \cdot slope \cdot w_{A_h}\right)^2\right]^{0.5} \qquad \text{A.3}$$

The heater rod was of square cross section with each side = 9 mm. The uncertainty in measuring the side using a vernier caliper was 0.1 mm. Since the area = (side)^2, the uncertainty in the area can be expressed as:

$$w_{A_h} = side \cdot 0.1^{-3} \cdot \sqrt{2} \qquad \text{A.4}$$

where the side is measured in mm. The uncertainty in the heater cross-sectional area w_{A_h} = ± 1.8 e^{-6} m^2. According to the raw material supplier, the thermal conductivity of the copper alloy used to manufacture the heater rod was 388 W/m-K according to the manufacturer. For the two heat input values listed above the uncertainty was evaluated using equation A.3 as:

q = 5 W, w_q = ± 0.64 W (± 12.8 %)

q= 32.4 W, w_q = ± 0.94 W (± 2.9 %)

The heat flux was calculated by dividing the heat input with the enhanced structure base area A. The base area measurement has an uncertainty, which was evaluated similar to the uncertainty in the heater rod cross-sectional area (w_{A_h}). The base area of most structures was a square of side L =10 mm. The uncertainty in this measurement with a vernier caliper was 0.1 mm. Therefore, the uncertainty in the structure base area is w_A = ± 2e^{-6} m^2.

The heat flux can be expressed as

$$q'' = \frac{q}{A} \qquad \text{A.5}$$

Combining equation A.1 and A.5, the resulting expression for uncertainty in q'' is

$$w_{q''} = \left[\left(\frac{w_q}{A} \right)^2 + \left(-\frac{q}{A^2} w_A \right)^2 \right]^{0.5} \qquad \text{A.6}$$

For the two heat input values the uncertainty in the heat fluxes was evaluated as

q'' = 5 W/cm^2, $w_{q''}$ = ± 0.65 W/cm^2 (± 13.6 %)

q'' = 32.4 W/cm^2, $w_{q''}$ = ± 1.1 W/cm^2 (± 3.4 %)

The temperature at the base of the enhanced structure (T_{wall}) was calculated using the slope of the linear curve fit and hence has an uncertainty associated with it. It can be expressed as

$$T_{wall} = T_1 - slope \cdot \Delta x \qquad \text{A.7}$$

where T_1 is the top most thermocouple reading, Δx the distance between this thermocouple and the base of the enhanced structure. The uncertainty in the measurement of Δx was 0.1 mm (similar to the uncertainty in location of the other thermocouples). The uncertainties with the other quantities have been described above. Combining equation A.1 and A.7 results in

$$w_{T_{wall}} = \left[\left(w_{T_1} \right)^2 + \left(- slope \cdot w_{\Delta x} \right)^2 + \left(- \Delta x \cdot w_{slope} \right)^2 \right]^{0.5} \qquad \text{A.8}$$

The uncertainty in T_{wall} was evaluated using equation A.8 for the two heat inputs as

q = 5 W, $w_{T_{wall}}$ = ± 0.13 ^{o}C

q = 34.2 W, $w_{T_{wall}}$ = ± 0.16 ^{o}C

Since T_{sat} is calculated as an average of two temperatures measured with two independent thermocouples immersed in the liquid pool, the uncertainty in the liquid saturation temperature is:

$$w_{T_{sat}} = \left[\left(w_{T_{sat1}}\right)^2 + \left(w_{T_{sat\,2}}\right)^2\right]^{0.5}$$

Numerically, $w_{T_{sat}} = \sqrt{2} \cdot 0.1 = 0.14\ ^{o}\text{C}$

Finally, the uncertainty in the wall superheat $\left(\Delta T_{wall} = T_{wall} - T_{sat}\right)$ was evaluated using equation A1 again:

$$w_{\Delta T_{sat}} = \left[\left(w_{T_{wall}}\right)^2 + \left(w_{T_{sat}}\right)^2\right]^{0.5}$$

For the two heat inputs,

q = 5 W, $w_{\Delta T_{wall}} = \pm\ 0.19\ ^{o}\text{C}$

q = 34.2 W, $w_{\Delta T_{wall}} = \pm\ 0.21\ ^{o}\text{C}$

APPENDIX B: DEDUCTION OF THE EQUATION (6.10)

Let us assume that the initial thickness of a liquid film created by a spreading bubble can be expressed as:

$$\delta_0 = C_3 SM\sqrt{r} \tag{B.1}$$

After a time interval Δt_v, a circular dried –up area of radius r' is created. The shapes are depicted in Figure B.1.

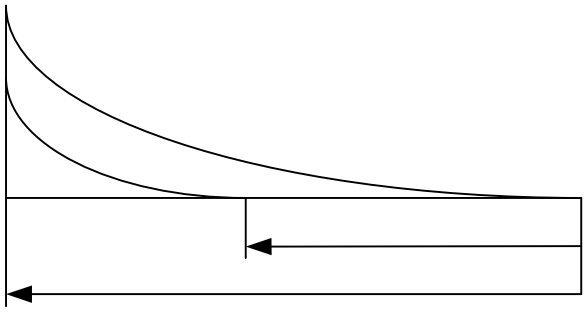

Figure B.1 Thin liquid film underneath a flattened bubble

With these assumptions, the initial volume of the liquid film trapped underneath one bubble is:

$$V_{initial} = \int_0^{r_0} 2\pi C_3 SMr\sqrt{r}\,dr = \frac{4}{5}\pi C_3 SMr_o^{\frac{5}{2}} \tag{B.2}$$

After the time interval Δt_v, the final volume of thin film liquid is:

$$V_{final} = \int_{r'}^{r_0} 2\pi C_3 SMr\sqrt{r - r'}\,dr \tag{B.3}$$

With the change of variable $r - r' = x$, equation (B.2) becomes:

$$V_{final} = \int_0^{r_0 - r'} 2\pi C_3 SM\left(x + r'\right)\sqrt{x}dx = 2\pi C_3 SM\left(\int_0^{r_0 - r'} x\sqrt{x}dx + \int_0^{r_0 - r'} r'\sqrt{x}dx\right)$$

After calculating the integrals,

$$V_{final} = 2\pi C_3 SM\left[\frac{2}{3}r'\left(r_o - r'\right)^{\frac{3}{2}} + \frac{2}{5}\left(r_o - r'\right)^{\frac{5}{2}}\right] \tag{B.4}$$

The quantity of liquid evaporated in the time interval Δt can be calculated by subtracting V_{final} from $V_{initial}$:

$$\Delta V = 2\pi C_3 SM\left[\frac{2}{5}r_o^{\frac{5}{2}} - \frac{2}{3}r'\left(r_o - r'\right)^{\frac{3}{2}} - \frac{2}{5}\left(r_o - r'\right)^{\frac{5}{2}}\right]$$

After some manipulations:

$$\Delta V = \frac{4}{5}\pi C_3 SMr_o^{\frac{5}{2}}\left[1 - \left(1 - \frac{r'}{r_o}\right)^{\frac{5}{2}} - \frac{5}{3}\left(\frac{r'}{r_o}\right)\left(1 - \frac{r'}{r_o}\right)^{\frac{3}{2}}\right] \tag{B.5}$$

Using equation (B.4), the latent heat dissipated can be expressed as:

$$q = \left(\rho_l h_{fg}\right)\frac{4}{5}\pi C_3 SMr_o^{\frac{5}{2}}\left[1 - \left(1 - \frac{r'}{r_o}\right)^{\frac{5}{2}} - \frac{5}{3}\left(\frac{r'}{r_o}\right)\left(1 - \frac{r'}{r_o}\right)^{\frac{3}{2}}\right] \tag{B.6}$$

Dividing q by the time interval Δt_v (equation 6.8) and by projected surface area (L^2) gives the latent heat flux (equation 6.10).

The expression $\left(\frac{r}{r'}\right)\left[1 - \left(1 - \frac{r'}{r}\right)^{\frac{5}{2}} - \frac{5}{3}\left(\frac{r'}{r}\right)\left(1 - \frac{r'}{r}\right)^{\frac{3}{2}}\right]$ needs to be evaluated for different values of the ratio $\frac{r'}{r}$. The results are included in Table B.1

Table B.1 Evaluation of expression (6.17)

Ratio $\frac{r'}{r}$	Expression (6.17)
0.1	0.89
0.2	0.95
0.3	0.99
0.4	1.03
0.5	1.06
0.6	1.08
0.7	1.08
0.8	1.08
0.9	1.05
1	1

APPENDIX C: THERMOPHYSICAL PROPERTIES OF PF 5060

Table C.1 Properties of PF 5060 at atmospheric pressure, 25°C

Property	Value
Boiling point	$56\left(^{o}C\right)$
Liquid density $\left(\rho_l\right)$	$1675\ \left(kg\cdot m^{-3}\right)$
Vapor density $\left(\rho_v\right)$	$12.68\left(kg\cdot m^{-3}\right)$
Dynamic viscosity $\left(\mu\right)$	$0.00064\left(kg\cdot m^{-1}\cdot s^{-1}\right)$
Specific heat $\left(c_p\right)$	$1050\ \left(J\cdot kg^{-1}\cdot K^{-1}\right)$
Latent heat of vaporization $\left(h_{fg}\right)$	$88\left(kJ\cdot kg^{-1}\right)$
Liquid thermal conductivity $\left(k_l\right)$	$0.057\left(W\cdot m^{-1}\cdot K^{-1}\right)$
Surface tension $\left(\sigma\right)$	$0.0012\left(N\cdot m^{-1}\right)$
Thermal expansion coefficient $\left(\beta\right)$	$0.0016\left(K^{-1}\right)$
Average molecular weight	338

REFERENCES

Anderson, T. M., and Mudawar, I., (1989), “Microelectronic Cooling by Enhanced Pool Boiling of a Dielectric Fluorocarbon Liquid,” Journal of Heat Transfer, vol. 111, pp. 752-759.

Arshad, J., and Thome, J. R., (1983), “Enhanced Boiling Surfaces: Heat Transfer Mechanism and Mixture Boiling,” Proceedings of ASME-JSME Thermal Engineering Joint Conference, vol.1, pp. 191-197.

Ayub, Z.H., and Bergles, A.E., (1987), "Pool Boiling from GEWA Surfaces in Water and R-113," Wärme-und Stoffübertragung, vol. 21, pp. 209-219.

Banerjee, K., Souri, S.J., Kapur, P., and Saraswat, K. C., (2001), “3-D ICs: A Novel Chip Design for Improving Deep-Submicrometer Interconnect Performance and Systems-on-Chip Integration, Proceedings IEEE, vol. 89, pp. 602-603.

Bhavnani, S., Fournelle, G., and Jaeger, R. C., (2001), “Immersion-Cooled Heat Sinks for Electronics: Insight from High-Speed Photography,” IEEE Transactions on Components and Packaging Technologies, vol. 24, pp. 166-176.

Bonjour, J. and Lallemand, M., (1998), “Flow Patterns During Boiling in a Narrow Space between Two Vertical Surfaces,” International Journal of Multiphase Flow, vol. 24, pp. 947-960.

Chien, L-H., and Webb, R. L., (1998a), “A Parametric Study of Nucleate Boiling on Structured Surfaces, Part II: Effect of Pore Diameter and Pore Pitch,” Journal of Heat Transfer, vol. 120, pp. 1049-1054.

Chien, L.-H. and Webb, R. L., (1998b), “Visualization of Pool Boiling on Enhanced Surfaces,” Experimental Thermal and Fluid Science, vol. 16, pp. 332-341.

Chien, L-H., and Webb, R. L., (1998c), “A Nucleate Boiling Model for Structured Enhanced Surfaces,” International Journal of Heat and Mass Transfer, vol. 41, pp. 2183-2195.

Chien, L.-H. and Chen, C.-L., (2001), “Experiments of Boiling on Cross-Grooved Surfaces in a Confined Space,” Proceedings of National Heat Transfer Conference, vol.1, pp. 175-182.

Danielson, R. D., Tousignant, L., and Bar-Cohen, A., (1987), “Saturated Pool Boiling Characteristics of Commercially Available Perfluorinated Inert Liquids,” Proceedings of ASME–JSME Thermal Engineering Joint Conference, vol. 3, pp. 419-430.

Fujie, K., Nakayama, W., Kuwahara, H., and Kakizaki, K., (1977), “Heat Transfer Wall for Boiling Liquids,” U.S. Patent 4,060,125.

Fujita, Y., Ohta, H., Uchida, S. and Nishikawa, K., (1988), “Nucleate Boiling Heat Transfer and Critical Heat Flux in Narrow Space between Rectangular Surfaces,” International Journal of Heat and Mass Transfer, vol. 31, pp. 229-239.

Ghiu, C.-D., Joshi, Y. K., and Nakayama, W., (2001), “Visualization Study of Pool Boiling from Transparent Enhanced structures,” Proceedings of the National Heat Transfer Conference, vol. 1, pp. 697-704.

Haider, I., and Webb, R.L., (1997), "A Transient Micro-Convection Model of Nucleate Pool Boiling," International Journal of Heat and Mass Transfer, vol. 40, pp. 3675-3688.

Ishibashi, E. and Nishikawa, K., (1969), “Saturated Boiling Heat Transfer in Narrow Spaces,” International Journal of Heat and Mass Transfer, vol. 12, pp. 863-894.

Katto, Y., Yokoya, S. and Teraoka, K., (1977), “Nucleate and Transition Boiling in a Narrow Space between two Horizontal, Parallel Disk Surfaces,” Bull. JSME 20, pp. 638-643.

Katto, Y. and Yokoya, S., (1966), “Experimental Study of Nucleate Pool Boiling in Case of Making Interference-Plate Approach to the Heating Surface,” Proceedings of the Third International Heat Transfer Conference, vol. 3, pp. 219-227.

Kline, S.J., and McClintock, F.A., (1953), "Describing Uncertainties in Single-Sample Experiments," Mechanical Engineering, vol. 75, pp. 3-8.

Kovalev, S.A.,Solov'yev, S.L., and Ovodkov, O.A., (1987), "Liquid Boiling on Porous Surfaces," Heat Transfer-Sov. Res., vol. 19 (3), pp. 109-120.

Marto, P. J., and Lepere, V. J., (1982), "Pool Boiling Heat Transfer from Enhanced Surfaces to Dielectric Fluids," Journal of Heat Transfer, vol. 104, pp. 292-299.

Mudawar, I., and Anderson, T. M., (1993), "Optimization of Enhanced Surfaces for High Flux Chip Cooling by Pool Boiling," Journal of Electronic Packaging, vol. 115, pp. 89-100.

Murthy, S., (2004), "Thin Two-Phase Heat Spreaders with Boiling Enhancement Microstructures for Thermal Management of Electronic Systems," Ph.D. dissertation, University of Maryland at College Park, MD.

Nakayama, W., Nakajima, T., Ohashi, S., and Kuwahara, H., (1989), "Modeling of Temperature Transient of Microporous Studs in Boiling Dielectric Fluid after Stepwise Power Application," Proceedings of the National Heat Transfer Conference, vol. 111, pp. 17-23.

Nakayama, W., Nakajima, T., and Hirasawa, S., (1984), "Heat Sink Studs Having Enhanced Boiling Surfaces For Cooling of Microelectronic Components," ASME Paper No. 84-WA/HT-89.

Nakayama, W., Daikoku, T., and Nakajima, T., (1982), "Effects of Pore Diameters and System Pressure on Saturated Pool Nucleate Boiling Heat Transfer from Porous Surfaces," Journal of Heat Transfer, vol.104, pp. 286-291.

Nakayama, W., Daikoku, T., Kuwahara, H., and Nakajima, T., (1980a), "Dynamic Model of Enhanced Boiling Heat Transfer on Porous Surfaces, Part I: Experimental Investigation," Journal of Heat Transfer, vol. 102, pp. 445-450.

Nakayama, W., Daikoku, T., Kuwahara, H., and Nakajima, T., (1980b), "Dynamic Model of Enhanced Boiling Heat Transfer on Porous Surfaces, Part II: Analytical Modeling," Journal of Heat Transfer, vol. 102, pp. 451-456.

Nowell, R.M., Bhavnani, S.H., and Jaeger, R.C., (1995), “Effect of Channel Width on Pool Boiling from a Microconfigured Heat Sink,” IEEE Transactions on Components, Packaging, and Manufacturing Technology-Part A, vol.18, pp. 534-539.

O’Connor, J. P., and You, S. M., (1995), “A Painting Technique to Enhance Pool Boiling Heat Transfer in Saturated FC-72,” Journal of Heat Transfer, vol. 117, pp. 387-393.

Pal, A., Joshi, Y., Beitelmal, M., Patel, C., and Wenger, T., (2002), “Design and Performance Evaluation of a Compact Thermosyphon,” IEEE Transactions on Components and Packaging Technologies, vol.25 No. 4, pp. 601-607.

Park, K.-A. and Bergles, A. E., (1988), “Effects of Size of Simulated Microelectronic Chips on Boiling and Critical Heat Flux,”, Journal of Heat Transfer, vol. 110, pp. 728-734.

Rainey, K. N. and You, S. M., (2001), “Effects of Heater Size and Orientation on Pool Boiling Heat Transfer from Microporous Coated Surfaces,” International Journal of Heat and Mass Transfer, vol. 44, pp. 2589-2599.

Rainey, K. N., and You, S. M., (2000), “Pool Boiling Heat Transfer from Plain and Microporous, Square Pin-Finned Surfaces in Saturated FC-72,” Journal of Heat Transfer, vol. 122, pp. 509-516.

Ramaswamy, C., Joshi, Y., Nakayama, W., and Johnson, W. B., (2003a), “Effects of Varying Geometrical Parameters on Boiling From Microfabricated Enhanced Structures,” Journal of Heat Transfer, vol. 125, pp. 103-109.

Ramaswamy, C., Joshi, Y., Nakayama, W., and Johnson, W. B., (2003b), “Semi-Analytical Model for Boiling from Enhanced Structures,” International Journal of Heat and Mass Transfer, vol. 46, pp. 4257-4269.

Ramaswamy, C., Joshi, Y., Nakayama, W., and Johnson, W. B., (2002), “High-Speed Visualization of Boiling from an Enhanced Structures,” International Journal of Heat and Mass Transfer, vol. 45, pp. 4761-4771.

Ramaswamy, C., (1999), “A Compact Two-Phase Thermosyphon Employing Microfabricated Boiling Enhancement Structures,” Ph.D. dissertation, University of Maryland at College Park, MD.

Ramaswamy, C., Joshi, Y., Nakayama, W. and Johnson, W.B., (1999), “Thermal Performance of a Compact Two-Phase Thermosyphon: Response to Evaporator Confinement and Transient Loads,” Journal of Enhanced Heat Transfer, vol. 6, pp. 279-288.

Ramaswamy, C., Joshi, Y., Nakayama, W., and Johnson, W. B., (1998), “Combined Effects of Sub-Cooling and Operating Pressure on the Performance of a Two-Chamber Thermosyphon,” Proceedings of the 6th Intersociety Conference on Thermal and Thermomechanical Phenomena in Electronic Systems, pp. 349-355.

Thome, J. R., (1990), Enhanced Boiling Heat Transfer, Hemisphere Publishing, New York, New York.

Webb, R. L., (1994), Principles of Enhanced Heat Transfer, John Wiley & Sons, New York, New York.

Webb, R.L., and Haider, I., (1992), "An Analytical Model for Nucleate Boiling on Enhanced Surfaces," Proceedings of the Engineering Foundation Conference on Pool and External Flow Boiling, pp. 345 - 360.

Xin, M.D., and Chao, Y.D., (1987), "Analysis and Experiment of Boiling Heat Transfer on T-shaped Finned Surfaces," Chemical Engineering Communications, vol. 50, pp. 185-199.

Yao, S.-C. and Chang, Y., (1983), “Pool Boiling Heat Transfer in a Confined Space,” International Journal of Heat and Mass Transfer, vol. 26, pp. 841-848.

3M Company, 1995, Specialty Fluids Newsletter, vol.1, No.1.